From uptake to primed cell wall defence: molecular mechanisms controlling beta-amino acid-induced immune priming in Arabidopsis

Chia-Nan Tao

A thesis submitted in partial fulfilment of the requirements for the degree of Doctor of Philosophy

The University of Sheffield
Faculty of Science
School of Biosciences

September 2023

Acknowledgements

This incredible journey commenced four years ago and now is close to the end. When I set foot in the United Kingdom in September 2019, it was hard to believe four years would pass so fast and even harder to imagine COVID-19 would happen a few months later. There are many people I wish to extend my thanks to, with the first and foremost my supervisor, Jurriaan Ton. Without his supervisory and steadfast support, the journey would not be as remarkable and fulfilling as it stands today. Undoubtedly, COVID-19 disrupted the progress, but Jurriaan remarkably attenuated its impact to insignificance. He is the ideal supervisor I could ever ask for, giving me enough freedom to explore the project but always there when I need advice and discussion. The Ministry of Education, Taiwan, mainly supports the PhD study. I want to thank the funding provided by my government for allowing me to study in the PhD program at the University of Sheffield and pursue my dream.

Many thanks to all the members of Ton's group, especially Roland, Sam, Mustafa, Adam and David. Roland was acting as my second supervisor during my first and second half year of PhD I shadowed him a lot to learn techniques ranging from pathogen inoculations to protein-protein interaction assay in the first year. He also laid the foundation for the research on FAH2. I feel fortunate and grateful to share office C207 with Sam, Mustafa and Adam. Working with these talented scientists inspires me massively; we share our views not only on science but also on life. They are always happy to give me a hand or a second opinion when needed. With them, any hardship or failure during my PhD became much more bearable. I truly believe that if we work together any goal is attainable. David is the person who keeps the lab running smoothly and serves as a reliable source of solutions for every challenge we confront. Without his technical support, going back to work after the COVID-19 lockdown would be more painful. He also acted as another pair of hands when I needed help. Besides them, I also want to thank all the past and present members of C45 and C51, as well as all those who crossed my path during my PhD journey. Thanking them for the kindness and help they showed me along the way.

Also, special thanks to Dr Laurent Zimmerli, who introduced the world of induced resistance and plant immunity to me. It has been more than 10 years since the date I started my summer internship at his lab. Little did I know at that time, this would turn

into my research interest and passion. Thank him willing to give an undergraduate student a chance to be involved in real research and glimpse how scientists work.

Lastly, but by no means least, my deepest thanks go to my family. Their love and financial support enabled me to chase my dream without fear. Even though we are in different countries, I know they will always be there to catch me if I fall. We seldom express our love to each other verbally because of our culture, but I can always feel it. Thanks, and I love you all, see you back in Taiwan.

Declaration and Acknowledgement of Collaborative Work

I, the author, confirm that the Thesis is my own work. I am aware of the University's Guidance on the Use of Unfair Means (www.sheffield.ac.uk/ssid/unfair-means). This work has not been previously been presented for an award at this, or any other, university. All co-authors of collaborative works present in this thesis have granted their approvement present the work. All the co-authors are acknowledged at the beginning of each chapter and their contributions are listed in the Author Contributions section in each chapter.

One publication has directly generated from this thesis. The publication is listed below.

Publication

Tao C-N, Buswell W, Zhang P, Walker H, Johnson I, Field K, Schwarzenbacher R, Ton J (2022) A single amino acid transporter controls the uptake of priming-inducing beta-amino acids and the associated tradeoff between induced resistance and plant growth. The Plant Cell 34: 4840-4856

Reproduced with permission from The Plant Cell.

Table of Contents

Acknowledgements i

Declaration and Acknowledgement of Collaborative Work iii

Publication iii

Table of Contents iv

List of Figures viii

List of Supplemental Figures ix

List of Supplemental Tables xi

List of Supplemental Data Set xi

Summary xii

Chapter 1: General Introduction 1

1.1 Plant innate immunity: PTI and ETI 2

1.2 Plant-acquired immunity: induced resistance 2

1.3 BABA-induced resistance 4

1.4 BABA is an endogenous stress signal 5

1.5 BABA: a potential crop protection agent? 5

1.6 IBI1: the Arabidopsis BABA receptor controlling IR and phytochemical stress via separate pathways 6

1.7 BABA-induced changes in plant metabolic, transcriptomic and epigenetic profiles 8

1.8 Molecular and cellular mechanisms driving BABA-IR 9

1.9 R-β-homoserine: a structural BABA analogue that is less phytotoxic than BABA 11

1.10 Scope of the PhD thesis 11

1.11 References 13

Chapter 2: A single amino acid transporter controls the uptake of priming-inducing beta-amino acids and the associated trade-off between induced resistance and plant growth 19

2.1 Abstract 20
2.2 Introduction 20
2.3 Results 23
2.3.1 Genome-wide screen for *impaired in RBH-immunity* (*iri*) mutants 23
2.3.2 Identification of *IRI1/LHT1* as a critical regulator of RBH-IR against *Hpa* . 25
2.3.3 LHT1 controls RBH uptake from the soil 25
2.3.4 Tolerance to RBH depends on LHT1 and not on catabolism 27
2.3.5 LHT1 also controls BABA uptake, BABA-IR and BABA tolerance 30
2.3.6 LHT1 transports both RBH and BABA 33
2.4 Discussion 36
2.4.1 Using annotated T-DNA insertion lines for a genome-saturating mutant screen 36
2.4.2 The role of LHT1 in plant-biotic interactions 37
2.4.3 The role of LHT1 in beta-amino acid-IR 38
2.4.4 RBH and BABA compete with proteinogenic amino acids for uptake by LHT1 40
2.4.5 LHT1: not just a transporter for proteinogenic amino acids 40
2.5 Methods 41
2.5.1 Biological material 42
2.5.2 Plant growth conditions 42
2.5.3 Mutant screen 42
2.5.4 Induced resistance (IR) assays 43
2.5.5 Plant growth assays 44
2.5.6 Genotyping verification by PCR and gene expression analysis by reverse transcription quantitative PCR (RT-qPCR) 44
2.5.7 Quantification of *in planta* RBH and BABA concentrations by hydrophilic interaction liquid chromatography coupled to quadrupole time-of-flight mass spectrometry 45

2.5.8 Yeast transformation 46
2.5.9 Yeast growth assays 46
2.5.10 Assessment of uptake and inhibition kinetics of LHT1 in yeast 47
2.6 Acknowledgements 48
2.7 Author Contributions 48
2.8 References 48
2.9 Supplemental Material 54
Chapter 3: The sphingolipid α-hydroxylase FAH2 interacts with the BABA receptor to regulate BABA-induced plant responses 63
3.1 Abstract 64
3.2 Introduction 65
3.3 Results 68
3.3.1 FAH2 physically interacts with IBI1 *in planta* 68
3.3.2 FAH2 regulates both BABA-IR and BABA-IS 71
3.3.3 Role of FAH2 and IBI1 in global sphingolipid profiles upon BABA and *Hpa* treatment 73
3.3.4 Identification of a FAH2- and IBI1-dependent VLCFA GIPC that is responsive to BABA and *Hpa* treatments 76
3.3.5 Role of FAH2 in the BABA-induced priming of pathogen-induced translocation of IBI1 from the ER to the cytosol 77
3.4 Discussion 80
3.4.1 FAH2, a interactor of IBI1 and a regulator of BABA-induced signalling 80
3.4.2 How can FAH2 regulate BABA-induced stress responses 82
3.4.3 Will FAH1, a FAH2 homolog, also interact with IBI1 and contribute in BABA-induced signalling? 83
3.4.4 FAH2 might control IBI1 translocation 83
3.5 Methods 84
3.5.1 Biological material 84

3.5.2 Plant growth conditions 84
3.5.3 BABA-induced resistance assay 84
3.5.4 BABA-induced stress assay 85
3.5.5 Subcellular localisation of IBI1-YFP 85
3.5.6 Real-time quantitative PCR analysis 86
3.5.7 Bimolecular fluorescence complementation assay 86
3.5.8 Co-immunoprecipitation assay 86
3.5.9 Sphingolipid profiling 87
3.6 Acknowledgements 88
3.7 Author Contributions 88
3.8 References 89
3.9 Supplemental Material 92
Chapter 4: A new player in the priming of cell wall defence by β-aminobutyric acid 96
4.1 Abstract 97
4.2 Introduction 97
4.3 Results 99
4.3.1 Morphology of primed callose papillae arresting early *Hpa* colonisation 99
4.3.2 Role of PMR4 in BABA-and RBH-IR against Hpa 101
4.3.3 Role of PMR4 in RBH- and BABA-induced penetration resistance 102
4.3.4 Role of PDLP proteins in RBH- and BABA-induced penetration resistance 103
4.3.5 BABA mobilises PDLP1 to germinating *Hpa* spores 105
4.4 Discussion 107
4.4.1 Penetration resistance against Hpa: a multifaceted immune response controlled diverse signalling pathways 107
4.4.2 The contribution of PMR4 to penetration resistance 107
4.4.3 The contribution of PDLPs to penetration resistance 108

4.5 Materials and Methods 109
4.5.1 Biological material and cultivation 109
4.5.2 Induced resistance bioassays 109
4.5.3 Three dimensional imaging of callose papillae by confocal microscopy . 110
4.5.4 Quantification of co-localisation between PDLP1-GFP and *Hpa* conidiospores 110
4.6 Acknowledgements 111
4.7 Author Contributions 111
4.8 References 111
4.9 Supplementarl Material 115
Chapter 5: General Discussion 118
5.1 RBH and BABA share the same cellular transporter but prime different defence pathways 119
5.2 The molecular mechanisms and biological relevance of RBH-induced resistance: a known unknown 122
5.3 BABA: a natural defence priming hormone? 124
5.4 RBH- and BABA-induced stress responses 127
5.5 Future exploitation of RBH and BABA in crop protection through dual application protocols. 128
5.6 References 129

List of Figures

Figure 1.1. Conceptual model of induced resistance (IR). 4
Figure 1.2. The model of BABA perception by IBI1 and downstream signalling. 8
Figure 1.3. Molecular mechanism of β-aminobutyric acid (BABA)- and R-β-homoserine (RBH)-induced resistance (IR) in Arabidopsis. 10
Figure 2.1. Genome-wide screen for impaired *in RBH-induced immunity* (*iri*) phenotypes in and characterisation of *iri1* mutants of Arabidopsis. 24
Figure 2.2. IRI1/LHT1 controls RBH-uptake and RBH-induced resistance against *Hpa*. 27

Figure 2.3. Overexpression of *LHT1* renders Arabidopsis susceptible to growth repression by RBH, which is antagonised by co-application of L-alanine..... 29
Figure 2.4. *LHT1* controls BABA-uptake and BABA-induced resistance against *Hpa*. 31
Figure 2.5. *LHT1* controls stress tolerance to BABA. 32
Figure 2.6. Characterisation of RBH and BABA uptake kinetics by LHT1 via heterologous expression in yeast. 35
Figure 3.1. A diagram of plant sphingolipid structure. 66
Figure 3.2. The fatty acid hydroxylase FAH2 interacts with the BABA receptor IBI1. 70
Figure 3.3. *FAH2* controls both BABA-induced resistance and stress. 72
Figure 3.4. Impacts of *FAH2* and *IBI1* on the global sphingolipid profiles of Arabidopsis. 75
Figure 3.5. Genotype- and treatment-dependent accumulation of GIPC18.0/3.24.1.0 and GIPC18.0/3.24.1.1. 77
Figure 3.6. Effects of the *fah2-1* mutation on the subcellular localisation of IBI1-YFP and transcription of the *35Spro::IBI1-YFP* cassette. 79
Figure 3.7. Model of the IBI1- and FAH2-dependent role of the GIPC 18.0.3/24.1.1 in BABA-IR against Hpa. 81
Figure 4.1. β-amino acid-induced resistance against *Hyaloperonospora arabidopsidis*. 100
Figure 4.2. Role of the callose synthase PMR4 in RBH- and BABA-induced penetration resistance. 102
Figure 4.3. Role of *PDLPs* in RBH- and BABA-induced penetration resistance against *Hpa*..... 104
Figure 4.4. BABA primes early translocation of PDLP1 to germinating *Hpa* conidiospores. 106
Figure 5.1. Molecular mechanism of R-β-homoserine (RBH)- and β-aminobutyric acid (BABA)-induced resistance (IR) in Arabidopsis. 121
Figure 5.2. Chemical structure of RBH and N-acyl-homoserine lactone……123

List of Supplemental Figures

Supplemental Figure 2.1. Validation of putative iri mutants at stage 3 of the mutant screen (supports Figures 2.1). 54-55

Supplemental Figure 2.2. Characterisation of RBH-IR in SALK/SAIL lines carrying independent T-DNA insertions in the same genes that are annotated to carry T-DNA insertions in *iri2-1*, *iri3-1* and *iri4-1* (supports Figures 2.1). 56
Supplemental Figure 2.3. Genetic characterisation of two independent lht1 mutant lines and the *LHT1* overexpression line (supports Figure 2.1). 57
Supplemental Figure 2.4. Transgenic overexpression of *LHT1* improves Arabidopsis growth on medium with L-alanine as the only N source, which is antagonised by co-application of RBH (supports Figure 2.3). 58
Supplemental Figure 2.5. Comparison of growth repression by low concentrations of BABA and RBH (supports Figure 2.5). 59
Supplemental Figure 2.6. RBH and BABA compete with L-alanine for LHT1 uptake and inhibit yeast growth (Supports Figure 2.6). 60
Supplemental Figure 2.7. RBH and BABA have minimal effects on yeast growth but cannot be used as N source by yeast (supports Figure 2.6). 60
Supplemental Figure 2.8. Transformation of the yeast *22Δ10α* mutant with *LHT1* rescues uptake of L-[^{14}C] alanine (supports Figure 2.6). 61
Supplemental figure 2.9. Modeling exact inhibitor constants (Ki) of RBH and BABA (supports Figure 2.6). 61
Supplemental Figure 2.10. Induction of LHT1 expression by *Hpa* (supports Figure 2.1). 62
Supplemental Figure 3.1. Green leaf area is reduced in *fah2-1* plants (Supports Figure 3.2). 92
Supplemental Figure 3.2. Sphingolipid composition is genotype-dependent (Supports Figure 3.3). 93
Supplemental Figure 3.3. Two-way ANOVA analysis on individual sphingolipids content (Supports Figure 3.4). 94
Supplemental Figure 3.4. *IBI1* expressed less in *fah2/35Spro::IBI1-YFP* (Supports Figure 3.5). 95
Supplemental Figure 4.1. *Hpa*-induced callose depositions in Col-0 and *pmr4-1* (Supports Figure 4.2). 116
Supplemental Figure 4.2. Co-localisation of PDLP1-GFP with Hpa (Supports Figure 4.4). 116
Supplemental Figure 4.3. RBH does not prime early translocation of PDLP1 to germinating Hpa conidiospores (Supports Figure 4.4). 117

List of Supplemental Tables

Supplemental Table 2.1. Primers used for characterisation of T-DNA insertion lines. 62
Supplemental Table 3.1. Primers used in this study and their sequences 95

List of Supplemental Data Set

As the consequence of the size, the supplemental data set listed below is provided separately as an excel workbook.

Supplemental Data Set 2.1. Annotated genomic T-DNA insertions of the 108 confirmed *iri* lines, RBH-IR phenotypes, and expression profiles of the associated T-DNA-tagged genes.

Summary

Besides innate immunity, plants have acquired immunity, which is based on immune memory from prior stress exposures. This memory enables plants to respond more effectively and rapidly to subsequent pathogen attacks, forming a resistant phenotype, known as induced resistance (IR) response. Two β-amino acids, (R)-β-homoserine (RBH) and β-aminobutyric acid (BABA), act as the stress stimulus triggering IR responses. The molecular mechanisms of RBH- and BABA-IR are still not fully understood, especially in the case of RBH, whose IR potential was only recently discovered. This PhD study aims to address this knowledge gap and enhance our comprehension of β-amino acid-induced resistance.

This work first looked into the mechanisms of RBH-IR by using a forward genetic screen with Arabidopsis (*Arabidopsis thaliana*) T-DNA insertion collection for mutants impaired in RBH-induced immunity (*iri*). An amino acid transporter, LYSINE HISTIDINE TRANSPORTER 1 (LHT1), was identified from the screen. Quantifying RBH and BABA content in the *LHT1* mutant and overexpression lines and an uptake experiment with yeast expressing *LHT1* revealed it acts as the primary transporter of RBH and BABA.

Next, FATTY ACID HYDROXYLASE 2 (FAH2), an interactor of the BABA receptor, IMPAIRED IN BABA-INDUCED IMMUNITY 1 (IBI1) was investigated. Induced resistance and growth response assays showed FAH2 regulates BABA-IR and BABA-induced stress. Furthermore, sphingolipid profiling of wildtype, *ibi1-1* and *fah2-1,* singled out a glycosyl inositol phosphorylceramide which might be a potential negative regulator of BABA-IR.

Finally, this work showed that RBH-IR and BABA-IR employ different regulatory mechanisms in relation to callose-associated penetration resistance, a shared IR response between these two chemicals. While BABA relies on PLASMODESMATA-LOCATED PROTEINs (PDLPs) and the callose synthase POWDERY MILDEW RESISTANT 4 (PMR4) to enhance callose-associated resistance, RBH-induced callose augmentation involves other callose synthases beyond PMR4, and independent from PDLPs. In summary, this thesis advances the understanding of molecular mechanisms underpinning RBH-IR and BABA-IR and provides candidate genes for future breeding programs.

Chapter 1: General Introduction

1.1 Plant innate immunity: PTI and ETI

Plants, like other eukaryotes, have a specialised innate immune system that enables them to detect and react to attack by microbial pathogens. The plant's innate immune system consists of two branches of defence; the first is activated by the conserved molecular patterns from pathogens (Jones and Dangl, 2006). These conserved patterns, such as flagellin and elongation factor Tu (EF-Tu) from bacteria and chitin oligomers from fungi, are known as microbe-associated molecular patterns (MAMPs) and can be detected by pattern recognition receptors (PRRs) on the cell membrane (Chisholm et al., 2006; Choi and Klessig, 2016). Plants react to the recognition of these molecular patterns by activating pattern-triggered immunity (PTI), which involves a range of defence mechanisms, including the production of reactive oxygen species (ROS) and antimicrobial compounds, stomatal closure, deposition of callose in cell walls, and induction of defence-related genes (Bigeard et al., 2015). A successful pathogen can secrete effectors to suppress PTI and cause effector-triggered susceptibility (ETS). As an evolutionary counter-response, plants have evolved intracellular receptors that perceive these pathogen effectors and activate the second branch of the innate immune response: effector-triggered immunity (ETI). Many of these intracellular receptors are nucleotide-binding leucine-rich (NLR) repeat proteins encoded by resistance genes (Förderer et al., 2022). Recent research revealed that NLRs assemble into oligomeric complexes, also known as resistosomes, which induce defence responses and typically lead to programmed cell death (Wang et al., 2019; Ma et al., 2020).

1.2 Plant-acquired immunity: induced resistance

Genetically susceptible plants that lack high levels of innate immunity can still protect themselves against pests and diseases via acquired immunity, which is based on a form of immune memory and develops upon recovery from an environmental stress stimulus, also known as ‘priming’. This memory enables plants to have quicker and more robust immune responses toward the subsequent pathogen invasion, resulting in a so-called induced resistance (IR) response against pathogens (De Kesel et al., 2021). There are three conceptual stages to IR: ***i***) the initial stress stimulus that triggers the memory, ***ii***) a stress-free recovery period, during which the memory develops, and

iii) the expression of the augmented defence response upon secondary challenge (Fig. 1.1). Although the initial stimulus is not limited to pathogen attacks, the best-characterised form of IR is called systemic acquired resistance (SAR), during which local pathogen infection acts as the initial stress stimulus and salicylic acid (SA) and N-hydroxypipecolic acid (NHP) act as memory-inducing signals in the distal plant parts during SAR establishment (De Kesel et al., 2021; Zeier, 2021). Besides pathogens, plant growth-promoting rhizobacteria and fungi can induce resistance. This induced systemic resistance (ISR) response to root colonisation by beneficial soil microbes can be differentiated from SAR on the basis of the underpinning signalling pathways. While SAR depends on SA and NHP, jasmonic acid (JA) and ethylene (ET) signalling are typically essential to the ISR (Pieterse et al., 2014). Some non-biotic agents, such as chemicals, can serve as potent elicitors of IR. These IR agents are often MAMPs or plant stress hormones, such as SA, or artificial analogues of thereof, such as 2,6-dichloroisonicotinic acid (INA) and benzothiadiazole (BTH; Yassin et al., 2021). In addition, β-amino acids have been reported to act as powerful IR agents in plants, particularly β-aminobutyric acid (BABA) and (R)-β-homoserine (RBH; Cohen et al., 2016; Buswell et al., 2018).

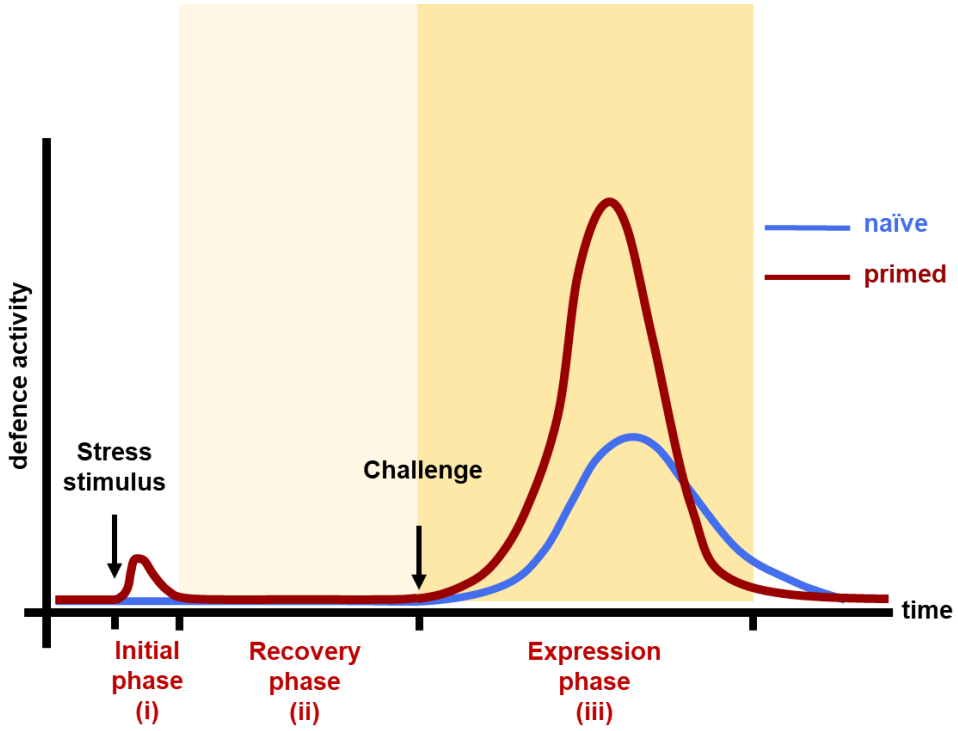

Figure 1.1. Conceptual model of induced resistance (IR). The blue and red lines represent the defence activity over time in naïve and primed plants, respectively. An IR event consists of three phases: (i) the initial phase, in which primed plants perceive stress stimuli and meagre and transient defence is triggered; (ii) the recovery phase, in which primed plants recover from the previous non-lethal event in a stress-free period and develop the stress memory; (iii) the expression phase, in which primed plants experience the second challenge while for naïve (unprimed) plants it is the first challenge. Both primed and naïve plants react to the challenge by launching defence activities, with primed plants responding faster and with more robust defence responses, known as IR than naïve plants.

1.3 BABA-induced resistance

The first record of disease suppression by BABA was published by Papavizas and Davey (1963), who showed that BABA application completely prevented root rot disease in pea by the oomycete pathogen, *Aphanomyces euteiches*, while α-aminobutyric acid only had a mild effect on disease suppression. However, it wasn't until 30 years later that Ygal Cohen (1994a, b) reported that BABA protects tomato (*Solanum lycopersicum*) and tobacco (*Nicotiana tobaccum*) against late blight and downy mildew, respectively. Since then, the resistance-inducing effects of BABA have been reported in a range of taxonomically unrelated crop species against a wide spectrum of diseases and pests (Cohen et al., 2016). For instance, BABA protects against commercially damaging plant pathogens and herbivores, such as potato late blight (Altamiranda et al., 2008), apple fire blight (Hassan and Buchenauer, 2007), pea

rust (Barilli et al., 2010a) and potato root-knot nematode (Mongae and Moleleki, 2015). Furthermore, treating harvested fruits with BABA has been reported to reduce postharvest disease incidence. For instance, BABA-treated fruits are more resistant to citrus green mould (Panebianco et al., 2014), mango anthracnose (Zhang et al., 2013) and *Rhizopus* rot (Wang et al., 2018). Remarkably, BABA-IR is not limited to biotic stress only; it can also enhance resistance against abiotic stresses, like drought (Jakab et al., 2005; Macarisin et al., 2009; Jisha and Puthur, 2016) and salt stress (Ton et al., 2005; Jisha and Puthur, 2016; Mostek et al., 2016).

1.4 BABA is an endogenous stress signal

A plausible explanation for the broad-spectrum effectiveness of BABA in plants is that it acts as an endogenous stress signal (Baccelli et al., 2017; Thevenet et al., 2017; Balmer et al., 2019). An increase in BABA has been detected in Arabidopsis after the application of both abiotic and biotic stresses. Furthermore, salt-stressed leaves from both monocot and dicot plants showed elevated concentrations, indicating that this stress-induced BABA accumulation is conserved across the plant kingdom (Thevenet et al., 2017). Further investigation of pathogen-induced BABA revealed that the plant immune system controls its accumulation, which is limited to local infection sites (Baccelli et al., 2017; Balmer et al., 2019). These findings strongly suggest that exogenous application of BABA hyperstimulates a natural and highly conserved acquired immune response in plants (Balmer et al., 2019).

1.5 BABA: a potential crop protection agent?

Over recent years, there has been increasing interest in the exploitation of BABA as a crop protection agent. Accordingly, it is relevant to know whether the mechanisms of BABA-IR in Arabidopsis are translatable to crops. In both tomato and lettuce (*Lactuca sativa*), only the R-enantiomer of BABA is effective in triggering IR (Cohen et al., 2010; Cohen et al., 2016), suggesting a similar perception mechanism. BABA potentiates SA-dependent defence and *pathogenesis-related* (*PR*) gene expression in tomato infected with *Pectobacterium carotovorum*, common bean (*Phaseolus vulgaris*) infected with *P. syringae* pv. *phaseolicola* and grapevine (*Vitis vinifera*) exposed to *Botrytis cinerea* (Farahani et al., 2016; Martinez-Aguilar et al., 2016; Wang et al., 2021).

BABA has also been reported to boost similar defences in different plant species, including callose deposition, reactive oxygen species production and lignin formation. For instance, BABA increases callose and H_2O_2 production in wheat (*Triticum aestivum*) upon inoculation with *Puccinia triticina* and in rice (*Oryza sativa L.*) upon challenge by root-knot nematodes (*Meloidogyne graminicola*; Ji et al., 2015; Bellameche et al., 2021). Furthermore, the augmented production of phenolic phytoalexins is recognised as a critical mechanism underpinning the BABA-IR mechanism, reducing the severity of pea rust causing by *Uromyces pisi* (Barilli et al., 2010b; Barilli et al., 2015).

Although BABA-IR has been described in many different plant species against a wide range of biotic and abiotic stresses, it is still rarely exploited in crop production. This is mainly due to its phytotoxicity when applied at higher concentrations (Yassin et al., 2021; Honig et al., 2023). In both Arabidopsis and tomato, relatively high concentrations of BABA repress plant growth and induce anthocyanin accumulation and chlorosis-like symptoms (Wu et al., 2010; Singh et al., 2023). BABA also delays fruit ripening in tomato and upregulates genes that are linked to abiotic stress (Wilkinson et al., 2018; Zapletalova et al., 2023).

Interestingly, in both tomato and Arabidopsis, BABA-IR and BABA-induced stress are enantiomer-specific: R-BABA provides protection but also causes stress phenotypes (Singh et al., 2023). As detailed in the below section, R-BABA is the active enantiomer that is perceived by the corresponding receptor in Arabidopsis. Thus, the beneficial IR response and unwanted stress response by BABA are likely based on a conserved perception mechanism. Understanding this mechanism can facilitate genetic strategies to uncouple BABA-IR from BABA-induced stress or chemical strategies to generate functional BABA analogues that induce resistance with less/no phytotoxicity.

1.6 IBI1: the Arabidopsis BABA receptor controlling IR and phytochemical stress via separate pathways

BABA-IR can be divided into two stages: the establishment of the primed state and the augmented defence response upon subsequent stress challenge. The first systematic studies of BABA-IR in the genetic model plant Arabidopsis revealed that BABA-primed plants show augmented activity of both SA- and ABA-dependent

pathways, depending on the challenging stress (Zimmerli et al. 2000; Ton & Mauch-Mani, 2014; Ton et al., 2005). The identification of the BABA receptor, IBI1, by Luna et al. (2014) provided a tractable system to study the perception and early signalling leading to the primed defence state. The *IBI1* gene was isolated by a screen for Arabidopsis mutants that are impaired in SA-independent BABA-induced immunity against *Hyaloperonospora arabidopsidis* (*Hpa*), named the *impaired in BABA-induced immunity 1* (*ibi1-1*) mutant. Map-based cloning revealed that the *ibi1-1* mutant carried a G to A point mutation at the first exon of an aspartyl tRNA synthetase, turning tryptophan into a premature stop codon that generates a truncated protein (Luna et al., 2014). Further computational modelling, biochemical experiments and site-directed mutagenesis provided evidence that the active R-enantiomer of BABA binds to the (L)-Asp-binding domain of the IBI1 protein (Luna et al., 2014; Buswell et al., 2018).

While binding between BABA and IBI1 triggers BABA-IR, it also blocks its canonical t-RNA synthetase activity in the cell, as evidenced by the accumulation of aspartic acid and enhanced phosphorylation of unanchored tRNA-binding EUKARYOTIC TRANSLATION INITIATION FACTOR 2 ALPHA SUBUNIT (eIF2α) in R-BABA treated plants (Luna et al., 2014; Fig. 1.2). The GENERAL CONTROL NON-DEREPRESSIBLE 2 (GCN2) pathway represents a salvation pathway, which is typically activated in response to limiting amino acid concentrations in the cell, leading to net reduction in gene translation (Lokdarshi and von Arnim, 2022). Luna et al. (2014) reported that the GCN2 pathway has a major contribution to the BABA-induced stress phenotype but also showed that it plays no role in BABA-IR, hence demonstrating that the undesirable stress response to BABA can be uncoupled from the desirable IR response to the agent.

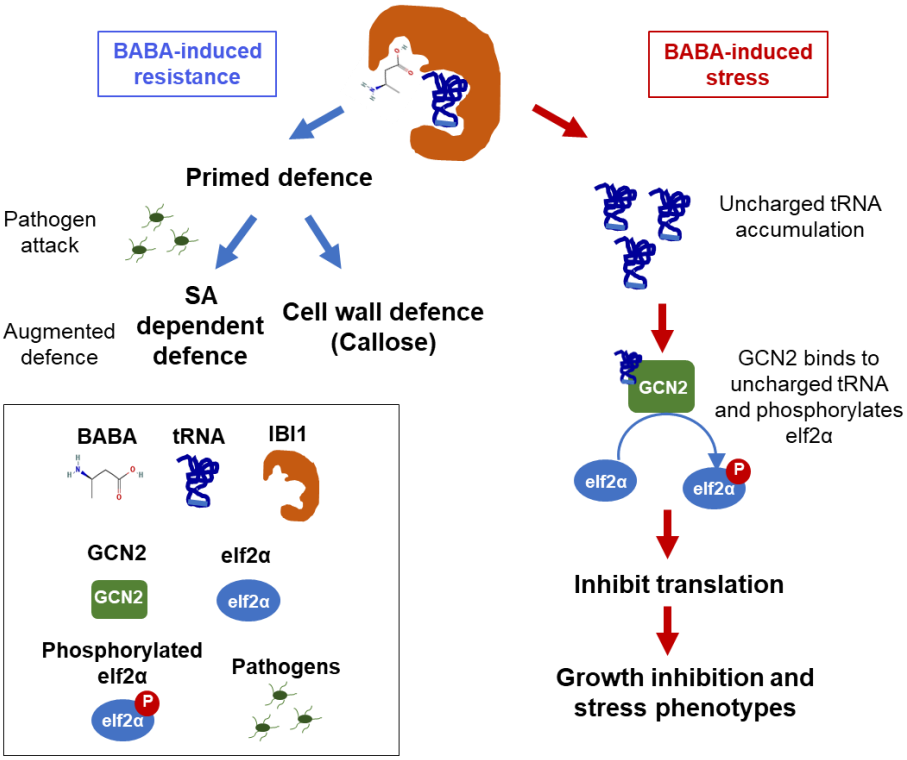

Figure 1.2. The model of BABA perception by IBI1 and downstream signalling. IBI1, a tRNA synthase, acts as the BABA receptor. BABA binding to IBI1 blocks its canonical function and initials two separated pathways. The first one is responsible for BABA-induced resistance (BABA-IR), which primes plant defence and allows augmented salicylic acid (SA) dependent and/or callose defence to be launched. The second pathway triggers BABA-induced stress. As BABA inhibits the canonical function of IBI1, uncharged tRNA accumulates in cells and binds to GENERAL CONTROL NONDEREPRESSIBLE 2 (GCN2). Following the binding between GCN2 and uncharged tRNA, GCN2 phosphorylates EUKARYOTIC TRANSLATION INITIATION FACTOR 2A (elf2α) and inhibits general translation, which leads to growth inhibition and stress phenotypes in plants.

1.7 BABA-induced changes in plant metabolic, transcriptomic and epigenetic profiles

Various metabolic increases have been reported after soil-drench plants with BABA, including amino acids, SA, SA-glucosides and metabolites belonging to the tricarboxylic acid cycle, such as citrate and fumarate (Pastor et al., 2014). BABA has also been shown to induce genome-wide changes in the transcriptome, including genes with defence-related functions against pathogens in Arabidopsis (Hegedűs et al., 2022). Similarly, genes encoding pathogen-related (PR) proteins, transcription factors, and genes involving JA and phenylpropanoid pathway metabolism were differentially expressed in rice 72 hours after BABA application (Desmedt et al., 2022).

Epigenetic changes can impact gene expression and responsiveness, and its importance in priming has been reported by various research groups (Hannan Parker et al., 2022; Harris et al., 2023). Significant increases in the acetylation at histone H3 lysine 3 and lysine 9 (H3K9K14Ac) and dimethylation at lysine 4 (H3K4Me2) at the promoter region of *PR1* and *FRK1* (*FLG22-INDUCED RECEPTOR-LIKE KINASE 1*) have been reported in BABA-treated Arabidopsis (Po-Wen et al., 2013). BABA also influences post-translational modifications to histones in crop plants: Meller et al. (2018) reported an increase of H3K4Me2 at *NONEXPRESSER OF PR GENES* 1(*NPR1*) by BABA treatment, which correlates with higher *NPR1* expression in potato (*Solanum tuberosum L.*). Besides histone modifications, BABA is also known to change DNA methylation, causing genome-wide hypo-methylation in the CHH context in tomato (Catoni et al., 2022). Interestingly, MORPHEUS' MOLECULE1 (MOM1), an essential component in RNA-directed DNA methylation (RdDM) and maintaining DNA methylation, was recently reported as a negative regulator in BABA-IR (Li et al., 2023; Miranda de la Torre et al., 2023). Hence, BABA appears to incur epigenetic changes in plants, which may contribute to the long-term priming of the agent.

1.8 Molecular and cellular mechanisms driving BABA-IR

The primed defence state is induced shortly after IBI1 binds to R-BABA. Luna et al. (2014) reported that BABA primes the pathogen-inducible trans-localisation of IBI1 from the endoplasmic reticulum (ER) membrane to the cytoplasm. It was hypothesised that the augmented cytosolic trans-localisation of IBI1 during pathogen attack of BABA-treated plants might allow it to interact with defence signalling proteins to mediate increased defence. Indeed, recent work by Schwarzenbacher et al. (2020) showed that IBI1 interacts with the cytosolic VASCULAR PLANT ONE ZINC FINGER transcription factors VOZ1 and VOZ2. Moreover, the *voz1/2* double mutant showed impaired BABA-induced priming of callose-associated penetration defence against *Hpa* (Schwarzenbacher et al., 2020). Since both VOZ1 and VOZ2 are transcriptionally responsive to ABA and repress ABA-induced expression of abiotic tolerance genes, while simultaneously promoting PTI response, Schwarzenbacher et al. (2020) concluded that the BABA-stimulated IBI1-VOZ1/2 interaction re-channels *Hpa*-induced ABA production towards defence gene expression, thereby preventing ABA-induced susceptibly and allowing for augmented PTI. Earlier studies have focused on

deciphering the defence responses, revealing that the augmented defence activity in BABA-primed plants depends on the challenging pathogen (Zimmerli et al., 2000, Ton et al. 2005). For instance, enhanced SA-dependent defences, including *PR1* expression and repression of coronatine-induced JA responses, were implicated as mechanisms contributing to BABA-IR against hemibiotrophic *Pseudomonas syringae* pv. *tomato* DC3000 in Arabidopsis (Fig. 1.3; Zimmerli et al., 2000; Tsai et al., 2011). Furthermore, BABA-IR against *Hpa*, a biotrophic oomycete, and BABA-IR against *Alternaria brassicicola*, a necrotrophic fungus, both rely largely on increased callose deposition at the cell wall (Zimmerli et al., 2000; Ton et al., 2005; Flors et al., 2008). Thus, BABA primes multiple defence pathways.

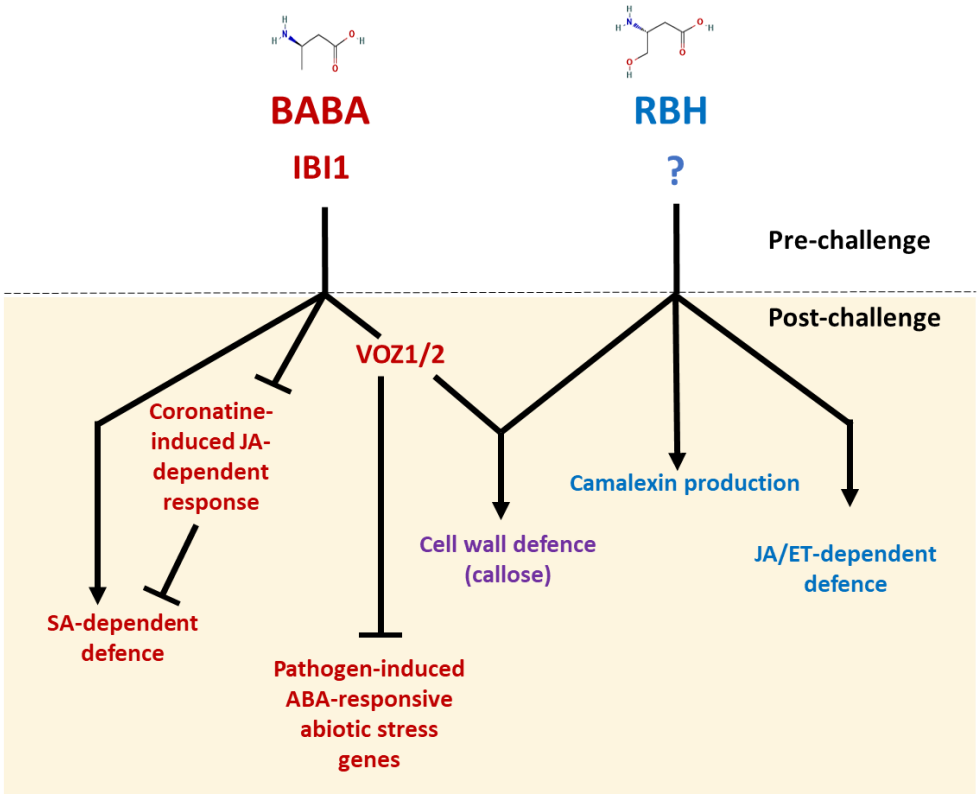

Figure 1.3. Molecular mechanism of β-aminobutyric acid (BABA)- and R-β-homoserine (RBH)-induced resistance (IR) in Arabidopsis. The IR mechanisms can be divided into two sectors: pre-challenge and post-challenge. In the pre-challenge phase, IBI1 perceives R-BABA, while the receptor for RBH is still unknown. After the pathogen challenge, BABA primes salicylic acid (SA)-dependent defence and also suppresses coronatine-induced jasmonic acid (JA)-dependent response, which can antagonise SA-dependent defence. The IBI1 interactors, VASCULAR PLANT ONE ZINC FINGER PROTEIN (VOZ) 1 and VOZ2 regulate the primed cell wall defence, callose, and also inhibit the expression of abscisic acid (ABA)-responsive abiotic stress genes, induced by pathogens. As for RBH, it enhances camalexin production and JA/ethylene (ET) dependent defence and, like BABA, augments callose.

1.9 R-β-homoserine: a structural BABA analogue that is less phytotoxic than BABA

From a screen of structural analogues of BABA for IR and stress in Arabidopsis, R-β-homoserine (RBH) emerged as a BABA analogue that induces high levels of resistance without concurrent phytotoxicity (Buswell et al., 2018). Further examination confirmed that RBH also induces stress-free resistance against *B. cinerea* in the tomato cultivar MicroTom (Buswell et al., 2018) and wild strawberry (*Fragaria vesca*; Badmi et al., 2019). Despite its structural similarity to BABA, the signalling mechanisms underpinning RBH-IR are dissimilar to BABA. This became evident by the finding that RBH elicits unaffected levels of IR against *Hpa* in the *ibi1* mutant of Arabidopsis, demonstrating that IBI1 is not required for RBH perception (Buswell et al., 2018). Also, while BABA is known to prime SA-dependent defences (Zimmlerli et al., 2000; Ton et al., 2005), RBH was found to prime JA and ethylene (ET)-dependent defence genes (Buswell et al., 2018), making it particularly effective against the necrotrophic fungus *Plectosphaerella cucumerina*. On the other hand, both RBH and BABA primed callose-related penetration defence against *Hpa*, representing a similar mechanism of IR by both agents (Fig. 1.3).

1.10 Scope of the PhD thesis

As a newly discovered IR reagent, the molecular mechanisms underpinning the perception and downstream signalling by RBH remain elusive. The work described in the second Chapter of this thesis has tried to address this knowledge gap by conducting a forward genetic screen for *impaired in RBH-immunity* (*iri*) mutants, using a genome-wide collection of fully annotated Arabidopsis T-DNA mutants. A total of 108 *iri* mutant lines were identified, showing partial or complete loss of RBH-IR. The 4 *iri* lines showing complete loss of RBH-IR were taken forward for further verification. Of these, the *iri* mutant phenotype of the *LYSINE HISTIDINE TRANSPORTER 1 (LHT1)* mutant could be confirmed by an independent T-DNA insertion in the same gene. Interestingly, the *iri1*/*lht1* mutant was also severely affected in BABA-IR to *Hpa*. Employing mass spectrometry-based quantification of RBH and BABA in leaves of wild-type, *iri1/lht1* mutant and *LHT1* overexpression lines after root application of both agents confirmed that this amino acid transporter gene acts as the primary transporter

of both β-amino acids. Induced resistance and growth responses assay in *lht1* and *35Spro: LHT1* plants furthermore revealed that LHT1 uptake activity controls the balance between IR and growth for both chemicals. Finally, this Chapter presents results on the kinetics of RBH and BABA uptake by LHT1 in transgenic yeast cells expressing *LHT1*. This analysis showed that both RBH and BABA act as competitive inhibitors of L-alanine uptake and that BABA has a slightly higher affinity toward LHT1 than RBH.

The third experimental Chapter focuses on the immediate signalling events after BABA perception by IBI1, and is based on the putative identification of FATTY ACID HYDROXYLASE 2 (FAH2) as an interactor of IBI1 (Schwarzenbacher et al. 2020). This Chapter firstly confirms the *in planta* interaction at the ER between IBI1 and FAH2 using Bimolecular Fluorescence Complementation (BiFC) and Co-immunoprecipitation (Co-IP). Furthermore, phenotypic evaluation of the *fah2-1* mutant revealed that FAH2 controls both BABA-IR and BABA-induced stress, while liquid chromatography coupled to tandem mass spectrometry profiling of wild-type, *fah2-1* and *ibi1-1* plants identified one glycosyl inositol phosphorylceramide as a potential negative regulator of BABA-IR. Finally, this Chapter has investigated the hypothesis that FAH2 controls BABA-induced priming of defence-related translocation of IBI1 from the ER to the cytosol.

Although the augmented defence responses during RBH-IR and BABA-IR differ, both chemicals prime callose-dependent penetration resistance against *Hpa* (Ton et al., 2005; Buswell et al., 2018). The fourth and final research chapter in this thesis aimed to study this aspect further by characterising the molecular and cellular components driving primed penetration resistance by RBH and BABA, using a combination of advanced light microscopy and genetic resources. Epi-fluorescence microscopy analysis revealed that only BABA-induced penetration resistance and not RBH-induced penetration resistance depends on POWDERY MILDEW RESISTANT 4 (PMR4), the main callose synthase responsible for pathogen-induced callose (Jacobs et al., 2003; Nishimura et al., 2003). A similar difference was found when analysing the role of PLASMODESMATA-LOCATED PROTEINs (PDLPs) in RBH- and BABA-IR since the *pdlp123* triple mutant was severely affected in penetration resistance by BABA but not by RBH. Further confocal scanning laser microscopy of a translational reporter line of PDLP1 revealed that BABA but not RBH primes early translocation of

PDLP1 to the sites of germinating conidiospores of *Hpa*, which precedes the augmented deposition of callose at these sites. These findings highlight that RBH-IR and BABA-IR are controlled by different pathways, which include the phenotypically similar priming of callose-associated penetration defence.

1.11 References

Altamiranda, E.A.G., Andreu, A.B., Daleo, G.R., and Olivieri, F.P. (2008). Effect of β-aminobutyric acid (BABA) on protection against *Phytophthora infestans* throughout the potato crop cycle. Australasian Plant Pathology 37, 421-427.

Baccelli, I., Glauser, G., and Mauch-Mani, B. (2017). The accumulation of β-aminobutyric acid is controlled by the plant's immune system. Planta 246, 791-796.

Badmi, R., Zhang, Y., Tengs, T., Brurberg, M.B., Krokene, P., Fossdal, C.G., Hytönen, T., and Thorstensen, T. (2019). Induced and primed defence responses of *Fragaria vescato Botrytis cinerea* infection, BioRxiv: 692491.

Balmer, A., Glauser, G., Mauch-Mani, B., and Baccelli, I. (2019). Accumulation patterns of endogenous β-aminobutyric acid during plant development and defence in *Arabidopsis thaliana*. Plant Biology 21, 318-325.

Barilli, E., Sillero, J.C., and Rubiales, D. (2010a). Induction of Systemic Acquired Resistance in Pea against Rust (*Uromyces pisi*) by Exogenous Application of Biotic and Abiotic Inducers. Journal of Phytopathology 158, 30-34.

Barilli, E., Prats, E., and Rubiales, D. (2010b). Benzothiadiazole and BABA improve resistance to *Uromyces pisi* (Pers.) Wint. in *Pisum sativum* L. with an enhancement of enzymatic activities and total phenolic content. European Journal of Plant Pathology 128, 483-493.

Barilli, E., Rubiales, D., Amalfitano, C., Evidente, A., and Prats, E. (2015). BTH and BABA induce resistance in pea against rust (*Uromyces pisi*) involving differential phytoalexin accumulation. Planta 242, 1095-1106.

Bellameche, F., Jasim, M.A., Mauch-Mani, B., and Mascher, F. (2021). Histopathological aspects of resistance in wheat to *Puccinia triticina*, induced by *Pseudomonas protegens* CHA0 and beta-aminobutyric acid. Phytopathologia Mediterranea 60, 441-453.

Bigeard, J., Colcombet, J., and Hirt, H. (2015). Signaling Mechanisms in Pattern-Triggered Immunity (PTI). Molecular Plant 8, 521-539.

Buswell, W., Schwarzenbacher, R.E., Luna, E., Sellwood, M., Chen, B., Flors, V., Pétriacq, P., and Ton, J. (2018). Chemical priming of immunity without costs to plant growth. New Phytologist 218, 1205-1216.

Catoni, M., Alvarez-Venegas, R., Worrall, D., Holroyd, G., Barraza, A., Luna, E., Ton, J., and Roberts, M.R. (2022). Long-lasting defence priming by β-aminobutyric acid in tomato is marked by genome-wide changes in DNA methylation. Frontiers in Plant Science 13, 836326.

Chisholm, S.T., Coaker, G., Day, B., and Staskawicz, B.J. (2006). Host-Microbe Interactions: Shaping the Evolution of the Plant Immune Response. Cell 124, 803-814.

Choi, H.W., and Klessig, D.F. (2016). DAMPs, MAMPs, and NAMPs in plant innate immunity. BMC Plant Biology 16, 232.

Cohen, Y. (1994a). 3-Aminobutyric acid induces systemic resistance against *Peronospore tabacina*. Physiological and Molecular Plant Pathology 44, 273-288.

Cohen, Y. (1994b). Local and Systemic Control of *Phytophthora infestans* In tomato plants By DL-3-amino-N-butanoic acids. Phytopathology 84, 55-59.

Cohen, Y., Rubin, A.E., and Kilfin, G. (2010). Mechanisms of induced resistance in lettuce against *Bremia lactucae* by DL-β-amino-butyric acid (BABA). European Journal of Plant Pathology 126, 553-573.

Cohen, Y., Vaknin, M., and Mauch-Mani, B. (2016). BABA-induced resistance: milestones along a 55-year journey. Phytoparasitica 44, 513-538.

De Kesel, J., Conrath, U., Flors, V., Luna, E., Mageroy, M.H., Mauch-Mani, B., Pastor, V., Pozo, M.J., Pieterse, C.M.J., Ton, J., and Kyndt, T. (2021). The Induced Resistance Lexicon: Do's and Don's. Trends in Plant Science 26, 685-691.

Desmedt, W., Kudjordjie, E.N., Chavan, S.N., Desmet, S., Nicolaisen, M., Vanholme, B., Vestergård, M., and Kyndt, T. (2022). Distinct chemical resistance-inducing stimuli result in common transcriptional, metabolic, and nematode community signatures in rice root and rhizosphere. Journal of Experimental Botany 73, 7564-7581.

Farahani, A.S., Taghavi, S.M., Afsharifar, A., and Niazi, A. (2016). Effect of beta-aminobutyric acid on resistance of tomato against Pectobacterium carotovorum subsp carotovorum. Journal of Plant Diseases and Protection 123, 155-161.

Flors, V., Ton, J., Van Doorn, R., Jakab, G., García-Agustín, P., and Mauch-Mani, B. (2008). Interplay between JA, SA and ABA signalling during basal and induced resistance against Pseudomonas syringae and Alternaria brassicicola. The Plant Journal 54, 81-92.

Förderer, A., Yu, D., Li, E., and Chai, J. (2022). Resistosomes at the interface of pathogens and plants. Current Opinion in Plant Biology 67, 102212.

Hannan Parker, A., Wilkinson, S.W., and Ton, J. (2022). Epigenetics: a catalyst of plant immunity against pathogens. New Phytologist 233, 66-83.

Harris, C.J., Amtmann, A., and Ton, J. (2023). Epigenetic processes in plant stress priming: Open questions and new approaches. Current Opinion in Plant Biology 75, 102432.

Hassan, M.A.E., and Buchenauer, H. (2007). Induction of resistance to fire blight in apple by acibenzolar-S-methyl and DL-3-aminobutyric acid. Journal of Plant Diseases and Protection 114, 151-158.

Hegedűs, G., Nagy, Á., Decsi, K., Kutasy, B., and Virág, E. (2022). Transcriptome datasets of β-Aminobutyric acid (BABA)-primed mono- and dicotyledonous plants, Hordeum vulgare and Arabidopsis thaliana. Data in Brief 41, 107983.

Honig, M., Roeber, V.M., Schmulling, T., and Cortleven, A. (2023). Chemical priming of plant defense responses to pathogen attacks. Frontiers in plant science 14, 1146577.

Jacobs, A.K., Lipka, V., Burton, R.A., Panstruga, R., Strizhov, N., Schulze-Lefert, P., and Fincher, G.B. (2003). An Arabidopsis callose synthase, GSL5, is required for wound and papillary callose formation. The Plant Cell 15, 2503-2513.

Jakab, G., Ton, J., Flors, V., Zimmerli, L., Métraux, J.-P., and Mauch-Mani, B. (2005). Enhancing Arabidopsis salt and drought stress tolerance by chemical priming for its abscisic acid responses. Plant Physiology 139, 267-274.

Ji, H.L., Kyndt, T., He, W., Vanholme, B., and Gheysen, G. (2015). Beta-aminobutyric acid-induced resistance against root-knot nematodes in rice is based on increased basal defense. Molecular Plant-Microbe Interactions 28, 519-533.

Jisha, K.C., and Puthur, J.T. (2016). Seed priming with BABA (β-amino butyric acid): a cost-effective method of abiotic stress tolerance in *Vigna radiata* (L.) Wilczek. Protoplasma 253, 277-289.

Jones, J.D.G., and Dangl, J.L. (2006). The plant immune system. Nature 444, 323-329.

Li, Z., Wang, M., Zhong, Z., Gallego-Bartolomé, J., Feng, S., Jami-Alahmadi, Y., Wang, X., Wohlschlegel, J., Bischof, S., Long, J.A., and Jacobsen, S.E. (2023). The MOM1 complex recruits the RdDM machinery via MORC6 to establish de novo DNA methylation. Nature Communications 14, 4135.

Lokdarshi, A., and von Arnim, A.G. (2022). Review: Emerging roles of the signaling network of the protein kinase GCN2 in the plant stress response. Plant Science 320, 111280.

Luna, E., van Hulten, M., Zhang, Y., Berkowitz, O., López, A., Pétriacq, P., Sellwood, M.A., Chen, B., Burrell, M., van de Meene, A., Pieterse, C.M.J., Flors, V., and Ton, J. (2014). Plant perception of β-aminobutyric acid is mediated by an aspartyl-tRNA synthetase. Nature Chemical Biology 10, 450-456.

Ma, S., Lapin, D., Liu, L., Sun, Y., Song, W., Zhang, X., Logemann, E., Yu, D., Wang, J., Jirschitzka, J., Han, Z., Schulze-Lefert, P., Parker, J.E., and Chai, J. (2020). Direct

pathogen-induced assembly of an NLR immune receptor complex to form a holoenzyme. Science 370, eabe3069.

MACARISIN, D., WISNIEWSKI, M.E., BASSETT, C., and THANNHAUSER, T.W. (2009). Proteomic analysis of β-aminobutyric acid priming and abscisic acid – induction of drought resistance in crabapple (*Malus pumila*): effect on general metabolism, the phenylpropanoid pathway and cell wall enzymes. Plant, Cell & Environmen 32, 1612-1631.

Martinez-Aguilar, K., Ramirez-Carrasco, G., Hernandez-Chavez, J.L., Barraza, A., and Alvarez-Venegas, R. (2016). Use of baba and ina as activators of a primed state in the common bean (*Phaseolus vulgaris* L.). Frontiers in Plant Science 7, 653.

Meller, B., Kuźnicki, D., Arasimowicz-Jelonek, M., Deckert, J., and Floryszak-Wieczorek, J. (2018). BABA-primed histone modifications in potato for intergenerational resistance to *Phytophthora infestans*. Frontiers in Plant Science 9, 1228.

Miranda de la Torre, J.O., Peppino Margutti, M.Y., Lescano López, I., Cambiagno, D.A., Alvarez, M.E., and Cecchini, N.M. (2023). The Arabidopsis chromatin regulator MOM1 is a negative component of the defense priming induced by AZA, BABA and PIP. Frontiers in Plant Science 14, 1133327.

Mongae, A., and Moleleki, L. (2015). The effect of β-aminobutyric acid (BABA) on root knot nematode and soft rot pathogen disease complexes in *Solanum tuberosum* plants. European Journal of Plant Pathology 142, 117-124.

Mostek, A., Börner, A., and Weidner, S. (2016). Comparative proteomic analysis of β-aminobutyric acid-mediated alleviation of salt stress in barley. Plant Physiology and Biochemistry 99, 150-161.

Nishimura, M.T., Stein, M., Hou, B.-H., Vogel, J.P., Edwards, H., and Somerville, S.C. (2003). Loss of a callose synthase results in salicylic acid-dependent disease resistance. Science 301, 969-972.

Panebianco, S., Vitale, A., Platania, C., Restuccia, C., Polizzi, G., and Cirvilleri, G. (2014). Postharvest efficacy of resistance inducers for the control of green mold on important Sicilian citrus varieties. Journal of Plant Diseases and Protection 121, 177-183.

Papavizas, G.C., and Davey, C.B. (1963). Effect of amino compounds and related substances lacking sulfur on *Aphanomyces* root rot of peas. Phytopathology 53, 116-122.

Pastor, V., Balmer, A., Gamir, J., Flors, V., and Mauch-Mani, B. (2014). Preparing to fight back: generation and storage of priming compounds. Frontiers in Plant Science 5, 295.

Pieterse, C.M.J., Zamioudis, C., Berendsen, R.L., Weller, D.M., Wees, S.C.M.V., and Bakker, P.A.H.M. (2014). Induced systemic resistance by beneficial microbes. Annual Review of Phytopathology 52, 347-375.

Po-Wen, C., Singh, P., and Zimmerli, L. (2013). Priming of the Arabidopsis pattern-triggered immunity response upon infection by necrotrophic *Pectobacterium carotovorum* bacteria. Molecular Plant Pathology 14, 58-70.

Schwarzenbacher, R.E., Wardell, G., Stassen, J., Guest, E., Zhang, P., Luna, E., and Ton, J. (2020). The IBI1 receptor of β-aminobutyric acid interacts with VOZ transcription factors to regulate abscisic acid signaling and callose-associated defense. Molecular Plant 13, 1455-1469.

Singh, R.R., Ameye, M., Haesaert, G., Deveux, M., Spanoghe, P., Audenaert, K., Rabasse, J.M., and Kyndt, T. (2023). Beta-Aminobutyric acid induced phytotoxicity and effectiveness against nematode is stereomer-specific and dose-dependent in tomato. Physiologia Plantarum 175, e13862.

Thevenet, D., Pastor, V., Baccelli, I., Balmer, A., Vallat, A., Neier, R., Glauser, G., and Mauch-Mani, B. (2017). The priming molecule β-aminobutyric acid is naturally present in plants and is induced by stress. New Phytologist 213, 552-559.

Ton, J., Jakab, G., Toquin, V.r., Flors, V., Iavicoli, A., Maeder, M.N., Métraux, J.-P., and Mauch-Mani, B. (2005). Dissecting the β-aminobutyric acid–induced priming phenomenon in Arabidopsis. The Plant Cell 17, 987-999.

Tsai, C.-H., Singh, P., Chen, C.-W., Thomas, J., Weber, J., Mauch-Mani, B., and Zimmerli, L. (2011). Priming for enhanced defence responses by specific inhibition of the Arabidopsis response to coronatine. The Plant Journal 65, 469-479.

Wang, J., Cao, S., Wang, L., Wang, X., Jin, P., and Zheng, Y. (2018). Effect of β-aminobutyric acid on disease resistance against *Rhizopus* rot in harvested peaches. Frontiers in Microbiology 9, 1505.

Wang, J., Wang, J., Hu, M., Wu, S., Qi, J., Wang, G., Han, Z., Qi, Y., Gao, N., Wang, H.W., Zhou, J.M., and Chai, J. (2019). Ligand-triggered allosteric ADP release primes a plant NLR complex. Science 364, eaav5868.

Wang, K.T., Li, C.H., Lei, C.Y., Zou, Y.Y., Li, Y.J., Zheng, Y.H., and Fang, Y. (2021). Dual function of VvWRKY18 transcription factor in the beta-aminobutyric acid-activated priming defense in grapes. Physiologia Plantarum 172, 1477-1492.

Wilkinson, S.W., Pastor, V., Paplauskas, S., Petriacq, P., and Luna, E. (2018). Long-lasting -aminobutyric acid-induced resistance protects tomato fruit against *Botrytis cinerea*. Plant Pathology 67, 30-41.

Wu, C.C., Singh, P., Chen, M.C., and Zimmerli, L. (2010). L-Glutamine inhibits beta-aminobutyric acid-induced stress resistance and priming in Arabidopsis. Journal of Experimental Botany 61, 995-1002.

Yassin, M., Ton, J., Rolfe, S.A., Valentine, T.A., Cromey, M., Holden, N., and Newton, A.C. (2021). The rise, fall and resurrection of chemical-induced resistance agents. Pest Management Science 77, 3900-3909.

Zapletalova, M., Rancurel, C., Industri, B., Bardin, M., Le Brigand, K., Nicot, P., Magnone, V., Seassau, A., Barbry, P., Potesil, D., Zdrahal, Z., Ponchet, M., and Lochman, J. (2023). BABA-induced pathogen resistance: a multi-omics analysis of the tomato response reveals a hyper-receptive status involving ethylene. Horticulture Research 10, uhad068.

Zeier, J. (2021). Metabolic regulation of systemic acquired resistance. Current Opinion in Plant Biology 62, 102050.

Zhang, Z., Yang, D., Yang, B., Gao, Z., Li, M., Jiang, Y., and Hu, M. (2013). β-Aminobutyric acid induces resistance of mango fruit to postharvest anthracnose caused by *Colletotrichum gloeosporioides* and enhances activity of fruit defense mechanisms. Scientia Horticulturae 160, 78-84.

Zimmerli, L., Jakab, G., Métraux, J.-P., and Mauch-Mani, B. (2000). Potentiation of pathogen-specific defense mechanisms in Arabidopsis by beta-aminobutyric acid. Proceedings of the national academy of sciences of the United States of America 97, 12920-12925.

Chapter 2: A single amino acid transporter controls the uptake of priming-inducing beta-amino acids and the associated trade-off between induced resistance and plant growth

Chia-Nan Tao[1], Will Buswell[1], Peijun Zhang[1], Heather Walker[1, 2], Irene Johnson[1], Katie Field[1], Roland Schwarzenbacher[1,3] and Jurriaan Ton[1]

[1] School of Biosciences, Institute for Sustainable Food, The University of Sheffield, Sheffield S10 2TN, United Kingdom

[2] *bi*OMICS Facility, Department of Animal and Plant Sciences, University of Sheffield, Sheffield S10 2TN, United Kingdom

[3] Present address: Department of Biosciences, Durham University, Durham, DH1 3LE, United Kingdom

The Plant Cell (2022) 34(12):4840-4856

2.1 Abstract

Selected beta-amino acids, such as beta-aminobutyric acid (BABA) and R-beta-homoserine (RBH), can prime plants for resistance against a broad spectrum of diseases. Here, we describe a genome-wide screen of fully annotated Arabidopsis T-DNA insertion lines for *impaired in RBH-induced immunity* (*iri*) mutants against the downy mildew pathogen *Hyaloperonospora arabidopsidis*, yielding 104 lines that were partially affected and four lines that were completely impaired in RBH-induced resistance. We confirmed the *iri1-1* mutant phenotype with an independent T-DNA insertion line in the same gene, encoding the high-affinity amino acid transporter LYSINE HISTIDINE TRANSPORTER 1 (LHT1). Uptake experiments with yeast cells expressing *LHT1* and mass spectrometry-based quantification of RBH and BABA in leaves of *lht1* mutant and *LHT1* overexpression lines revealed that LHT1 acts as the main transporter for cellular uptake and systemic distribution of RBH and BABA. Subsequent characterisation of *lht1* mutant and *LHT1* overexpression lines for induced resistance and growth responses revealed that the levels of LHT1-mediated uptake determine the trade-off between induced resistance and plant growth by RBH and BABA.

2.2 Introduction

The innate immune system enables plants to perceive and react to attacks by pathogens and herbivores. The basal component of this regulatory system is under the control of pattern recognition receptors (PRRs) that perceive molecular non-self-patterns from the attacker or damaged-self patterns that form during an attack (Choi and Klessig, 2016). Following recognition of these alarm signals, a signaling network is initiated that orchestrates the induction of cellular defence mechanisms, including reactive oxygen species (ROS), callose-rich cell wall depositions and the induction of defence-related genes (Chisholm et al., 2006; Bigeard et al., 2015). Besides this pattern-triggered immunity (PTI), innate immunity can be triggered by susceptibility-inducing pathogen effectors. If the challenged plant expresses a resistance (R) gene that can recognize the activity of such a pathogen effector, the innate immune response is referred to as effector-triggered immunity (ETI; Cui et al., 2015). In addition to innate immunity, plants can acquire long-lasting resistance, which develops after

recovery from biotic stress. This induced resistance (IR) is typically based on the priming of the innate immune system, which mediates a faster and/or stronger induction of inducible defences upon secondary attack (Wilkinson et al., 2019; De Kesel et al., 2021). Moreover, IR can be triggered by root colonisation of selected plant beneficial microbes or treatment with specific chemical agents, such as microbe-associated molecular patterns, volatile organic compounds and non-proteinogenic β-amino acids (Mauch-Mani et al., 2017; De Kesel et al., 2021).

β-amino butyric acid-induced resistance (BABA-IR) has emerged as a popular model system to study the molecular mechanisms controlling immune priming in plants. BABA-IR has been reported in more than 40 plant species against different types of pathogens (Cohen, 1994; Cohen et al., 2016). In Arabidopsis (*Arabidopsis thaliana*), BABA primes both salicylic acid (SA) dependent and independent defense mechanisms and protects plants against biotrophic, hemibiotrophic and necrotrophic pathogens (Zimmerli et al., 2000; Ton et al., 2005; Schwarzenbacher et al., 2020). Recent evidence suggests that BABA accumulates during exposure to biotic and abiotic stress (Thevenet et al., 2017), which provides biological relevance and supports previous evidence that an aspartyl tRNA aspartase, IMPAIRED IN BABA-INDUCED DISEASE IMMUNITY 1 (IBI1), acts as a plant receptor for BABA (Luna et al., 2014). BABA was also suggested to act as a microbial rhizosphere signal, based on the finding that induced systemic resistance (ISR) upon root colonization by *Pseudomonas simiae* WCS417 is blocked in the *ibi1-1* mutant (Luna et al., 2014). Despite the apparently high efficiency by which plant roots are capable of taking up BABA from the soil (Zimmerli et al., 2000; Ton et al., 2005), a cellular transporter for this well-known priming agent has not been identified.

Although BABA-IR is effective against a broad spectrum of plant diseases, high doses of BABA results in major growth reduction (Wu et al., 2010; Luna et al., 2014). This undesirable side effect is partly caused by disruptive binding of R-BABA to the aspartic acid-binding pocket of the IBI1 enzyme, causing the accumulation of uncharged $tRNA^{Asp}$ and GCN2 (GENERAL CONTROL NON-DEREPRESSIBLE 2)-dependent inhibition of translation (Luna et al., 2014; Buswell et al., 2018). To search for less phytotoxic IR analogs of BABA, we previously screened a small library of structurally related β-amino acids for IR activity and phytotoxicity in Arabidopsis. This screen resulted in the identification of R-β-homoserine (RBH), which induces resistance in

Arabidopsis and tomato (*Solanum lycopersicum* L.) cultivar Micro-Tom against biotrophic and necrotrophic pathogens without growth reduction (Buswell et al., 2018). A recent study comparing four IR agents for their effectiveness in strawberry (*Fragaria × ananassa*) against *Botrytis cinerea* also identified RBH as the most effective IR agent without negative effects on plant growth (Badmi et al., 2019). Like BABA, RBH primes defense activity of callose-rich papillae, which in Arabidopsis are formed at relatively early stages of infection by the biotrophic oomycete *Hyaloperonospora arabidopsidis (Hpa).* Interestingly, despite its structural similarity to BABA, RBH does not require the IBI1 receptor to induce resistance in Arabidopsis (Buswell et al., 2018). Furthermore, unlike BABA, RBH does not prime salicylic acid (SA)-dependent induction of gene expression but primes camalexin production upon infection by *Hpa* and the expression of jasmonic acid (JA)-dependent defence genes after infection by the necrotrophic fungus *Plectosphaerella cucumerina* (Zimmerli et al., 2000; Ton et al., 2005; Buswell et al., 2018). Hence, RBH-induced resistance (RBH-IR) is controlled by partially distinct pathways relative to BABA-IR. Importantly, the molecular mechanisms responsible for the uptake and perception of RBH are unknown.

In this study, we conducted a genome-wide screen of Arabidopsis T-DNA insertion mutants for *impaired in RBH-induced immunity* (*iri*) phenotypes against *Hpa*, yielding 104 and four lines that are partially and completely impaired in RBH-IR, respectively. Of the latter, we characterized the *iri1* mutant, which is affected in the high-affinity amino acid transporter LYSINE HISTIDINE TRANSPORTER 1 (LHT1). We provide evidence that the level of LHT1-mediated uptake determines the balance between IR and plant tolerance by RBH and BABA. Furthermore, mass spectrometry analysis of leaves from RBH- and BABA-treated wild-type, *lht1* mutant and *LHT1*-overexpressing plants revealed that LHT1 is critical for the uptake and systemic distribution of both RBH and BABA, while uptake experiments with *LHT1*-expressing yeast cells demonstrated that LHT1 acts as a high-affinity transporter of BABA and RBH. In support of other studies that have linked LHT1 to plant-microbe interactions and plant immunity, we conclude that LHT1 acts as a master regulator of the trade-off between growth and IR by priming-inducing beta-amino acids.

2.3 Results

2.3.1 Genome-wide screen for *impaired in RBH-immunity* (*iri*) mutants

To search for new regulatory genes of RBH-induced resistance, we screened 23,547 T-DNA insertion lines from the SALK and SAIL collections (Alonso and Ecker, 2006) for an *impaired in RBH-induced immunity* (*iri*) phenotype against *Hpa*. This set of T-DNA insertion lines covers >90% of all annotated protein-coding genes in the Arabidopsis genome. In contrast to conventional ethyl methanesulfonate (EMS)-based mutant screens, which rely on the selection of mutant phenotypes in individual plants, the collection of fully annotated homozygous T-DNA insertion mutants allowed us to screen five genetically identical seedlings per line for quantification of the *iri* mutant phenotype, including partial loss of RBH-IR. To reduce false positives, we performed the screen in three successive stages. In the first stage, we screened seedlings in 400-well trays, in which the soil was soaked to saturation with RBH to a final soil concentration of ~0.5 mM, followed by inoculation with *Hpa* conidiospores and scoring for visual sporulation at 5-7 days post inoculation (dpi; Fig. 2.1A). Each tray yielded ~1-2 lines displaying sporulation for at least two seedlings/well by 7 dpi; these lines were selected and rescreened during stage 2, using the same 400-well tray selection system. Stage 2 yielded 427 putative *iri* mutant lines (Fig. 2.1A). These putative *iri* mutant lines were taken forward for final validation in stage 3, which was based on categorical scoring of *Hpa* colonization in trypan-blue-stained leaves from control- and RBH-treated plants (0.5 mM) of each candidate line (Fig. 2.1A). To validate the statistical robustness of this screening stage, we conducted a pilot experiment that compared *Hpa* colonization between 40 pots of Col-0 seedlings pre-treated with either water or RBH (0.5 mM). Categorical scoring of trypan blue-stained leaves confirmed statistically uniform distributions of *Hpa* colonization within each treatment (Supplemental Fig. 2.1A). Of the 427 putative *iri* lines from stage 2, we confirmed 104 lines as having partially impaired RBH-IR in stage 3, as evidenced by statistically enhanced levels of *Hpa* colonization in RBH-treated mutant plants compared to RBH-treated wild-type plants, while still showing a statistically significant reduction in *Hpa* colonization by RBH treatment compared to the water controls (Fig. 2.1A, Supplemental Fig. 2.1B and Supplemental Data Set 2.1). An additional four lines, named *iri1-1* to *iri4-1*, showed a full impairment of RBH-IR, as indicated by statistically

identical levels of *Hpa* colonization between RBH- and water-treated plants within each line (Fig. 2.1A, Supplemental Fig. 2.1B and Supplemental Data Set 2.1).

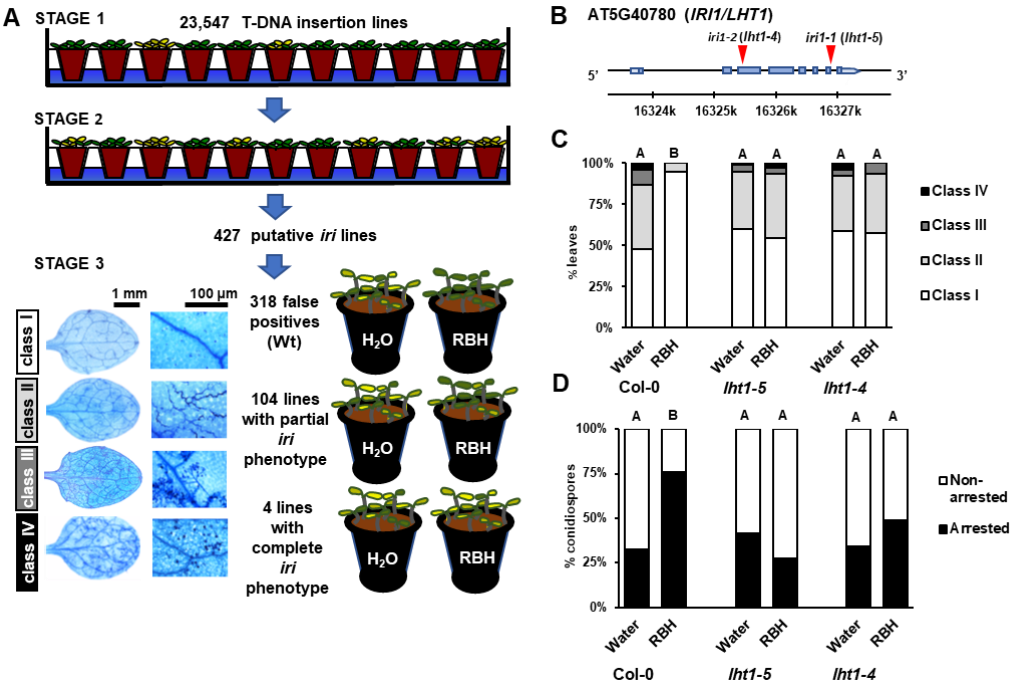

Figure 2.1. Genome-wide screen for *impaired in RBH-induced immunity* (*iri*) phenotypes in and characterisation of *iri1* mutants of Arabidopsis. (A) Scheme of the 3 successive selection stages of *iri* mutant screen of 23,547 T-DNA insertion lines from the SALK/SAIL collection. Small populations of ~5 seedlings per line were screened (stage 1) and rescreened (stage 2) for sporulation by *Hyalopoeronospora arabidopsidis* WACO9 (*Hpa*) upon soil-drenching treatment with 0.5 mM R-β-homoserine (RBH) and subsequent inoculation with *Hpa* conidionspores (top). Putative *iri* lines were validated in controlled RBH-induced resistance (RBH-IR) assays by categorising leaves from water- and RBH-treated (0.5 mM) plants into four *Hpa* colonisation classes at 5-7 days post inoculation (dpi; bottom; Supplemental Fig. 1). Photos of trypan-blue leaves on the bottom left indicate the *Hpa* colonization classes, ranging from healthy leaves (I), hyphal colonisation with without conidiospores (II), hyphal colonization with conidiophores (III) to extensive hyphal colonisation with conidiophores and deposition of sexual oospores (IV). **(B)** Gene model of the *IRI1* gene (At5g40780) encoding the Lysine Histidine Transporter1 (LHT1) protein. Red triangles indicate two independent T-DNA insertions in the *lht1-5 (iri1-1)* and *lht1-4 (iri1-2)* mutants, respectively, to confirm involvement of the *LHT1* gene in RBH-IR against *Hpa.* **(C)** Quantification of RBH-IR against *Hpa* in leaves of Col-0, *lht1-5* and *lht1-4.* Shown are frequency distributions of trypan-blue-stained leaves across the four *Hpa* colonization classes (see A). Different letters indicate statistically significant differences between samples at 6 dpi (Fisher's exact tests + Bonferonni FDR; $p < 0.05$; n = 70-80 leaves). **(D)** Quantification of arrested *Hpa* colonization by callose. *Hpa*-induced callose was analysed in aniline blue/calcofluor-stained leaves by epifluorescence microscopy. Shown are percentages of callose-arrested and non-arrested conidiospores at 3 dpi, as detailed by Schwarzenbacher et al. (2020). Different letters indicate statistically significant differences in frequencies between samples (Fisher's exact tests + Bonferoni FDR; $p < 0.05$; n > 100 conidiospores).

2.3.2 Identification of *IRI1/LHT1* as a critical regulator of RBH-IR against *Hpa*

Since SALK/SAIL lines can carry multiple T-DNA insertions and/or T-DNA-induced mutations (Alonso and Ecker, 2006), it is possible that the *iri* mutant phenotypes are caused by mutations in genes other than those identified and annotated by PCR border recovery analysis. To address this possibility, we quantified RBH-IR in independent T-DNA insertion lines in the annotated genes for each of the four complete *iri* lines (Fig. 2.1B, C and Supplemental Fig. 2.2A, B). Since RBH-IR against *Hpa* in Arabidopsis is associated with greater effectiveness of callose-rich papillae (Buswell et al., 2018), we quantified the effectiveness of callose-mediated cell wall defense at 3 dpi, as detailed previously (Schwarzenbacher et al., 2020). All original *iri* lines consistently lacked RBH-IR and concomitantly failed to augment callose-mediated defense upon RBH treatment (Fig. 2.1D, and Supplemental Fig. 2.2C), confirming the importance of this post-invasive defense barrier in RBH-IR against *Hpa*. However, independent T-DNA insertions in the annotated genes inactivated in *iri2-1*, *iri3-1* or *iri4-1* did not affect RBH-IR and showed wild-type levels of callose-mediated defense against *Hpa* (Supplemental Fig. 2.2C), indicating that their *iri* phenotypes are caused by T-DNA-induced mutations in other genes. By contrast, an independent T-DNA insertion mutant (*iri1-2*) in the annotated gene disrupted in *iri1-1* displayed a complete *iri* phenotype (Fig. 2.1B, C) and was concomitantly impaired in RBH-induced priming of callose defense (Fig. 2.1D). The *iri1-1* and *iri1-2* mutants carry a T-DNA insertion in the 5th intron and the 2nd intron of *LYSINE HISTIDINE TRANSPORTER1* (*LHT1*; At5g40780; Fig. 2.1B and Supplemental Fig. 2.3A, B), respectively. *LHT1* encodes a high-affinity amino acid transporter for acidic and neutral amino acids in roots and mesophyll cells (Chen and Bush, 1997; Hirner et al., 2006; Svennerstam et al., 2007). We will therefore refer to *IRI1* as *LHT1* hereafter.

2.3.3 LHT1 controls RBH uptake from the soil

Since LHT1 was characterized as an amino acid transporter (Chen and Bush, 1997), we hypothesized that the lack of RBH-IR in *lht1* mutants (*lht1-5*, for *iri1-1*; and *lht1-4*, for *iri1-2*) might be caused by impaired RBH uptake from the soil. To test this hypothesis, we determined RBH concentrations after saturating the soil with increasing RBH concentrations in the leaves of Col-0, *lht1-5* and a previously characterized *LHT1* overexpression line (Hirner et al., 2006; *35Spro:LHT1*), which

shows a 27-fold higher *LHT1* expression level than Col-0 plants under our experimental conditions (Supplemental Fig. 2.3C). At 2 days after soil treatment, we harvested replicate leaf tissues for RBH quantification by hydrophilic interaction liquid chromatography coupled to quadrupole time-of-flight mass spectrometry (HILIC-Q-TOF; Fig. 2.2A) or challenged the leaves with *Hpa* to quantify RBH-IR (Fig. 2.2B). The three genotypes differed statistically in their RBH shoot concentrations after soil treatment with increasing RBH concentrations, as evidenced by a highly statically significant interaction between soil treatment and genotype (two-way ANOVA; $p<0.001$; Fig. 2.2A). For both Col-0 and *35Spro:LHT1,* RBH shoot accumulation showed a dose-dependent rise with increasing RBH concentrations in the soil. The *35Spro:LHT1* seedlings accumulated statistically higher RBH concentrations in their shoots than Col-0 after saturating the soil to a final concentration of 0.15 mM or 0.5 mM RBH, whereas RBH concentrations in the shoot of *lht1-5* were hardly detectable by HILIC-Q-TOF and failed to show a dose-dependent increase with RBH soil treatment (Fig. 2.2A). The observed variation in RBH shoot concentrations correlated with RBH-IR intensity against *Hpa* (Fig. 2.2B); while RBH failed to induce statistically significant levels of resistance in *lht1-5* at all concentration tested, *35Spro:LHT1* plants showed increased levels of RBH-IR compared to Col-0 at all RBH concentrations tested. Notably, the relatively low concentration of 0.05 mM RBH failed to protect Col-0 against *Hpa* seedlings, whereas the same RBH concentration induced a statistically significant reduction in *Hpa* colonization in *35Spro:LHT1* (Fig. 2.2B). Thus, RBH uptake from the soil by LHT1 increases by overexpression of *LHT1*, which in turn boosts RBH-IR against *Hpa*.

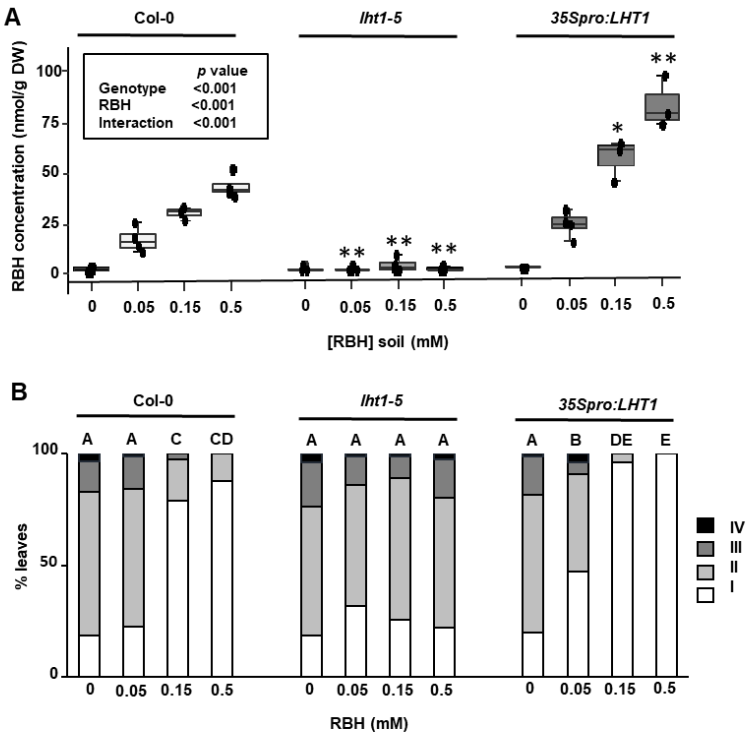

Figure 2.2. *IRI1/LHT1* controls RBH-uptake and RBH-induced resistance against *Hpa*. (A) Quantification of RBH in leaves of Col-0 (wild-type), *lht1-5 (*mutant) and *35Spro:LHT1* (over-expression) plants after soil-drench treatment with increasing RBH concentrations. Leaves were collected at 2 days after soil-drench treatment with RBH and analysed by HILIC-Q-TOF. Boxplots show median (middle bar), interquartile range (IQR; box), 1.5 x IQR (whiskers) and replication units (single dots) of leaf RBH concentrations (nmol/g DW). Inset shows *p*-values of statistically significant effects on RBH concentration by genotype, soil treatment and interaction thereof (2-way ANOVA). Asterisks indicate statistically significant differences to Col-0 for each soil treatment (Welch t-test; **: $p<0.01$; *: $0.01<p<0.05$). **(B)** Quantification of RBH-induced resistance against *Hpa* Col-0, *iri1-1/lht1-5* and *35Spro:LHT1*. Two-week-old seedlings were soil-drenched with increasing concentrations of RBH and challenge-inoculated with *Hpa* conidiospores 2 days later. Shown are frequency distributions of trypan-blue-stained leaves across four *Hpa* colonisation classes at 6 dpi (see Fig. 2.1A). Different letters indicate statistically significant differences between samples (Fisher's exact tests + Bonferroni FDR; $p < 0.05$; n = 70-90 leaves).

2.3.4 Tolerance to RBH depends on LHT1 and not on catabolism

In contrast to BABA, RBH induces resistance in Arabidopsis without concomitant growth inhibition (Buswell et al., 2018). To examine whether LHT1 controls tolerance to RBH, we quantified seedling growth of Col-0, *lht1-5*, and *35Spro:LHT1* on Murashige and Skoog (MS) agar medium. To strengthen the evidence that RBH-induced phytotoxicity in *35Spro:LHT1* depends on LHT1 uptake, we conducted this experiment in the presence of increasing concentrations of L-Ala, a high-affinity substrate of LHT1 (Hirner et al., 2006), expecting that if tolerance is controlled by LHT1-dependent uptake, the L-Ala in the medium would outcompete RBH for uptake

and antagonise RBH-induced phytotoxicity. Indeed, while green leaf areas (GLA) of Col-0 and *lht1-5* were unaffected by increasing concentrations of RBH after 1 week of growth, growth of the *35Spro:LHT1* overexpression line showed a dose-dependent repression with increasing RBH concentrations, which was antagonized by L-Ala in a dose-dependent manner (Fig. 2.3A, B). Together with our earlier finding that RBH uptake increased in the *35Spro:LHT1* line (Fig. 2.2A), these results indicate that natural tolerance of Arabidopsis to RBH (Buswell et al., 2018) is determined by RBH uptake capacity of LHT1.

To exclude a role for catabolism in RBH tolerance, we repeated the experiment on MS medium without inorganic nitrogen (N_{inorg}; NO_3^- and NH_4^+), supplemented with increasing concentrations of RBH and L-Ala. Importantly, Arabidopsis failed to grow on agar medium without N_{inorg} (Supplemental Fig. 2.4), and increasing RBH concentrations in the growth medium failed to rescue growth. Hence, Arabidopsis cannot metabolise RBH as a N source, which rules out metabolic breakdown (catabolism) as a mechanism of RBH tolerance. By contrast, increasing L-Ala concentrations added to the agar medium rescued seedling growth of all genotypes, albeit to varying degrees. While *35Spro:LHT1* seedlings showed the strongest growth response to increasing L-Ala concentrations, Col-0 displayed an intermediate growth response, followed by a relatively weak growth response in *lht1-5* (Supplemental Fig. 2.4), thus confirming the contribution of LHT1 to L-Ala uptake (Hirner et al., 2006; Svennerstam et al., 2007; Svennerstam et al., 2011). Notably, increasing RBH concentrations in the presence of L-Ala caused a dose-dependent growth reduction in *35Spro:LHT1* seedlings but not in Col-0 or *lht1-5* (Supplemental Fig. 2.4), which supports our conclusion that increased RBH uptake through *LHT1* overexpression renders Arabidopsis sensitive to RBH-induced stress due to accumulation of phytotoxic RBH concentrations that cannot be catabolised. Thus, tolerance of Arabidopsis to RBH is controlled by LHT1-dependent uptake of RBH, rather than catabolism of RBH.

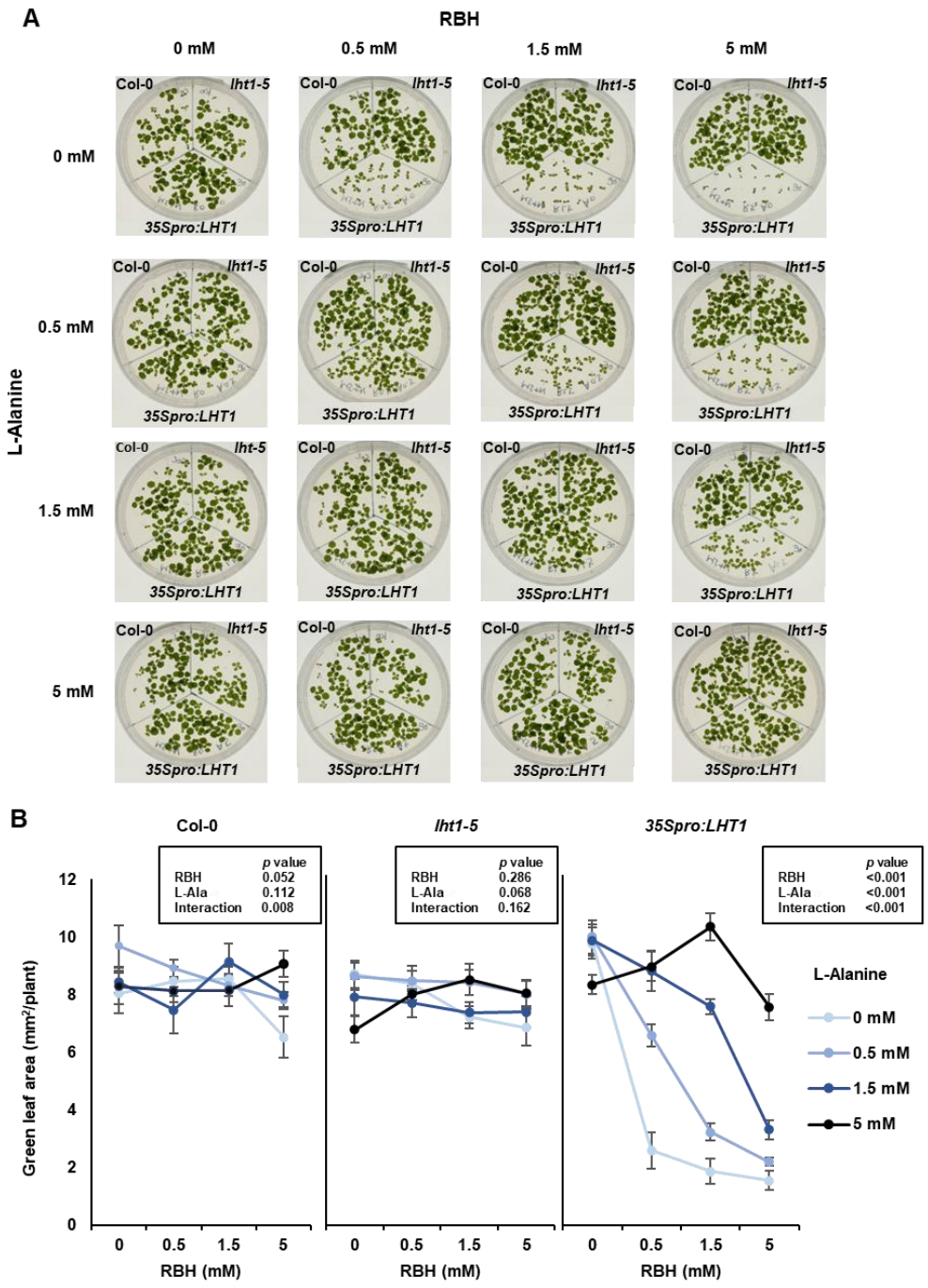

Figure 2.3. Overexpression of *LHT1* renders Arabidopsis susceptible to growth repression by RBH, which is antagonized by co-application of L-alanine. (A) *LHT1*-dependent effects of RBH and L-alanine on plant growth. Shown are 2-week-old seedlings of Col-0 (upper left), *lht1-5* (upper right), and *35Spro: LHT1* (bottom) grown on MS agar plates, supplemented with 10 mM $(NH_4)_2SO_4$ and increasing concentrations of RBH and/or L-alanine. **(B)** Quantification of green leaf area (GLA ± SEM; n=7-19) in 1-week-old Col-0, *lht1-5,* and *35Spro:LHT1* seedlings from the same experiment. Inset shows *p*-values of effects on GLA by RBH concentration, L-alanine concentration and their interaction inside each genotype (two-way ANOVA).

2.3.5 LHT1 also controls BABA uptake, BABA-IR and BABA tolerance

Given the published broad substrate range of the LHT1 transporter for acidic and neutral amino acids (Hirner et al., 2006; Svennerstam et al., 2007), we examined whether LHT1 also plays a role in the uptake of BABA. To this end, we harvested replicate shoot tissues of Col-0 and *lht1-5* seedlings to quantify *in planta* concentrations of BABA at 2 days after saturating the soil with increasing concentrations of the chemical (0, 0.025, 0.05, 0.15 and 0.5 mM), using HILIC-Q-TOF (Fig. 2.4A). While saturating the soil on which Col-0 seedlings grew with increasing BABA concentrations resulted in a dose-dependent increase of BABA concentrations in the shoot (Fig. 2.4A), a similar treatment of the *lht1-5* mutant failed to increase shoot BABA concentrations (Fig. 2.4A), indicating that BABA uptake is dependent on LHT1. To corroborate this, we saturated the soil of Col-0, *lht1-5* and *35Spro:LHT1* seedlings with increasing BABA concentrations and scored BABA-IR against *Hpa* (Fig. 2.4B). As reported previously, BABA was more efficient than RBH in protecting Col-0 against *Hpa* (Buswell et al., 2018), already reducing *Hpa* colonization at 0.025 mM BABA and reaching maximum levels of resistance at concentrations of 0.05 mM and higher (Fig. 2.4B). The *35Spro:LHT1* line showed even higher levels of resistance at 0.025 mM BABA compared to Col-0, indicating that these seedlings are sensitized to respond to BABA. By contrast, the *lht1-5* mutant was severely compromised in its effectiveness of BABA-IR, and only displayed weak levels of IR at soil BABA concentrations of 0.25 mM and 0.5 mM (Fig. 2.4B). Thus, like RBH-IR, BABA-IR depends on a functional LHT1 transporter and is enhanced by overexpression of *LHT1*.

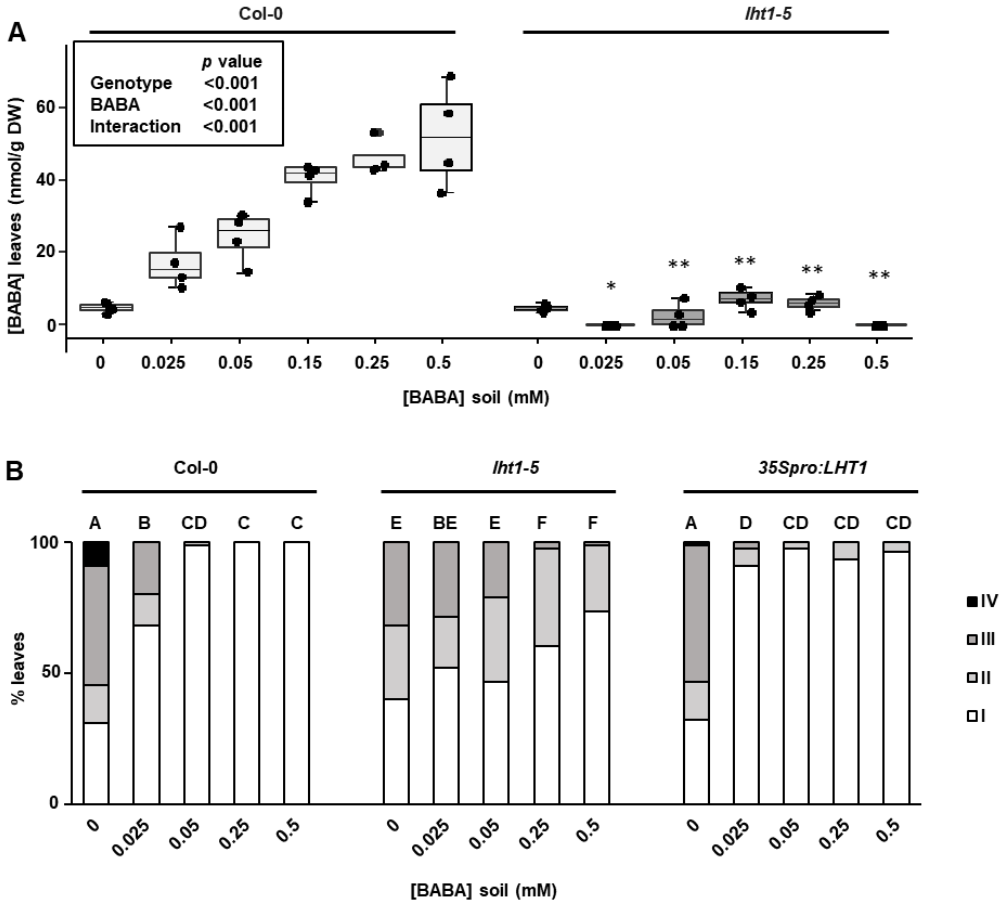

Figure 2.4. LHT1 controls BABA-uptake and BABA-induced resistance against *Hpa*. (A) Quantification of BABA in leaves of Col-0 (wild-type) and *lht1-5* (mutant) plants after soaking the soil to saturation with increasing BABA concentrations. Leaves were collected at 2 days after soil treatment and analyzed by HILIC-Q-TOF. Boxplots show median (middle bar), interquartile range (IQR; box), 1.5 x IQR (whiskers) and replication units (single dots) of leaf BABA concentrations (nmol/g DW). Inset shows *p*-values of statistically significant effects on BABA concentration by genotype, soil treatment and their interaction (two-way ANOVA). Asterisks indicate statistically significant differences to Col-0 for each soil treatment (Welch t-test; **, $p<0.01$; *, $0.01<p<0.05$). **(B)** Quantification of BABA-induced resistance against *Hpa* in Col-0, *lht1-5* and *35Spro:LHT1* seedlings. Two-week-old seedlings had the soil of their pots saturated with increasing concentrations of BABA and challenge-inoculated with *Hpa* conidiospores 2 days later. Shown are frequency distributions of trypan blue-stained leaves across four *Hpa* colonization classes at 6 dpi (see Figure 2.1A). Different letters indicate statistically significant differences between samples (Fisher's exact tests + Bonferroni FDR; $p < 0.05$; n = 70-80 leaves).

To determine whether LHT1 also controls BABA-induced phytotoxicity, we quantified the growth of Col-0, *lht1-5* and *35Spro:LHT1* seedlings growing on MS agar plates supplemented with phytotoxic concentrations of BABA. As shown in Fig. 5, GLA values of Col-0 after 1 week of growth declined with increasing BABA concentrations. This BABA-induced stress increased dramatically in *35Spro:LHT1* seedlings and decreased in *lht1-5* seedlings (Fig. 2.5A, B). The fact that *lht1-5* seedlings still showed growth repression at higher BABA concentrations suggests that additional

mechanisms contribute to BABA-induced phytotoxicity. To compare the severity of RBH- and BABA-induced phytotoxicity, we cultivated Col-0, *Iht1-5* and *35Spro:LHT1* seedlings on MS agar plates containing the same doses of RBH or BABA (0.25 mM, 0.5 mM, 1 mM or 2.5 mM). Of the three genotypes tested, only *35Spro:LHT1* seedlings were affected in growth by both chemicals at concentrations of 0.25 mM and above (Supplemental Fig. 2.5A), with BABA causing more severe growth repression than RBH (Supplemental Fig. 2.5B). Quantification of green leaf areas of *35Spro:LHT1* across all inhibitor concentrations confirmed that BABA is more potent in repressing growth than RBH (Supplemental Fig. 2.5B). Collectively, our results indicate that LHT1 is the dominant transporter for BABA uptake from the soil, controlling both BABA-IR and BABA-induced stress.

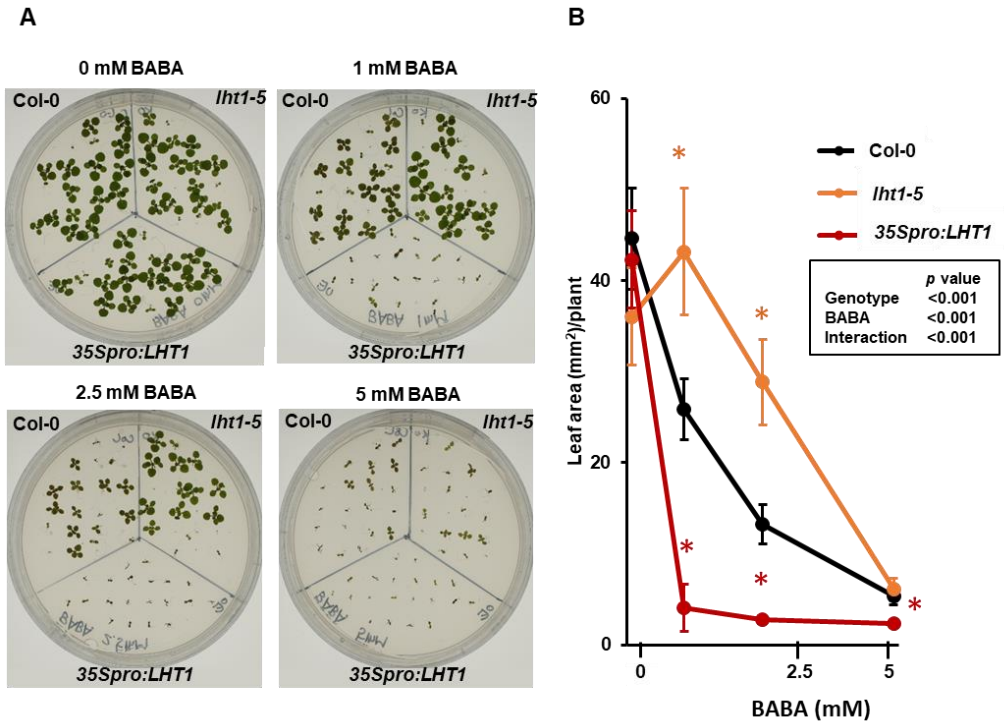

Figure 2.5. LHT1 controls stress tolerance to BABA. (A) Effects of BABA on growth by Col-0, *Iht1-5, 35Spro:LHT1* Shown are 2-week-old seedlings of Col-0 (upper left), *Iht1-5* (upper right), and *35Spro:LHT1* (bottom) grown on MS agar plates, supplemented with increasing concentrations of BABA. **(B)** Average green leaf areas (GLA ± SEM; n=14-20) of 1-week-old Col-0, *Iht1-5*, *35Spro:LHT1* plants from the same experiment. Asterisks indicate statistically significant differences compared to Col-0 at each BABA concentration (Welch t-tests + Bonferroni FDR; $p < 0.05$).

2.3.6 LHT1 transports both RBH and BABA

Having established that LHT1 is responsible for the uptake of RBH and BABA, we next examined the kinetics by which LHT1 transports these β-amino acids. To this end, we heterologously expressed the Arabidopsis *LHT1* coding sequence in the yeast (*Saccharomyces cerevisiae*) 22Δ10α strain, which lacks ten amino acid transporter genes and is completely deficient in the uptake of amino acids (Besnard et al., 2016). In contrast to empty vector (EV)-transformed 22Δ10α cells, the *LHT1*-expressing 22Δ10α strain was capable of growing on agar plates containing 1 mM L-Ala as the only nitrogen (N) source (Fig. 2.6A), while supplementing liquid growth medium without inorganic $(NH_4)_2SO_4$ with increasing L-Ala concentrations steadily improved growth by *LHT1*-expressing 22Δ10α cells (Fig. 2.6B). Increasing RBH and BABA concentrations in liquid growth medium with 1 mM L-Ala repressed growth by *LHT1*-expressing 22Δ10α cells completely (Supplemental Fig. 2.6A, B), despite the fact that both chemicals only marginally repressed 22Δ10α growth in liquid medium with 10 mM $(NH_4)_2SO_4$ as an N source (Supplemental Fig. 2.7). These results not only show that yeast fails to metabolize RBH and BABA, but they also suggest that increasing RBH and BABA concentrations outcompete L-Ala for cellular uptake.

To study the kinetics of RBH and BABA uptake, we carried out experiments with ^{14}C-labeled L-Ala in the absence and presence of RBH or BABA. To this end, we incubated EV- and *LHT1*-expressing 22Δ10α cells for 2, 5 and 10 min in buffer containing 50 µM or 500 µM L-Ala with a fixed amount of ^{14}C-L-Ala for incubation, after which we quantified cellular L-Ala uptake by ^{14}C scintillation. In contrast to EV-transformed cells, *LHT1*-expressing cells showed a linear uptake for L-Ala over time (Supplemental Fig. 2.8), confirming the functionality of the transporter in yeast. To determine whether RBH and BABA competitively inhibit the LHT1 transporter for L-Ala uptake, we incubated *LHT1*-expressing cells for 5 min in buffer containing increasing concentrations L-Ala and a fixed amount of ^{14}C- L-Ala in the presence or absence of 500 µM RBH or 500 µM BABA (Fig. 2.6C, D). Plotting the uptake velocity (V_{uptake}; fmol L-Ala/cell) against L-Ala concentration revealed a dose-dependent increase until saturation (V_{max}; Fig. 2.6C, D). Based on these data, we calculated that LHT1 has a Km value of 9.4 µM for L-Ala-uptake, which is in line with previously reported Km values for acidic and neutral amino acids (Hirner et al., 2006). Although V_{uptake} in the presence of either 500 µM RBH or 500 µM BABA decreased across a lower range L-Ala concentration, it still

reached similar V_{max} values at higher L-Ala concentrations, indicating that RBH and BABA are competitive inhibitors of L-Ala uptake by LHT1. To calculate the inhibition constants (Ki) of RBH and BABA, we conducted further uptake experiments in the presence of multiple inhibitor concentrations (0, 250, and 1,000 µM RBH/BABA) and increasing L-Ala concentrations. We generated Dixon plots of the inverse uptake velocity ($1/V_{uptake}$) against inhibitor concentration (Cornish-Bowden, 1974; Yoshino & Murakami, 2009) to determine Ki values at the intersecting lines of the different L-Ala concentrations (1, 5, 25, 50, 250 µM; Fig. 2.6E, F). Predicted intersects were called at modelled RBH/BABA concentrations that had the smallest $1/V_{uptake}$ range between the various L-Ala concentrations (Supplemental Fig. 2.9), revealing a Ki of 87.9 µM for RBH and a Ki of 68.9 µM for BABA (Fig. 2.6E, F). Hence, LHT1 is a transporter of both beta-amino acids and shows a higher affinity for BABA than for RBH.

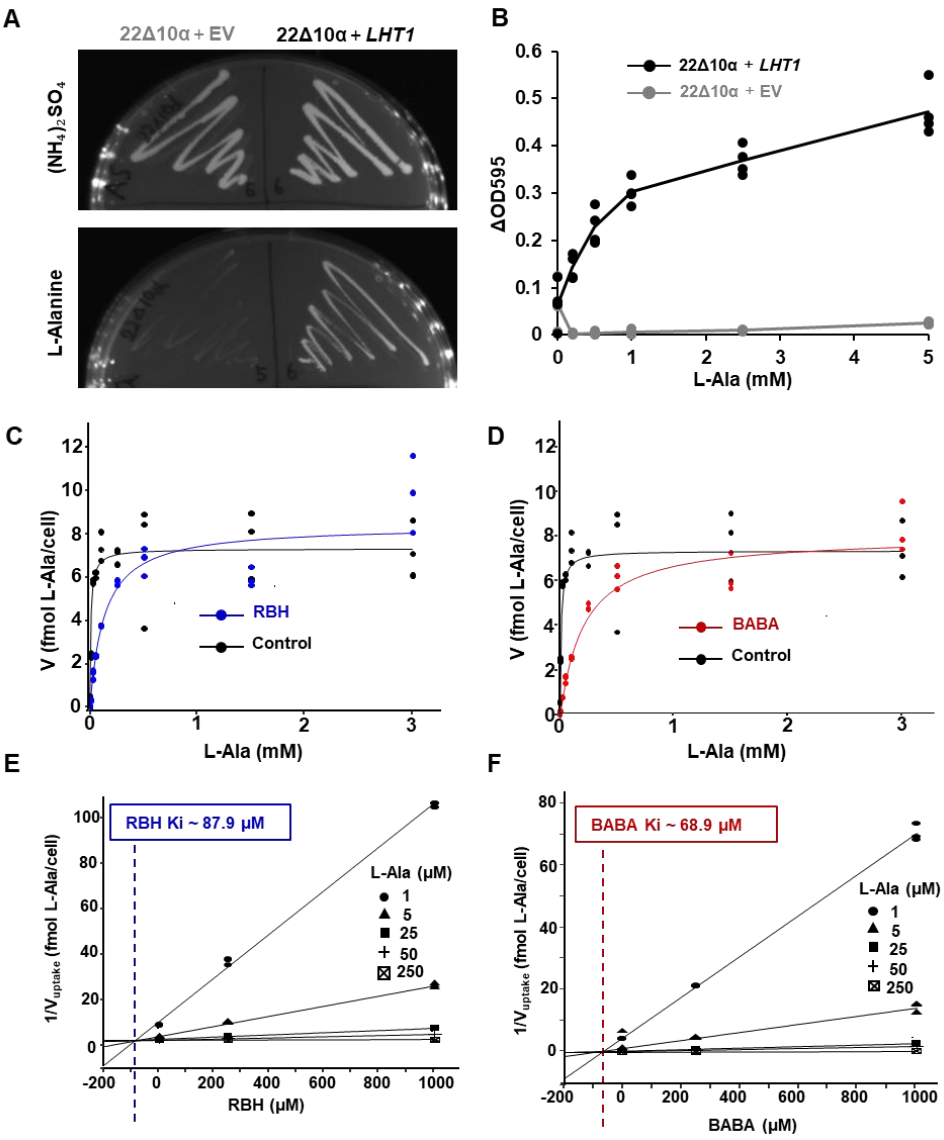

Figure 2.6. Characterization of RBH and BABA uptake kinetics by LHT1 via heterologous expression in yeast. (A, B) Transformation of the yeast mutant 22Δ10α (Besnard et al., 2016) with Arabidopsis *LHT1* rescues growth on agar (A) or liquid medium (B) with L-alanine (L-Ala) as the only nitrogen source. Shown in **(A)** are growth phenotypes of empty vector (EV)- and *LHT1*-transformed 22Δ10α cells on agar medium supplemented with inorganic nitrogen (10 mM $(NH_4)_2SO_4$; top) or 1 mM L-alanine (bottom). **(B)** Growth of EV- and *LHT1*-transformed 22Δ10α in liquid medium supplemented with increasing L-Ala concentrations. Data points and lines represent individual measurements and means of ΔOD595 values (n=4), respectively. **(C, D)** Competitive inhibition of LHT1-dependent uptake of L-Ala by RBH (**C**; blue) and BABA (**D**; red). Uptake velocities by LHT1 were determined in the presence of increasing L-Ala concentrations containing 50 nCi ^{14}C-labeled L-Ala with and without 500 µM RBH **(C)** or BABA **(D)**. Data points represent average L-Ala uptake velocities (fmol L-Ala/cell; n=3) over a 5-min time window. In the absence of RBH or BABA, the Km for L-Ala-uptake by LHT1 was 9.4 µM. Competitive inhibition by RBH and BABA is shown by a decrease in Km but not Vmax. **(E, F)** Dixon plots to determine the inhibition constants (Ki) of RBH **(E)** and BABA **(F)**. Ki values were determined in the presence of increasing L-Ala concentrations containing a fixed amount of 50 nCi ^{14}C-labeled L-Ala and 0, 250 and 1,000 µM of RBH or BABA. Data points represent mean values of inverse L-Ala uptake velocities over a 5-min time window (cell/fmol L-Ala; n=3). Dotted vertical lines indicate intercepts at Ki values of RBH and BABA (see also Supplemental Figure 2.9).

2.4 Discussion

2.4.1 Using annotated T-DNA insertion lines for a genome-saturating mutant screen

We used a genome-covering collection of Arabidopsis T-DNA insertion lines in a forward mutant screen for regulatory genes of IR. The availability of homozygous T-DNA insertions with high genomic coverage (Alonso and Ecker, 2006) facilitates a near genome-saturating screen. The use of this resource has several benefits compared to conventional mutant screens. First, the availability of T-DNA flanking sequences mapped to the Arabidopsis genome allows for immediate identification of gene candidates without having to commit to a time-consuming generation of mapping populations and linkage analysis. Second, the collection of homozygous mutant lines enables the screening of small populations that all carry the same mutant allele, which facilitates the identification of partial (leaky) mutant phenotypes, as illustrated by the identification of 104 *iri* lines that are partially affected in RBH-IR (Fig. 2.1A; Supplemental Fig. 2.1B, and Supplemental Data Set 2.1). This relatively high number of partial *iri* mutants supports the notion that IR is a highly quantitative form of resistance, relying on the additive contribution of multiple genes (Ton et al. 2006; Ahmad et al. 2010, Wilkinson et al. 2019). Thus, the within-genotype replication of this screen enables selection for genes that make a quantitative contribution to complex multigenic traits. A disadvantage of using annotated T-DNA insertion lines in a forward mutant screen is that a single T-DNA insertion line can carry multiple mutations (O'Malley et al., 2015). These mutations are not necessarily covered by the annotated T-DNA flanking sequences, since they can be caused by truncated T-DNA elements or mis-repairs of integration sites from abortive T-DNA integrations (leaving mutational footprints; Gelvin, 2021). Indeed, several other studies have reported that mutant phenotypes in this collection of T-DNA insertion lines do not always co-segregate with the annotated T-DNA insertion (De Muyt et al., 2009; Dobritsa et al., 2011; Wilson-Sánchez et al., 2014). To account for this issue, we validated the mutant phenotypes of the four complete *iri* mutants in independent T-DNA insertion lines of their disrupted annotated genes for both RBH-IR and augmented cell wall defence against *Hpa* (Fig. 2.1C, D and Supplemental Fig. 2.2). Even though the *iri* phenotypes of the four original mutant lines were robust and reproducible (Fig. 2.1C, D and Supplemental Fig. 2.2), only the phenotype of the *lht1-5* (*iri1-1*) mutant could be confirmed in an independent

T-DNA insertion line in the annotated disrupted gene. Identifying the causal mutation in the other three *iri* lines will require thermal asymmetric interlaced PCR (TAIL-PCR) to identify flanking sequences of alternative T-DNA insertions or conventional linkage analysis in segregating mapping populations.

2.4.2 The role of LHT1 in plant-biotic interactions

IRI1 encodes the broad-range amino acid transporter LHT1. Cellular transporters play important roles in the control of plant-pathogen interactions by facilitating pathogen feeding (Elashry et al., 2013; Marella et al., 2013), secretion of antibiotic compounds (Lu et al., 2015; Khare et al., 2017), transporting defense plant hormones (Serrano et al., 2013), or contributing to plant defense responses (Liu et al., 2010; Yang et al., 2014). Furthermore, the *LHT1* ortholog *LjLHT1.2* in birdsfoot trefoil (*Lotus japonicus*) is transcriptionally induced by arbuscular mycorrhizal fungi (AMF; Guether et al., 2011), suggesting that it facilitates AMF-dependent uptake of organic nitrogen. Given the role of LHT1 in IR, it is tempting to speculate that LHT1 also plays a role in mycorrhiza-IR (Cameron et al., 2013). In Arabidopsis, LHT1 has been implicated in the direct regulation of SA-dependent disease resistance. Liu et al. (2010) reported that *lht1* mutant lines had increased basal resistance against the hemibiotrophic bacterium *Pseudomonas syringae* pv. *tomato*, the hemibiotrophic fungus *Colletotrichum higginsianum*, and the biotrophic fungus *Erysiphe cichoracearum*. The study furthermore provided evidence that LHT1 controls plant immunity by cellular uptake of L-glutamine (L-Gln), which is a precursor of the redox-buffering compound glutathione. Liu et al. (2010) proposed that the lower L-Gln uptake capacity in *lht1* mutants suppresses cellular redox buffering capacity, thereby enabling augmented elicitation of ROS and SA-dependent defences upon pathogen attack. In our experiments, statistically significant differences in basal defence against the biotrophic oomycete *Hpa* between wild-type and *lht1* mutant plants was only observed once (Fig. 2.4B) while no significant difference were found in Fig. 2.1C and 2.2B, in contrast to the results shown by Liu et al. (2010). This discrepancy may be explained by the fact that we used relatively young plants (2- to 3-week-old seedlings), which do not express SA-dependent age-related resistance (ARR; Kus et al., 2002). Indeed, other studies have reported that *lht1* seedlings display normal growth phenotypes without the enhanced SA levels observed in older plants (Liu et al., 2010; Zhang et al., 2022).

Accordingly, it is possible that glutamine-dependent redox regulation contributes to age-related resistance in older plants. Since *LHT1* expression is lower in seedlings (Hirner et al., 2006), it is also possible that other amino transporters contribute to the cellular delivery of glutamine in these younger seedlings, such as AMINO ACID PERMEASE 1 (AAP1; Boorer et al., 1996) or CATIONIC AMINO ACID TRANSPORTER 8 (CAT8; Yang et al., 2010). Interestingly, in contrast to the negative role of LHT1 in innate immunity reported by Liu et al. (2010), a recent study by Yoo et al. (2020) revealed that LHT1 contributes positively to ETI-related resistance in Arabidopsis against *Pseudomonas syringae* pv. *maculicola* carrying the avirulence gene *AvrRpt2*. Moreover, Zhang et al. (2022) showed that LHT1 is the dominant transporter responsible for increased amino acid uptake during early PTI against pathogenic *Pseudomonas syringae*, when it has a positive contribution to resistance by restricting bacterial colonization. Hence, LHT1 has been reported to have both positive and negative roles in innate plant resistance. It should be noted, however, that the immune-related function of LHT1 described in our study is related to IR by priming-inducing β-amino acids, rather than innate resistance.

2.4.3 The role of LHT1 in beta-amino acid-IR

Our results have shown that LHT1 is the dominant transporter for cellular uptake of RBH and BABA from the soil (Fig. 2.2A and 2.4A). LHT1 localizes to the cell membrane (Hirner et al., 2006), which enables cellular import of RBH and BABA from the apoplast. *LHT1* is expressed in root tips, lateral roots and mature leaves (Hirner et al., 2006), enabling cellular uptake of RBH and BABA in both roots and leaves. Since *LHT1* is not expressed in the leaf vein, we propose that the activity of RBH and BABA in leaves is preceded by long-distance transport via the xylem and apoplastic distribution in the leaves. While BABA was applied exogenously in our experiments, recent studies have reported that biotic and abiotic stresses can elicit low concentrations of endogenous BABA in Arabidopsis (Thevenet et al., 2017; Balmer et al., 2019). Under these conditions, BABA only accumulates in locally stressed tissues and not systemically in non-stressed tissues (Balmer et al., 2019), indicating that stress-induced accumulation of BABA does not contribute to systemic defense signaling. Although the biosynthesis pathway of stress-induced BABA remains unknown, it seems plausible that this local biosynthesis occurs inside the cell. The Ki

values of RBH (87.9 µM) and BABA (68.9 µM) indicate that these beta amino acids have marginally lower affinities for LHT1 than endogenous alpha-amino acids (Hirner et al., 2006). Since alpha-amino acids typically reach apoplastic concentrations between 1 µM to 10 µM (Zhang et al., 2022), it would be difficult for BABA to compete with these substrates. Moreover, *Hpa*-induced BABA concentrations do not exceed 25 ng/g fresh weight (242.7 nM; Thevenet et al. 2017), which seems too low to be a competitive substrate for LHT1. Hence, cellular uptake of BABA by LHT1 does not appear to play a major role in *Hpa*-induced BABA accumulation, which would also explain why the *lht1* mutant and *35Spro:LHT1* overexpression lines were not majorly affected in basal resistance to *Hpa* (Fig. 2.2B). Nevertheless, we cannot exclude that *Hpa* locally induces much higher BABA concentrations in the cells directly interacting with the parasite, and that LHT1 plays a role in countering diffusion of this intracellular BABA into the apoplast. In this context, it is interesting to note that *Hpa* infection induces *LHT1* expression (Sonawala et al. 2018; Supplemental Fig. S10), which could play a role in upholding defense-inducing intracellular concentrations of BABA in *Hpa*-challenged cells and would also explain why stress-induced BABA is not distributed systemically (Balmer et al. 2019).

While our results provide strong evidence that LHT1 is the dominant transporter for the uptake of RBH and BABA (Fig. 2.2-6), they do not necessarily mean that the contribution of LHT1 to RBH-IR or BABA-IR solely depends on its uptake activity. For instance, while treatment with 0.05 mM RBH resulted in similar foliar concentrations in both *35Spro:LHT1* and wild-type plants (Fig. 2.2A), this relatively low RBH concentration only triggered a significant IR response in *35Spro:LHT1* plants and not in wild-type plants. This uncoupling of RBH concentration from IR suggests that the function of LHT1 in RBH-IR may involve an additional defense signaling activity that becomes active at low RBH concentrations. Such a transporter-receptor co-functionality (transceptor activity) has been reported for NITRATE TRANSPORTER 1.1 (NRT1.1) for nitrate uptake and signaling. Replacing Pro-492 with Leu-492 in NRT1.1 disabled the nitrate transport activity of this protein but not its ability to induce *NRT2.1* expression (Ho et al., 2009), which is a nitrate-responsive gene that has concomitantly been linked to the regulation of disease resistance (Camanes et al., 2012). Although no amino acid transporters have been reported with receptor co-functionality (Dinkeloo et al., 2018), it is tempting to speculate that LHT1 might act as

a transceptor of β-amino acids. Site-directed mutagenesis of LHT1 and testing whether its RBH and BABA transport activity can be uncoupled from its role in RBH-IR and BABA-IR would be required to test this attractive hypothesis.

Since the *lht1* mutant still displayed residual levels of BABA-IR and BABA-induced stress after treatment with high BABA doses (Fig. 2.4B, 2.5B), we cannot exclude the possibility that other amino acid transporters have a minor contribution to BABA uptake. A recent study reported that LHT2 has a similar substrate specificity as LHT1, including several D-amino acids and 1-aminocyclopropane-1-carboxylate (ACC; Choi et al., 2019), and could thus have a complementary contribution to BABA uptake.

2.4.4 RBH and BABA compete with proteinogenic amino acids for uptake by LHT1

We used *LHT1*-expressing yeast cells to assess competitive inhibition of L-Ala uptake by RBH and BABA. Our uptake assays revealed a Km for LHT1 of 9.4 µM for L-Ala (Fig. 2.6C), which supports previously reported Km values of LHT1 for proteinogenic amino acids (Hirner et al., 2006). Furthermore, the inhibitory kinetics of RBH or BABA on L-Ala uptake confirmed competitive inhibition, as evidenced by the fact that L-Ala uptake in the presence of RBH or BABA still reached maximum velocities at higher L-Ala concentrations (Fig. 2.6C, D). Of the two beta-amino acids, BABA had a lower Ki than RBH (68.9 µM vs 87.9 µM), suggesting that LHT1 has a higher affinity for BABA than RBH (Fig. 2.6E, F). This difference in affinity is consistent with our observation that BABA has a stronger inhibitory effect on growth of *35Spro:LHT1* than RBH (Supplemental Fig. 2.5). Since the affinity of LHT1 has been reported to be similar or higher for a range of acidic and neutral amino acids, including L-Gln (Hirner et al., 2006; Svennerstam et al., 2007), our results also explain previous findings by Wu et al. (2010), who showed that BABA-induced phytotoxicity in Arabidopsis can be alleviated by co-application with L-Gln.

2.4.5 LHT1: not just a transporter for proteinogenic amino acids

Although LHT1 was initially identified as a transporter for proteinogenic amino acids (Chen and Bush, 1997), subsequent studies have shown that it transports a much wider range for non-proteinogenic amino acids, such as the ethylene precursor ACC

(Shin et al., 2015) and xenobiotic amino acid conjugates (Chen et al., 2018; Jiang et al., 2018). Consistent with this broad-spectrum uptake activity, we showed that LHT1 is the main transporter of the β-amino acids RBH and BABA. Of particular interest is the regulatory function of LHT1 in the trade-off between beta-amino acid-IR and plant growth. For BABA, overexpression of *LHT1* in Arabidopsis increased BABA-IR at the relatively low concentration of 0.025 mM BABA (Fig. 2.4B) but it also dramatically increased plant sensitivity to BABA-induced growth repression (Fig. 2.5A, B and Supplemental Fig. 2.5A, B). However, RBH elicited high levels of IR in wild-type plants at soil concentrations of 0.15 mM RBH and above (Fig. 2.2B) but did not repress growth across all concentrations tested (Fig. 2.3A, B), supporting our earlier conclusion that RBH induces disease resistance without costs on plant growth (Buswell et al. 2018). Interestingly, *35Spro:LHT1* overexpression plants increased the level of IR at relatively low RBH concentrations (Fig. 2.2B), but also repressed growth in a dose-dependent manner (Fig. 2.3A, B and Supplemental Fig. 2.5A, B). Direct comparison of RBH- and BABA-induced growth repression in *35Spro:LHT1* plants confirmed that BABA is more active than RBH (Supplemental Fig. 2.5B), which is also apparent from the IR response (Fig. 2.2B, 2.4B). It is worth noting that the molecular mechanisms of RBH-induced stress remain unclear, and its lower toxicity in plants might come from a combination of uptake and intracellular modes of action.

The observed trade-offs between beta-amino acid-IR and plant growth reveal two important conclusions. First, like BABA, RBH can repress plant growth, but this phytotoxicity depends on LHT1-dependent uptake capacity rather than RBH catabolism. Second, our results show that the trade-off between beta-amino acid-IR and growth can be optimized in favor of the IR response by manipulating the *LHT1* gene. This conclusion holds major translational value for breeding programs aiming to exploit BABA-IR in vegetable crops that are protected by BABA but also suffer from BABA-induced phytotoxicity (Cohen et al., 2016; Yassin et al., 2021).

2.5 Methods

2.5.1 Biological material

All Arabidopsis (*Arabidopsis thaliana*) genotypes were in accession Columbia-0 (Col-0). The *iri1-1* mutant (*lht1-5*) and *iri1-2* mutant (*lht1-4*) were described previously by Svennerstam et al. (2007) and Liu et al. (2010); the *35Spro: LHT1* overexpression lines were described by Hirner et al. (2006). The *iri* mutant screen was performed with fully annotated T-DNA insertion lines from the SALK and SAIL collections (Alonso *et al.*, 2003) and purchased from the Nottingham Arabidopsis Stock Centre (sets N27941, N27951, N27942, N27943, N27944, N27945). The annotated T-DNA insertions in *iri1-1* (SALK_115555), *iri1-2* (SALK_036871), *iri2-1* (SALK_204380), SAIL_902_B08, *iri3-1* (SALK_118654), SALK_078838, *iri4-1* (SALK_076708) and SALK_046376 were confirmed by PCR before further testing (Supplemental Table 2.1), as described below. *Hyaloperonospora arabidopsidis* strain WACO9 was maintained in its asexual cycle by alternate conidiospore inoculations of Col-0 and Ws NahG plants.

2.5.2 Plant growth conditions

For soil-based IR experiments, seeds were sown in a 2:1 (v/v) Scott's Levington M3 compost/sand mixture and stratified for 2-4 days in the dark at 4°C. Plants were subsequently cultivated under short-day conditions (8-h light; Sylvania GroLux T8 36W or Valoya NS1 LED); 150 µmol photons m^{-2} s^{-1}; 21°C; and 16-h dark; 18°C) with a ~60% relative humidity (RH). Plants for seed propagation were grown in long-day growth conditions (16-h light; Sylvania GroLux T8 36W); 150 µmol photons m^{-2} s^{-1}; 21°C; and 8-h dark; 18°C) with ~60% RH. For plate assays, seeds were surface sterilized (vapor-phase sterilization method) prior to sowing on half-strength Murashige and Skoog (MS) medium (pH = 5.7 and 1% sucrose), solidified with 1.5% agar (w/v).

2.5.3 Mutant screen

Approximately 10-15 seeds for each seed line were sown in individual wells of 400-well trays (Teku JP 3050/230 H). Each tray was filled with ~2.4 L of compost/sand mixture. After sowing, stratification of seeds and seed germination, seedlings were thinned to five seedlings/well. Two-week-old seedlings were treated with RBH by watering each tray with 1.5 L of 2x concentrated RBH solution (1 mM), which was left

overnight to saturate the soil. Excess RBH solution (~300 mL) was removed the next morning, resulting in a final soil concentration of ~0.5 mM RBH. Challenge inoculation was performed at 2 days after RBH treatment by spraying seedlings with a suspension of *Hpa* conidiospores (10^5 spores/mL). Trays were sealed with clingfilm after inoculation to maintain 100% RH and promote infection. To verify RBH-IR, each tray contained three randomly distributed wells with Col-0 seedlings. Furthermore, to verify favorable conditions for *Hpa* disease, three additional wells with Col-0 seedlings were cut out from each tray and left outside during RBH-uptake to prevent RBH-IR prior to inoculation. At 5-7 dpi, trays were visually inspected for *Hpa* sporulation when sporulation on Col-0 seedlings in the untreated wells of the tray became apparent. Lines developing sporulation within 7 dpi were scored as stage 1 *impaired in RBH-induced-immunity* (S1 *iri*) lines, while nongerminated lines were scored as stage 1 nongerminated (S1 *ug*). All S1 *iri* and S1 *ug* lines were pooled for the stage 2 screen in 400-well trays, as described above. S1 *iri* lines allowing visible sporulation in two screens time were scored as Stage 2 *iri* (S2 *iri*). S1 *ug* lines that germinated upon rescreening and showed sporulation were re-tested for S2 *iri* phenotypes. Of the 26,631 T-DNA insertion lines, 23,547 lines germinated and could be screened for *iri* mutant phenotypes. The 427 putative *iri1* lines selected after stage 2 were pooled for seed bulking and validated by controlled IR assays in stage 3 (S3) of the screen, as described below.

2.5.4 Induced resistance (IR) assays

Two-week-old seedlings were grown in 60-mL pots, after which the soil was saturated with water, *(R)*-β-homoserine (Sigma-Aldrich; #03694), or R/S-BABA (Sigma-Aldrich, #A44207) to the indicated concentrations, as described previously (Buswell et al., 2018). Two days after chemical treatment, seedlings were spray-inoculated with a suspension of *Hpa* conidiospores (10^5 spores/mL) and maintained in 100% RH to promote infection. Leaves were collected at 6-7 dpi for trypan blue staining for microscopy scoring of *Hpa* colonization by categorizing them into four classes, ranging from healthy leaves (I) to heavily colonized leaves (IV), as described in detail by Schwarzenbacher et al. (2020). To investigate augmented induction of cell wall defense by chemical priming treatment, leaves were harvested at 3 dpi for aniline blue/calcofluor staining and analysis by epifluorescence microscopy (Leica DM6B;

light source: CoolLED pE-2; 365 nm excitation filter, L 425 nm emission filter, 400 nm dichroic filter). For each genotype/treatment combination, germinated coniodiospores on 10 leaves from independent seedlings were scored either as arrested (spores or germ tubes fully encased in callose), or non-arrested by callose depositions (no callose or lateral callose deposition along the germ tube/hyphae), as detailed by Schwarzenbacher *et al.* (2020). Statistical differences in in *Hpa* colonization or callose defense were analyzed by pairwise Fisher's exact tests, using R software (v 3.5.1). For multiple comparisons, an additional Bonferroni multiple correction was applied, using the R package 'fifer' (fifer_1.1.tar.gz).

2.5.5 Plant growth assays

Surface-sterilized seeds were sown onto half-strength MS agar plates and cultivated for 2 weeks under standard plant growth conditions, as indicated above. Photographs were taken after 1 and 2 weeks of growth with a Nikon D5300 digital camera. Green leaf areas (GLA) were quantified from digital photographs of 1- or 2-week-old seedlings, using Fiji/ImageJ software (Rueden et al., 2017). Statistical differences in the natural logarithm of (1+GLA) were analyzed by two-way ANOVA, using R software (v 3.5.1).

2.5.6 Genotyping verification by PCR and gene expression analysis by reverse transcription quantitative PCR (RT-qPCR)

Genomic T-DNA insertions of all *iri1, iri2, iri3 and iri4* lines were confirmed by PCR using LP+RP and LBb1.3/ LB3+RP primers (Supplemental Table S2) To quantify *LHT1* expression levels by RT-qPCR, shoot tissues from five 2-week-old seedlings were collected and combined as one biological replicate. A total of five replicates were collected at the same time and snap-frozen in liquid nitrogen and homogenized. Total RNA was extracted using an RNeasy Plant Mini Kit (Qiagen, cat. no. 74904) and first-strand cDNA was synthesized from 800 ng total RNA using a Maxima First Strand cDNA Synthesis Kit (Thermo Fisher, cat. no. K1641). The cDNA was diluted 20 times in nuclease-free water before qPCR. All qPCR reactions were performed with 2 µL diluted cDNA and primer concentrations at a final concentration of 250 nM in a Rotor-Gene Q real-time PCR cycler (Qiagen, Q-Rex v1.0), using a Rotor-Gene SYBR Green

PCR Kit (Qiagen, cat. no. 204074). The qPCR amplification of *LHT1* was performed with gene-specific primers (FP: ATCTCCGGCGTTTCTCTTGCTG, RP: GCCCATGCGATTGTTGAGTAGCTG) and normalized to the transcript levels of two housekeeping genes (At1g13440 [*GLYCERALDEHYDE-3-PHOSPHATE DEHYDROGENASE C2*, *GAPC2*], and At2g28390 [*MONENSIN SENSITIVITY 1*, *MON1*]), as detailed previously (Schwarzenbacher et al., 2020).

2.5.7 Quantification of *in planta* RBH and BABA concentrations by hydrophilic interaction liquid chromatography coupled to quadrupole time-of-flight mass spectrometry

Shoot tissues were collected at 2 days after soil-drenching and divided into four replicate tubes per treatment (five plants per tube, from separate trays), frozen at –80°C, freeze-dried and weighed. Dry tissue was crushed and extracted into 1 mL of cold extraction buffer (methanol: water: formic acid, 10:89.99:0.01, v/v/v). Extracts were centrifuged at 16,000 g for 5 min at 4℃, after which each supernatant was divided between three aliquots. RBH and BABA standards were prepared as individual standards from 0.1 to 100 µM. Separation was performed with a Waters Acquity HILIC BEH C18 analytical column, 1.7-mm particle size, 2.1 x 50 mm. The mobile phase was 20 mM ammonium formate with 0.1% (v/v) formic acid (A) and acetonitrile with 0.1% (v/v) formic acid (B). The gradient started at 99% (v/v) A and reached 65% (v/v) A in 4 min. The gradient changed to 1% (v/v) A up to 6 min and was held there for 1.5 min and then returned to initial conditions. The solvent flow rate was 0.3 mL min^{-1}, with an injection volume of 4 µL. Mass spectra were recorded in positive electro-spray ionization mode, using a Waters UPLC system interfaced to a Waters quadrupole time-of-flight mass spectrometer (Q-TOF; G2Si Synapt). Nitrogen was used as the drying and nebulizing gas. Desolvation gas flow was adjusted to approximately 150 L/h and the cone gas flow was set to 20 L/h with a cone voltage of 5 V and a capillary voltage of 2.5 kV. The nitrogen desolvation temperature was 280°C and the source temperature was 100°C. The instrument was calibrated in 20-1,200 m/z range with a sodium formate solution. Leucine enkephalin (Sigma-Aldrich, St. Louis MO, USA) in methanol: water (50:50, v/v) with 0.1% (v/v) formic acid was simultaneously introduced into the qTOF instrument via the lock-spray needle for recalibrating the *m/z* axis. Quantification of amino acids in tissues was based on the standard curves, using

MassLynx v4.1 software (Waters, Elstree UK). Amino acids identities were confirmed by co-elution of product fragment ions with parent ions and matching peak retention times to individual amino acid standards. Statistical differences in RBH and BABA between genotypes and soil-drench treatments were tested by two-way ANOVA followed by Welch t-tests to test cross-genotype differences at each RBH/BABA concentration, using R software (v 3.5.1).

2.5.8 Yeast transformation

The *LHT1* (At5g40780) coding sequence with stop codon was amplified from wild-type Col-0 cDNA with Phusion High-Fidelity DNA Polymerase (New England Biolabs, #M0530L) and cloned into the pENTR plasmid (Invitrogen). *LHT1* was then subcloned into pDR196 (Meyer et al., 2006) by restriction (EcoRI and XhoI) and ligation **(**T4 DNA ligase). Empty vector (EV)- and *LHT1*-harboring plasmids were confirmed by Sanger sequencing and introduced into competent cells of the 22Δ10α strain (Besnard et al., 2016), using heat shock transformation (Gietz and Schiestl, 2007).

2.5.9 Yeast growth assays

To assess the growth of *LHT1*- and EV-transformed 22Δ10α yeast strains, cells were first cultivated in liquid Yeast Nitrogen Base (YNB) medium (Alfa Aesar, #H26271, without amino acids and ammonium sulfate) supplemented with 10 mM ammonium sulfate at 30℃ and 220 rpm for 2 days. Cells were washed by centrifugation at room temperature (3,000 g; 5 min) and resuspended in distilled water to an OD_{600} of 0.3-0.5. To assess whether yeast can metabolize RBH and BABA, 5 µL of the cell suspension was added to 2 mL Yeast Nitrogen Base and increasing concentrations of RBH or BABA (0.2–5 mM). To assess toxicity of RBH and BABA, 5 uL of the suspension was added to 2 mL YNB medium with 10 mM ammonium sulfate and increasing concentrations of RBH or BABA (0.2–5 mM). To assess competition between L-Ala and RBH or BABA, 5 µL of the suspension was added to 2 mL YNB medium supplemented with 1 mM L-Ala and increasing concentrations of RBH or BABA (0.2–5 mM). cultures were incubated at 30℃ with 220 rpm shaking for 3 days, after which the OD_{595} was determined in a plate reader (FLUOstar OPTIMA; BMG LABTECH; Germany).

2.5.10 Assessment of uptake and inhibition kinetics of LHT1 in yeast

Transformed 22Δ10α cells were grown in YNB medium supplemented with 10 mM $(NH_4)_2SO_4$ at 30℃ with shaking at 220 rpm for 2 days. Yeast cells were collected by centrifugation at room temperature (3000 g; 5 min), washed in distilled water, and resuspended in ice-cold washing buffer (0.6 M sorbitol, 50 mM sodium phosphate, pH 4.5) to OD_{600} of 5. Before the uptake assay, cells were energized by adding 1 M glucose (final concentration 50 mM) to the growth medium for 10 min. To assess time-dependent uptake of L-[^{14}C] Ala in EV- and *LHT1*-transformed cells (Supplemental Fig. S6), 1.5-mL of the energized cell culture was added to 1.5 mL uptake buffer, containing 50 nCi L-[^{14}C]Ala (158 mCi/mmol; Perkin Elmer; NEC856) with unlabeled L-Ala (50 or 500 µM). After 2, 5 or 10 min of incubation in a thermomixer (Grant bio ES-20; Grant Instruments; UK; 30℃, 220 rpm), the cell suspensions were mixed with 2 mL ice-cold water and kept on ice to inhibit L-Ala uptake. Cells were then centrifuged (3000 g; 5 min; 4°C) and washed four times with 2 mL ice-cold water, after which pellets were stored at –20°C for quantification of radioactivity the following day. To determine uptake and inhibition kinetics (Fig. 2.6C,D), *LHT1*-transformed cells were incubated in the same uptake medium, containing 50 nCi L-[^{14}C] Ala with increasing concentrations (1–3,000 µM) of unlabeled L-Ala and/or 500 µM inhibitory RBH or BABA. After 5 min of incubation, cells were washed, collected, and stored as described above. To assess radioactivity, frozen pellets were resuspended in 750 µL distilled water, from which 200 µL was loaded onto Combusto-Pads (Perkin Elmer, part number 5067034) and combusted in a sample oxidizer (Model 307 Sample Oxidizer; Perkin Elmer; USA). Trapped $^{14}CO_2$ was quantified by liquid scintillation counting (Tri-Carb 3100TR; Perkin Elmer; USA). L-Ala uptake velocities over the 5-min time window (V_{uptake}) were expressed as fmol L-Ala/cell and plotted against the L-Ala concentration, using the R package drc (Ritz et al., 2015) to determine the kinetics of L-Ala uptake in the absence and presence of RBH or BABA.

To estimate inhibition constants (Ki) of RBH and BABA (Fig. 2.6E,F), L-Ala uptake velocities were determined in the presence of 0, 250 and 1,000 µM RBH or BABA, using a medium containing increasing concentrations of L-Ala (1, 5, 25, 50, 250 µM) with a fixed quantity of 50 nCi L-[^{14}C]Ala. Dixon plots were created by plotting inverse L-Ala uptake velocities ($1/V_{uptake}$) against inhibitor concentration (RBH or BABA), after

which five linear models for each L-Ala concentration were generated using the *lm* function (R base). Exact Ki values of RBH and BABA were determined by modeling 1,200 $1/V_{uptake}$ values in the range between -200 to 1,000 µM of the inhibitor concentration using the *predict()* function (R base), after which Ki values were selected by calculating the inhibitor concentration yielding the minimum range in $1/V_{uptake}$.

2.6 Acknowledgements

We thank Dr. Henrik Svennerstam for providing the seeds of the *35Spro:LHT1* line, Professor Guillaume Pilot for providing the 22Δ10α yeast line, Professor Stephen Rolfe and Dr. Pedro Rocha for advice on the enzyme kinetic experiment. We thank Dr. Karin Posthuma (Enza Zaden) for advice and support throughout the project. We gratefully acknowledge PhD student support from The De Laszlo Foundation. This work was supported by a grant from the European Research Council (ERC; no. 309944 "Prime-A-Plant") to J.T., a Research Leadership Award from the Leverhulme Trust (no. RL-2012-042) to J.T., a BBSRC-IPA grant to J.T. (BB/P006698/1) and Supplementary grant from Enza Zaden to J.T., and a ERC-PoC grant to JT (no. 824985 "ChemPrime). K.F. is supported by a European Research Council Consolidator Grant (MYCOREV - 865225). The authors declare no financial conflict of interest.

2.7 Author Contributions

J.T. conceived the research; C.-N.T, W.B., P.Z., R.S., and J.T. designed the experiments; C.-N.T (Figs. 2.1, 2.4, 2.5, 2.6, Supplemental Figs. 2.2, 2.3, 2.5, 2.6) , W.B. (Figs. 2.1, 2.2, 2.3, Supplemental Figs. 2.1), P.Z. (Figs. 2.4, 2.5, 2.6, Supplemental Figs. 2.3, 2.4, 2.6, 2.7, 2.8, 2.10), H.W. (Figs. 2.2, 2.4), I.J. (Figs. 2.6, Supplemental Figs. 2.8), and K.F. (Fig. 2.6) conducted the experiments; C.-N.T, W.B., P.Z., and J.T. analyzed the data; C.-N.T, W.B., and J.T. wrote the paper.

2.8 References

Ahmad, S., Gordon-Weeks, R., Pickett, J., and Ton, J. (2010). Natural variation in priming of basal resistance: from evolutionary origin to agricultural exploitation. Molecular Plant Pathology 11, 817-827.

Alonso, J.M., and Ecker, J.R. (2006). Moving forward in reverse: genetic technologies to enable genome-wide phenomic screens in Arabidopsis. Nature Reviews Genetics 7, 524-536.

Badmi, R., Zhang, Y., Tengs, T., Brurberg, M.B., Krokene, P., Fossdal, C.G., Hytönen, T., and Thorstensen, T. (2019). Induced and primed defense responses of *Fragaria vesca* to *Botrytis cinerea* infection. bioRxiv, 692491.

Balmer, A., Glauser, G., Mauch-Mani, B., and Baccelli, I. (2019). Accumulation patterns of endogenous beta-aminobutyric acid during plant development and defense in *Arabidopsis thaliana*. Plant Biology 21, 318-325.

Besnard, J., Pratelli, R., Zhao, C., Sonawala, U., Collakova, E., Pilot, G., and Okumoto, S. (2016). UMAMIT14 is an amino acid exporter involved in phloem unloading in Arabidopsis roots. Journal of Experimental Botany 67, 6385-6397.

Bigeard, J., Colcombet, J., and Hirt, H. (2015). Signaling mechanisms in pattern-triggered immunity (PTI). Molecular Plant 8, 521-539.

Boorer, K.J., Frommer, W.B., Bush, D.R., Kreman, M., Loo, D.D.F., and Wright, E.M. (1996). Kinetics and specificity of a H+ amino acid transporter from *Arabidopsis thaliana*. Journal of Biological Chemistry 271, 2213-2220.

Buswell, W., Schwarzenbacher, R.E., Luna, E., Sellwood, M., Chen, B., Flors, V., Pétriacq, P., and Ton, J. (2018). Chemical priming of immunity without costs to plant growth. New Phytologist 218, 1205-1216.

Camanes, G., Pastor, V., Cerezo, M., Garcia-Andrade, J., Vicedo, B., Garcia-Agustin, P., and Flors, V. (2012). A Deletion in NRT2.1 Attenuates *Pseudomonas syringae*-induced hormonal perturbation, resulting in primed plant defenses. Plant Physiology 158, 1054-1066.

Cameron, D.D., Neal, A.L., van Wees, S.C.M., and Ton, J. (2013). Mycorrhiza-induced resistance: more than the sum of its parts? Trends in Plant Science 18, 539-545.

Chen, L., and Bush, D.R. (1997). LHT1, a lysine-and histidine-specific amino acid transporter in Arabidopsis. Plant Physiology 115, 1127-1134.

Chen, Y., Yan, Y., Ren, Z.-F., Ganeteg, U., Yao, G.-K., Li, Z.-L., Huang, T., Li, J.-H., Tian, Y.-Q., Lin, F., and Xu, H.-H. (2018). AtLHT1 Transporter can facilitate the uptake and translocation of a Glycinergic-Chlorantraniliprole conjugate in *Arabidopsis thaliana*. Journal of Agricultural and Food Chemistry 66, 12527-12535.

Chisholm, S.T., Coaker, G., Day, B., and Staskawicz, B.J. (2006). Host-microbe interactions: shaping the evolution of the plant immune response. Cell 124, 803-814.

Choi, H.W., and Klessig, D.F. (2016). DAMPs, MAMPs, and NAMPs in plant innate immunity. BMC plant biology 16, 1-10.

Choi, J., Eom, S., Shin, K., Lee, R.-A., Choi, S., Lee, J.-H., Lee, S., and Soh, M.-S. (2019). Identification of Lysine Histidine Transporter 2 as an 1-Aminocyclopropane Carboxylic Acid Transporter in Arabidopsis thaliana by Transgenic Complementation Approach. Frontiers in plant science 10, 1092.

Cohen, Y. (1994). 3-Aminobutyric acid induces systemic resistance against *Peronospore tabacina*. Physiological and Molecular Plant Pathology 44, 273-288.

Cohen, Y., Vaknin, M., and Mauch-Mani, B. (2016). BABA-induced resistance: milestones along a 55-year journey. Phytoparasitica 44, 513-538.

Cornish-Bowden, A. (1974). A simple graphical method for determining the inhibition constants of mixed, uncompetitive and non-competitive inhibitors (Short Communication). Biochemical Journal: Molecular Aspects 137, 143-144.

Cui, H., Tsuda, K., and Parker, J.E. (2015). Effector-triggered immunity: from pathogen perception to robust defense. Annunal Review Plant Biology 66, 487-511.

De Kesel, J., Conrath, U., Flors, V., Luna, E., Mageroy, M.H., Mauch-Mani, B., Pastor, V., Pozo, M.J., Pieterse, C.M., and Ton, J. (2021). The induced resistance lexicon: Do's and don'ts. Trends in Plant Science 26, 685-691.

De Muyt, A., Pereira, L., Vezon, D., Chelysheva, L., Gendrot, G., Chambon, A., Lainé-Choinard, S., Pelletier, G., Mercier, R., and Nogué, F. (2009). A high throughput genetic screen identifies new early meiotic recombination functions in *Arabidopsis thaliana*. PLoS Genetics 5, e1000654.

Dinkeloo, K., Boyd, S., and Pilot, G. (2018). Update on amino acid transporter functions and on possible amino acid sensing mechanisms in plants. In Seminars in cell & developmental biology (Elsevier), pp. 105-113.

Dobritsa, A.A., Geanconteri, A., Shrestha, J., Carlson, A., Kooyers, N., Coerper, D., Urbanczyk-Wochniak, E., Bench, B.J., Sumner, L.W., and Swanson, R. (2011). A large-scale genetic screen in Arabidopsis to identify genes involved in pollen exine production. Plant Physiology 157, 947-970.

Elashry, A., Okumoto, S., Siddique, S., Koch, W., Kreil, D.P., and Bohlmann, H. (2013). The AAP gene family for amino acid permeases contributes to development of the cyst nematode *Heterodera schachtii* in roots of Arabidopsis. Plant Physiology Biochemistry 70, 379-386.

Gelvin, S.B. (2021). Plant DNA Repair and *Agrobacterium* T-DNA Integration. International Journal of Molecular Sciences 22, 8458.

Gietz, R.D., and Schiestl, R.H. (2007). High-efficiency yeast transformation using the LiAc/SS carrier DNA/PEG method. Nature Protocols 2, 31-34.

Guether, M., Volpe, V., Balestrini, R., Requena, N., Wipf, D., and Bonfante, P. (2011). LjLHT1.2-a mycorrhiza-inducible plant amino acid transporter from *Lotus japonicus*. Biology and Fertility of Soils 47, 925-936.

Hirner, A., Ladwig, F., Stransky, H., Okumoto, S., Keinath, M., Harms, A., Frommer, W.B., and Koch, W. (2006). Arabidopsis LHT1 is a high-affinity transporter for cellular amino acid uptake in both root epidermis and leaf mesophyll. The Plant Cell 18, 1931-1946.

Ho, C.-H., Lin, S.-H., Hu, H.-C., and Tsay, Y.-F. (2009). CHL1 functions as a nitrate sensor in plants. Cell 138, 1184-1194.

Jiang, X., Xie, Y., Ren, Z., Ganeteg, U., Lin, F., Zhao, C., and Xu, H. (2018). Design of a new Glutamine-Fipronil conjugate with alpha-amino acid function and its uptake by A-thaliana Lysine Histidine Transporter 1 (AtLHT1). Journal of Agricultural and Food Chemistry 66, 7597-7605.

Khare, D., Choi, H., Huh, S.U., Bassin, B., Kim, J., Martinoia, E., Sohn, K.H., Paek, K.-H., and Lee, Y.J.P.o.t.N.A.o.s. (2017). Arabidopsis ABCG34 contributes to defense against necrotrophic pathogens by mediating the secretion of camalexin. Proceedings of the National Academy of Sciences of the United States of America 114, E5712-E5720.

Kus, J.V., Zaton, K., Sarkar, R., and Cameron, R.K. (2002). Age-related resistance in Arabidopsis is a developmentally regulated defense response to *Pseudomonas syringae*. The Plant Cell 14, 479-490.

Liu, G., Ji, Y., Bhuiyan, N.H., Pilot, G., Selvaraj, G., Zou, J., and Wei, Y. (2010). Amino acid homeostasis modulates salicylic acid–associated redox status and defense responses in Arabidopsis. The Plant Cell 22, 3845-3863.

Lu, X., Dittgen, J., Piślewska-Bednarek, M., Molina, A., Schneider, B., Svato¡, A., Doubský, J., Schneeberger, K., Weigel, D., and Bednarek, P. (2015). Mutant allele-specific uncoupling of PENETRATION3 functions reveals engagement of the ATP-binding cassette transporter in distinct tryptophan metabolic pathways. Plant Physiology 168, 814-827.

Luna, E., Van Hulten, M., Zhang, Y., Berkowitz, O., López, A., Pétriacq, P., Sellwood, M.A., Chen, B., Burrell, M., and Van De Meene, A. (2014). Plant perception of β-aminobutyric acid is mediated by an aspartyl-tRNA synthetase. Nature chemical biology 10, 450-456.

Marella, H.H., Nielsen, E., Schachtman, D.P., and Taylor, C.G. (2013). The Amino Acid Permeases AAP3 and AAP6 are involved in root-knot nematode parasitism of Arabidopsis. Molecular Plant-Microbe Interactions 26, 44-54.

Mauch-Mani, B., Baccelli, I., Luna, E., and Flors, V. (2017). Defense priming: an adaptive part of induced resistance. Annual Review of Plant Biology 68, 485-512.

Meyer, A., Eskandari, S., Grallath, S., and Rentsch, D. (2006). AtGAT1, a high affinity transporter for γ-aminobutyric acid in *Arabidopsis thaliana*. Journal of Biological Chemistry 281, 7197-7204.

O'Malley, R.C., Barragan, C.C., and Ecker, J.R. (2015). A user's guide to the Arabidopsis T-DNA insertion mutant collections. In Plant Functional Genomics (Springer), pp. 323-342.

Ritz, C., Baty, F., Streibig, J.C., and Gerhard, D. (2015). Dose-response analysis using R. PLoS One 10, e0146021-e0146021.

Rueden, C.T., Schindelin, J., Hiner, M.C., DeZonia, B.E., Walter, A.E., Arena, E.T., and Eliceiri, K.W. (2017). ImageJ2: ImageJ for the next generation of scientific image data. Bmc Bioinformatics 18, 1-26.

Schwarzenbacher, R.E., Wardell, G., Stassen, J., Guest, E., Zhang, P., Luna, E., and Ton, J. (2020). The IBI1 receptor of β-aminobutyric acid interacts with VOZ transcription factors to regulate abscisic acid signaling and callose-associated defense. Molecular Plant 13, 1455-1469.

Serrano, M., Wang, B., Aryal, B., Garcion, C., Abou-Mansour, E., Heck, S., Geisler, M., Mauch, F., Nawrath, C., and Métraux, J.-P. (2013). Export of salicylic acid from the chloroplast requires the multidrug and toxin extrusion-like transporter EDS5. Plant Physiology 162, 1815-1821.

Shin, K., Lee, S., Song, W.-Y., Lee, R.-A., Lee, I., Ha, K., Koo, J.-C., Park, S.-K., Nam, H.-G., and Lee, Y. (2015). Genetic identification of ACC-RESISTANT2 reveals involvement of LYSINE HISTIDINE TRANSPORTER1 in the uptake of 1-aminocyclopropane-1-carboxylic acid in Arabidopsis thaliana. Plant Cell Physiology 56, 572-582.

Sonawala, U., Dinkeloo, K., Danna, C.H., McDowell, J.M., and Pilot, G. (2018). Review: Functional linkages between amino acid transporters and plant responses to pathogens. Plant Science 277, 79-88.

Svennerstam, H., Ganeteg, U., Bellini, C., and Nasholm, T. (2007). Comprehensive screening of Arabidopsis mutants suggests the lysine histidine transporter 1 to be involved in plant uptake of amino acids. Plant Physiology 143, 1853-1860.

Svennerstam, H., Jamtgard, S., Ahmad, I., Huss-Danell, K., Nasholm, T., and Ganeteg, U. (2011). Transporters in Arabidopsis roots mediating uptake of amino acids at naturally occurring concentrations. New Phytologist 191, 459-467.

Thevenet, D., Pastor, V., Baccelli, I., Balmer, A., Vallat, A., Neier, R., Glauser, G., and Mauch-Mani, B. (2017). The priming molecule β-aminobutyric acid is naturally present in plants and is induced by stress. New Phytologist 213, 552-559.

Ton, J., Jakab, G., Toquin, V., Flors, V., Iavicoli, A., Maeder, M.N., Métraux, J.-P., and Mauch-Mani, B. (2005). Dissecting the β-aminobutyric acid–induced priming phenomenon in Arabidopsis. The Plant Cell 17, 987-999.

Wilkinson, S.W., Mageroy, M.H., Lopez Sanchez, A., Smith, L.M., Furci, L., Cotton, T.E.A., Krokene, P., and Ton, J. (2019). Surviving in a hostile world: plant strategies to resist pests and diseases. Annual Review Phytopathology 57, 505-529.

Wilson-Sánchez, D., Rubio-Díaz, S., Muñoz-Viana, R., Pérez-Pérez, J.M., Jover-Gil, S., Ponce, M.R., and Micol, J.L. (2014). Leaf phenomics: a systematic reverse genetic screen for Arabidopsis leaf mutants. The Plant Journal 79, 878-891.

Wu, C.-C., Singh, P., Chen, M.-C., and Zimmerli, L. (2010). L-Glutamine inhibits beta-aminobutyric acid-induced stress resistance and priming in Arabidopsis. Journal of Experimental Botany 61, 995-1002.

Yang, H., Bogner, M., Stierhof, Y.-D., and Ludewig, U. (2010). H+-Independent glutamine transport in plant root tips. PLos One 5, e8917.

Yang, H., Postel, S., Kemmerling, B., and Ludewig, U. (2014). Altered growth and improved resistance of Arabidopsis against *Pseudomonas syringae* by overexpression of the basic amino acid transporter AtCAT1. Plant, Cell & Environment 37, 1404-1414.

Yassin, M., Ton, J., Rolfe, S.A., Valentine, T.A., Cromey, M., Holden, N., and Newton, A.C. (2021). The rise, fall and resurrection of chemical-induced resistance agents. Pest Management Science 77, 3900-3909.

Yoshino, M., and Murakami, K. (2009). A graphical method for determining inhibition constants. Journal of Enzyme Inhibition and Medicinal Chemistry 24, 1288-1290

Yoo, H., Greene, G.H., Yuan, M., Xu, G., Burton, D., Liu, L., Marques, J., and Dong, X. (2020). Translational Regulation of Metabolic Dynamics during Effector-Triggered Immunity. Molecular Plant 13, 88-98.

Zhang, X., Khadka, P., Puchalski, P., Leehan, J.D., Rossi, F.R., Okumoto, S., Pilot, G., and Danna, C.H. (2022). MAMP-elicited changes in amino acid transport activity contribute to restricting bacterial growth. Plant Physiology 189, 2315-2331.

Zimmerli, L., Jakab, G., Métraux, J.-P., and Mauch-Mani, B. (2000). Potentiation of pathogen-specific defense mechanisms in Arabidopsis by β-aminobutyric acid. Proceedings of the National Academy of Sciences of the United States of America 97, 12920-12925.

2.9 Supplemental Material

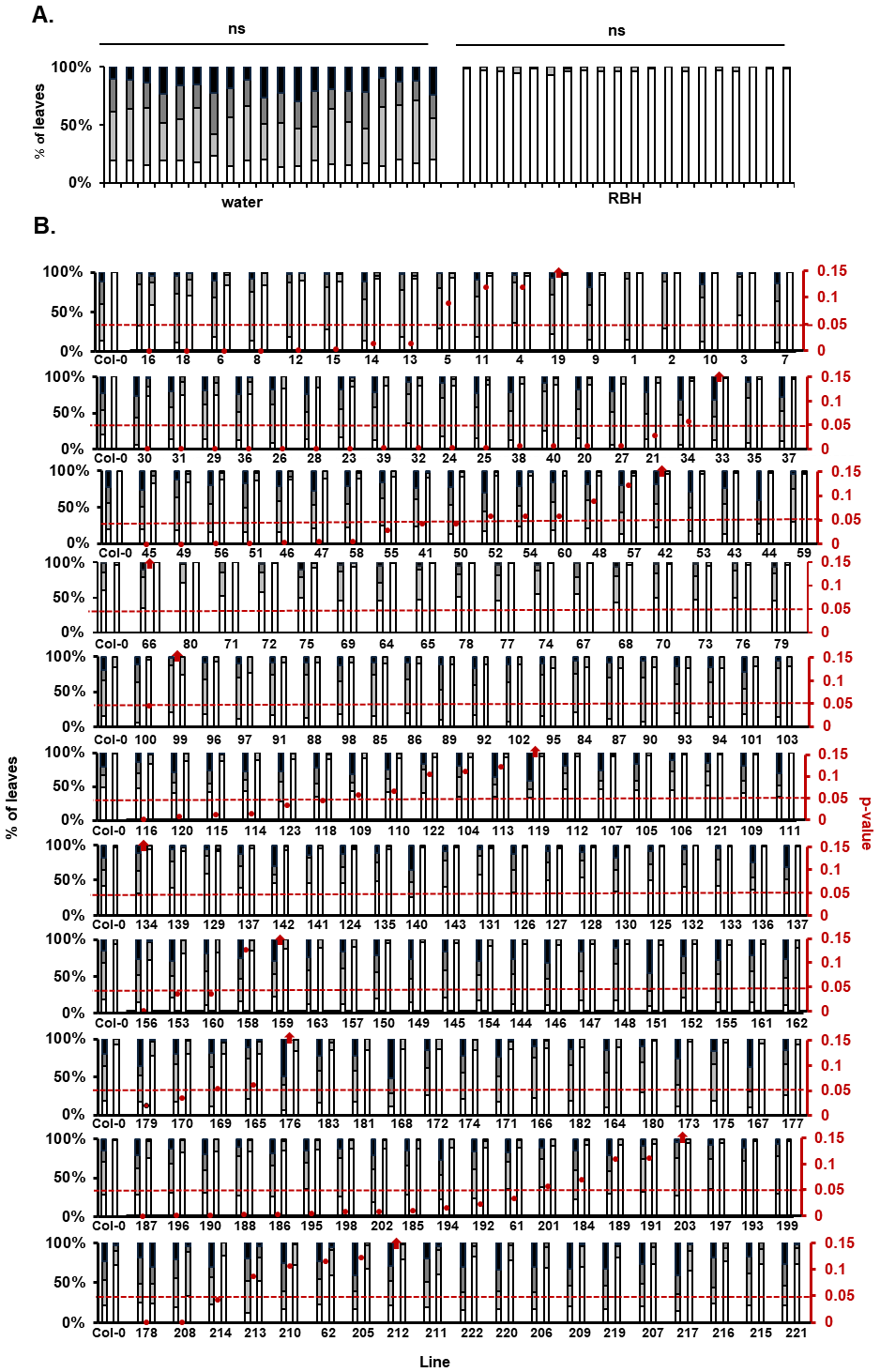

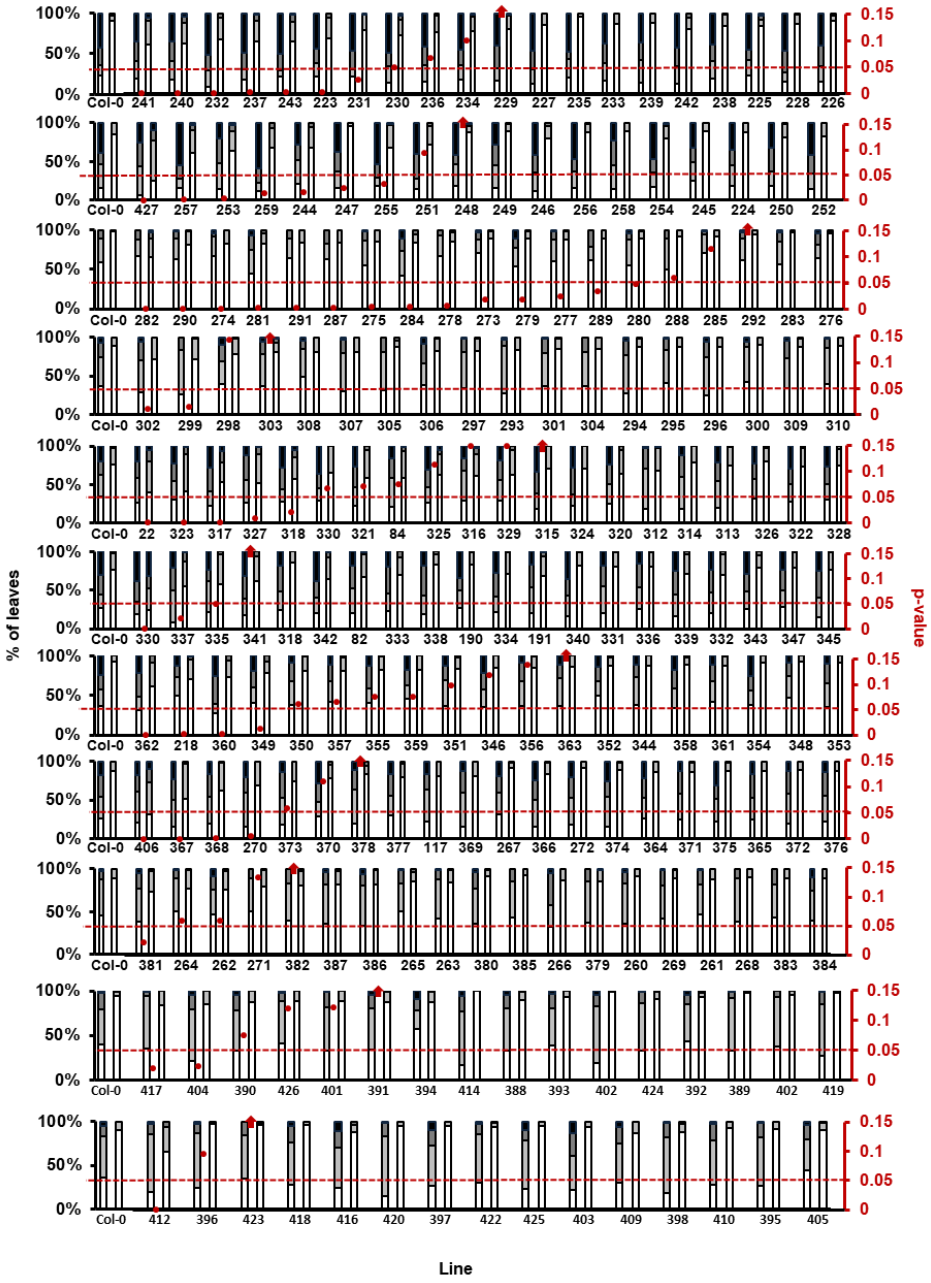

Supplemental Figure 2.1. Validation of putative *iri* mutants at stage 3 of the mutant screen. (supports Figures 2.1). (A) Experiment to confirm statistical robustness of the bioassay system used to verify putative *iri* mutants. The results demonstrate uniformity of *Hpa* colonization between 20 independent batches of naïve (water-treated) plants and between 20 independent batches of plants showing RBH-IR (right). Shown are levels of *Hpa* colonization in leaves of water-treated (left) and RBH-treated (right) seedlings (Col-0 wild-type) within one experiment. Each batch consisted of one 60-mL pot containing 20-30 seedlings. Two-week-old seedlings had the soil in their pots saturated with water or RBH to a final concentration of 0.5 mM, and were inoculated with *Hpa* two days later. At 6-7 dpi, leaves were harvested for trypan-blue staning (n = 60-80) and microscopically assigned to four different classes of *Hpa* colonization (see Fig. 2.1A for details). Robustness of the bioassay assay system is indicated by the lack of statistically significant differences in *Hpa* colonization between independent batches of the same treatment (Fisher's Exact Test, $p < 0.05$). **(B)** Quantification of RBH-IR against *Hpa* in 427 putative *iri* lines, using the RBH-IR bioassay. The red y-axis on the right shows the *p*-values of the difference in *Hpa* colonization between RBH-treated mutant seedlings and RBH-treated Col-0 seedlings within each sub-experiment (Fisher's Exact Test), indicating loss of RBH-IR. The dotted line indicates the threshold of significance ($p = 0.05$).

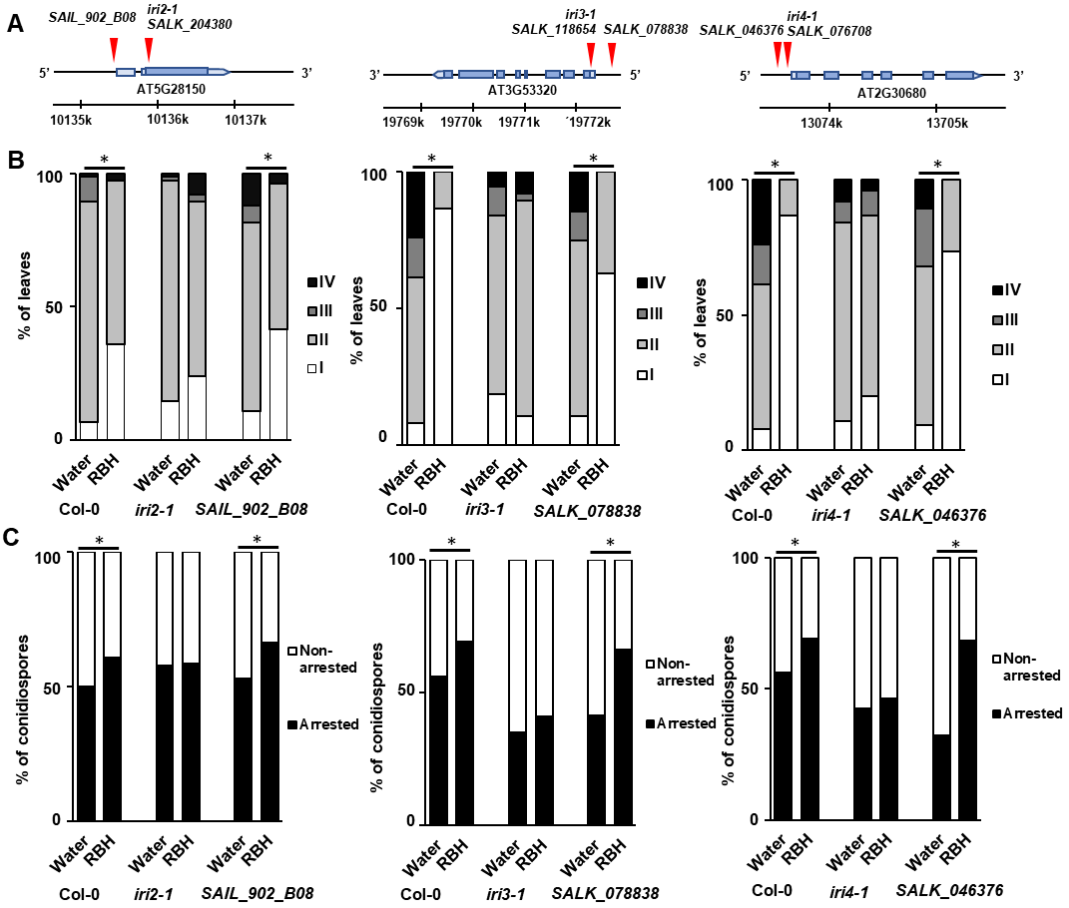

Supplemental Figure 2.2. Characterization of RBH-IR in SALK/SAIL lines carrying independent T-DNA insertions in the same genes that are annotated to carry T-DNA insertions in *iri2-1*, *iri3-1* and *iri4-1* (supports Figures 2.1). (A) Gene models and positions of T-DNA insertions, shown as red triangles, for *iri2-1*, *iri3-1* and *iri4*-1, as well as independent SAIL/SALK lines carrying different T-DNA insertions in the same genes, respectively. **(B)** Quantification of RBH-IR against *Hpa* in leaves of mutants carrying the T-DNA insertion indicated above. Two-week-old seedlings had the soil in their pots saturated with water or RBH to a final concentration of 0.5 mM RBH, and were challenged with *Hpa* conidiospores 2 days later. Shown are frequency distributions of trypan blue-stained leaves across the four *Hpa* colonization classes (Figure 2.1A) at 7 dpi. Asterisks indicate statistically significant differences between water- and RBH-treated samples (Fisher's exact tests; $p < 0.05$; n=70-80 leaves). **(C)** Quantification of arrested *Hpa* colonization by callose at 3 dpi. *Hpa*-induced callose was analyzed in aniline blue/calcofluor-stained leaves by epifluorescence microscopy. Shown are percentages of callose-arrested and non-arrested conidiospores as detailed by Schwarzenbacher et al. (2020). Different letters indicate statistically significant differences in frequencies between water- and RBH-treated plants (Fisher's exact tests; $p < 0.05$; n>100 conidiospores).

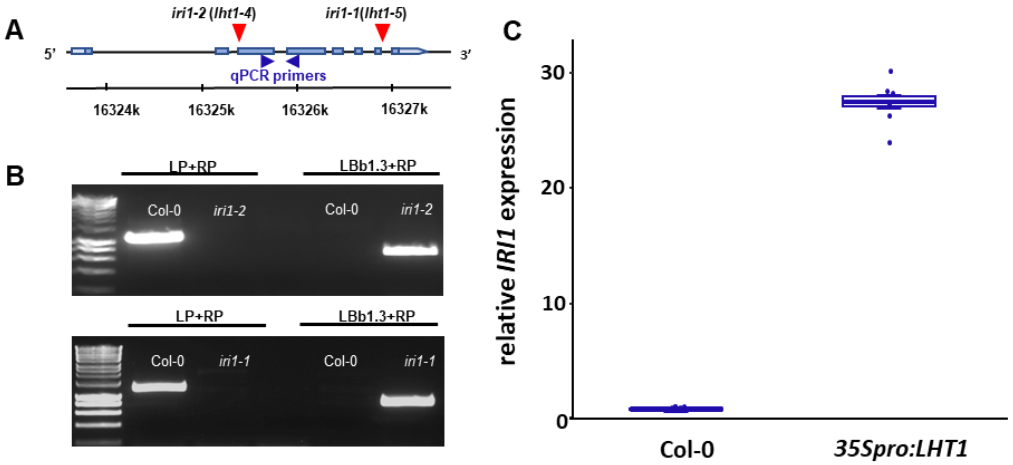

Supplemental Figure 2.3. Genetic characterization of two independent *lht1* mutant lines and the *LHT1* overexpression line (supports Figure 2.1). (A) Gene model of *LHT1*. Red triangles indicate T-DNA insertions in the *lht1-5* (*iri1-1*) and *lht1-4* (*iri1-2*) mutants. Dark blue arrows indicate aligned locations of the primers used for RT-qPCR analysis (see below). **(B)** Confirmation of T-DNA insertions by PCR. Shown are PCR products of the expected sizes in Col-0, *lht1-5* (*iri1-1*) and *lht1-4* (*iri1-2*), using gene-specific primers (LP+RP) and the left-border primer of the T-DNA in combination with the gene-specific RP primer (LBb1.3+RP). Primer sequences are listed in Supplemental Table S1. **(C)** RT-qPCR quantification of LHT1 expression levels in Col-0 and the overexpression line *35Spro:LHT1*. Biologically replicated samples (n=5) were harvested from 2-week-old seedlings under the same growth conditions as our IR assay. Boxplots show median (middle bar), interquartile range (IQR; box), 1.5 x IQR (whiskers) and replication units (single dots) of relative expression values normalized to the mean relative expression value of Col-0.

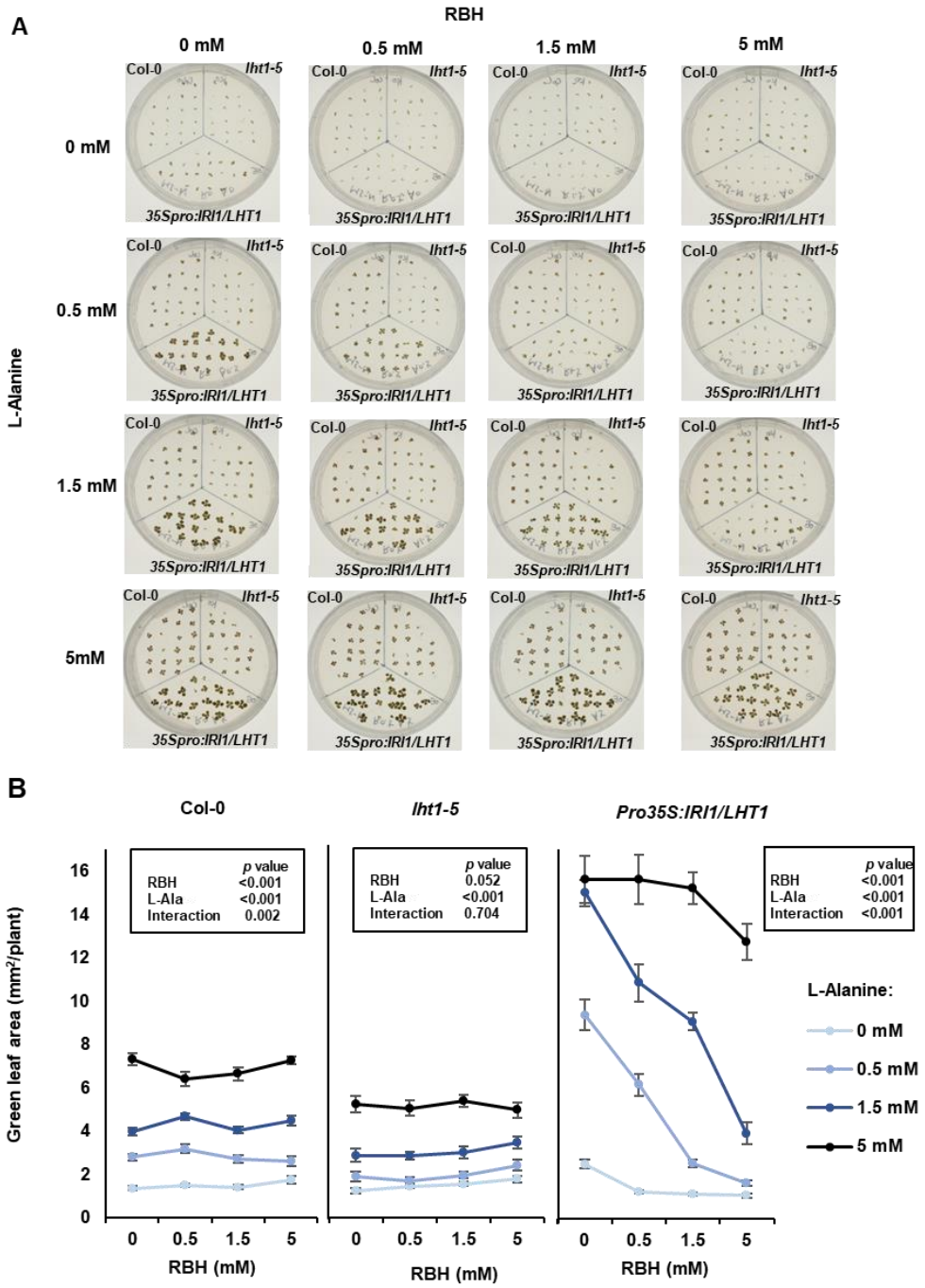

Supplemental Figure 2.4. Transgenic overexpression of *LHT1* improves Arabidopsis growth on medium with L-alanine as the only N source, which is antagonized by co-application of RBH (supports Figure 2.3). (A) Shown are 2-week-old seedlings of Col-0 (upper left), *lht1-5* (upper right), and *35Spro:LHT1* (bottom) on MS agar plates without inorganic N and supplemented with increasing concentrations of RBH and/or L-alanine. All genotypes failed to grow on medium with RBH as the only N source. **(B)** Green leaf areas (GLA ± SEM; n=10-19) of 2-week-old Col-0, *lht1-5*, and *35Spro:LHT1* seedlings from the same experiment. Insets show *p*-values of the effects on GLA by RBH concentration, L-alanine concentration and their interaction for each genotype (2-way ANOVA).

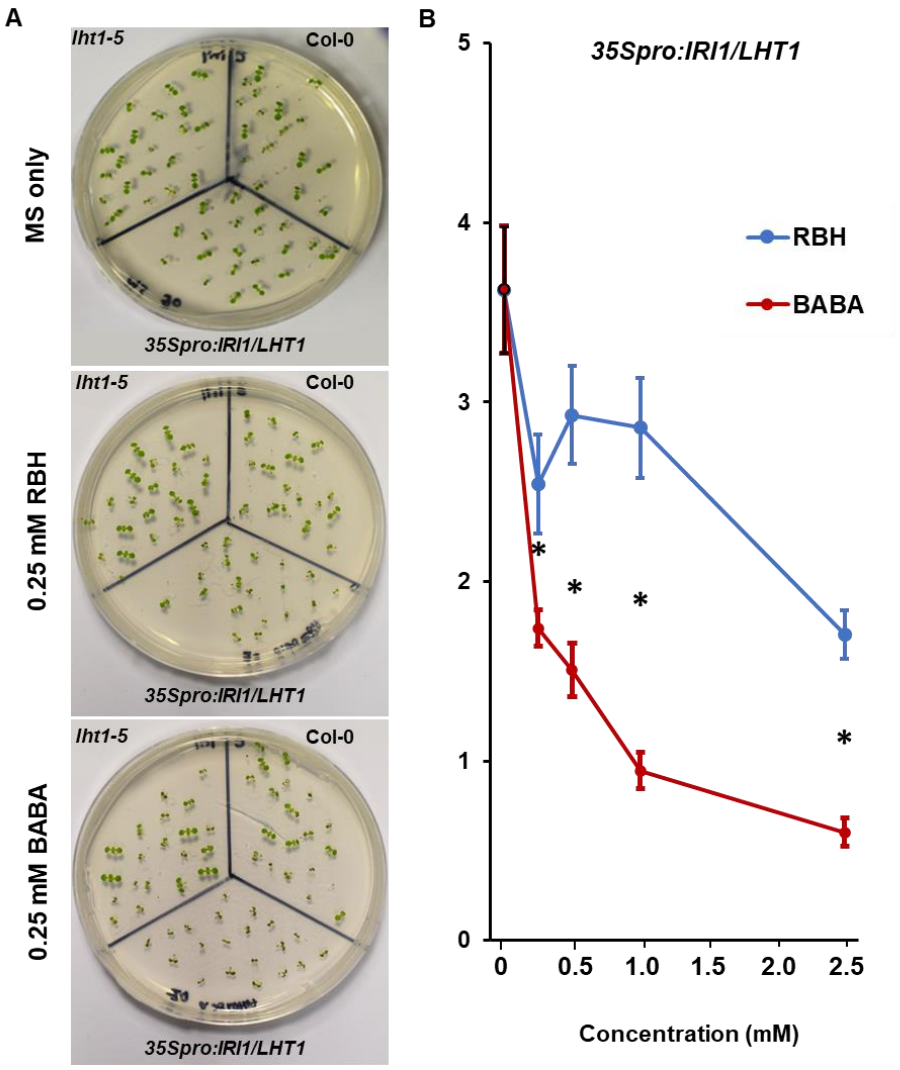

Supplemental Figure 2.5. Comparison of growth repression by low concentrations of BABA and RBH (supports Figure 2.5). (A) Representative photographs of growth phenotypes for Col-0 (upper right), *lht1-5* (upper left) and *35Spro:LHT1* seedlings in the presence of 0.25 mM RBH or BABA. Shown are 1-week-old seedlings grown on MS agar plates with or without 0.25 mM RBH or BABA. **(B)** Quantification of green leaf area (GLA ± SEM; n=17-20) in 1-week-old *35Spro:LHT1* seedlings grown on MS agar with relatively low concentrations of RBH or BABA. Asterisks indicate statistically significant differences in GLA between RBH and BABA treatments (Welch's t-test; $p < 0.05$).

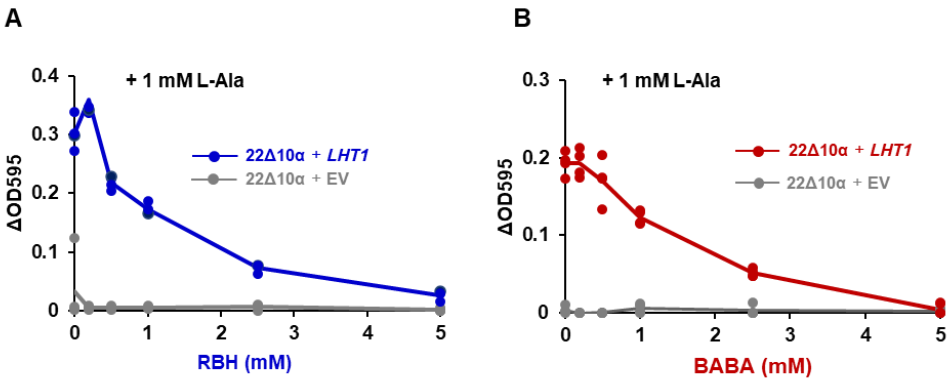

Supplemental Figure 2.6. RBH and BABA compete with L-alanine for LHT1 uptake and inhibit yeast growth (Supports Figure 2.6). (A, B) Growth of EV- and *LHT1*-transformed 22Δ10α in liquid medium supplemented with increasing L-Ala concentrations, 1 mM L-Ala + increasing RBH concentrations **(A)**, or 1 mM L-Ala + increasing BABA concentrations **(B)**. Growth was quantified spectrophotometrically as ΔOD_{595} values (OD_{595} – OD_{595} of medium without yeast). Data points and lines represent individual measurements and means of ΔOD_{595} values (n=4) after 3 days of growth, respectively.

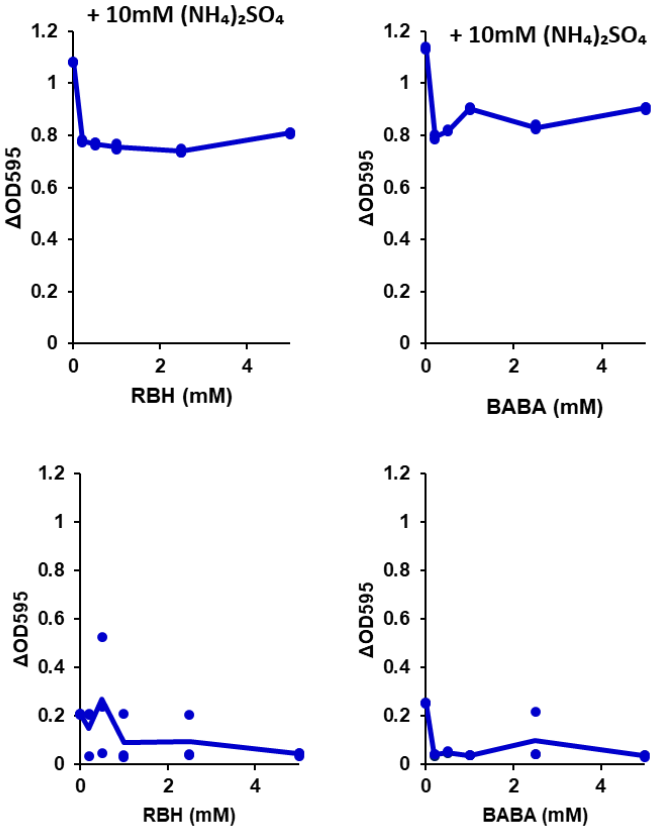

Supplemental Figure 2.7. RBH and BABA have minimal effects on yeast growth but cannot be used as N source by yeast (supports Figure 2.6). The yeast mutant strain 22Δ10α (Besnard et al., 2016) was transformed with Arabidopsis *LHT1* and grown in liquid growth medium with (top) or without $(NH_4)_2SO_4$ (bottom), co-supplied with increasing concentrations of RBH (left) or BABA (right). Growth was quantified spectrophotometrically by determining ΔOD_{595} values (OD_{595} - OD_{595} of medium without yeast). Lines represent average ΔOD_{595} values (n=4) after growth for 3 days.

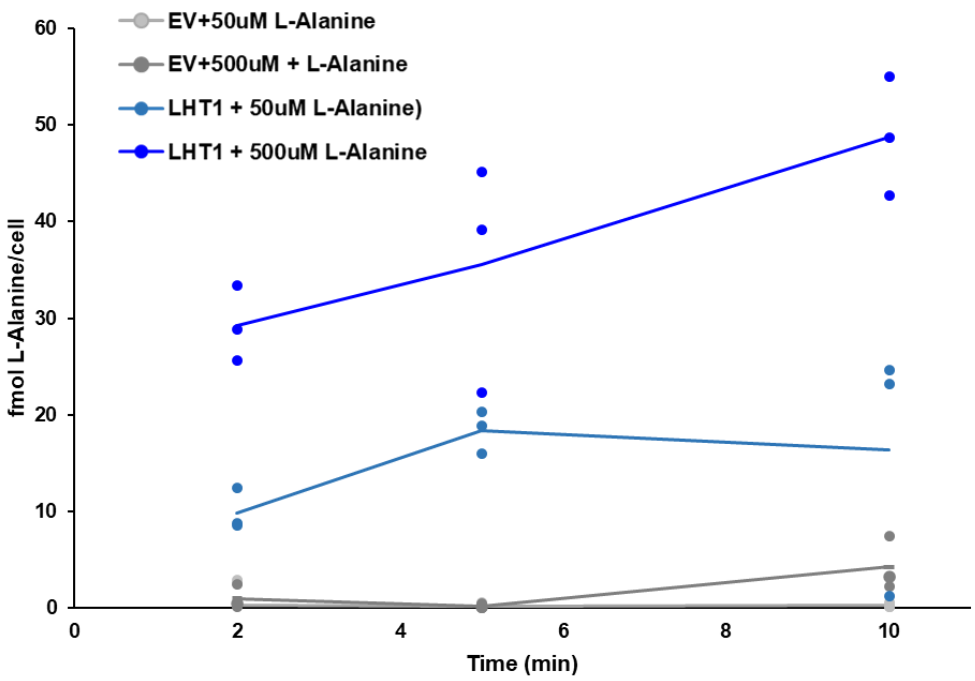

Supplemental Figure 2.8. Transformation of the yeast 22Δ10α mutant with *LHT1* rescues uptake of L-[^{14}C] alanine (supports Figure 2.6). Empty vector (EV)- and *LHT1*-transformed cells were incubated for 2, 5 or 10 min. in the presence of 50 or 500 µM L-Ala with 50 nCi ^{14}C-labeled L-Ala. Lines represent average cellular L-Ala concentrations (fmol L-Ala/cell; ±SEM; n=3).

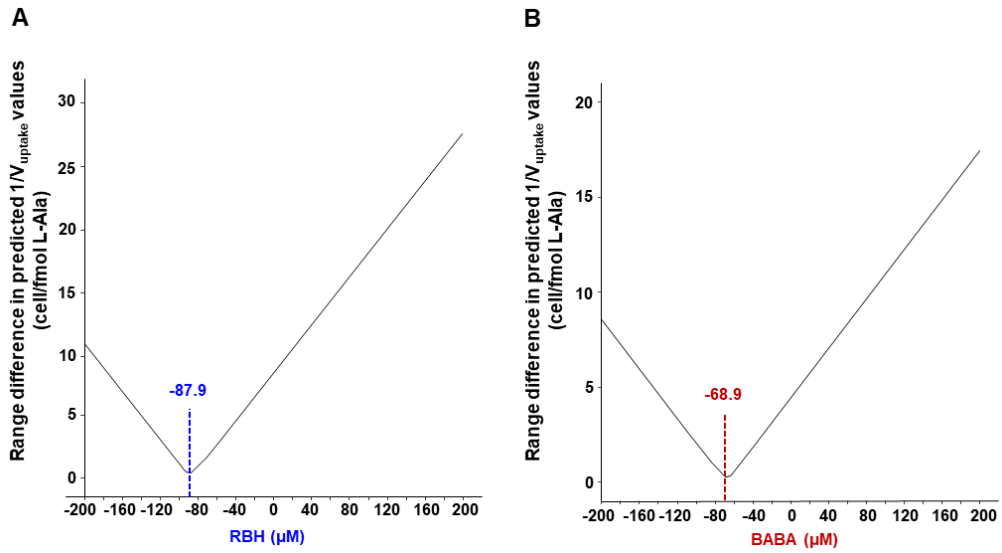

Supplemental figure 2.9. Modeling exact inhibitor constants (Ki) of RBH (A) and BABA (supports Figure 2.6). Shown are predicted range between inverse uptake velocities ($1/V_{uptake}$) at different L-Ala concentrations across a range of inhibitor concentrations. Predicted values were calculated from the linear models in the Dixon plots (Figure 2.6E,F). The Ki values by RBH and BABA were determined as the concentration yielding the minimum range.

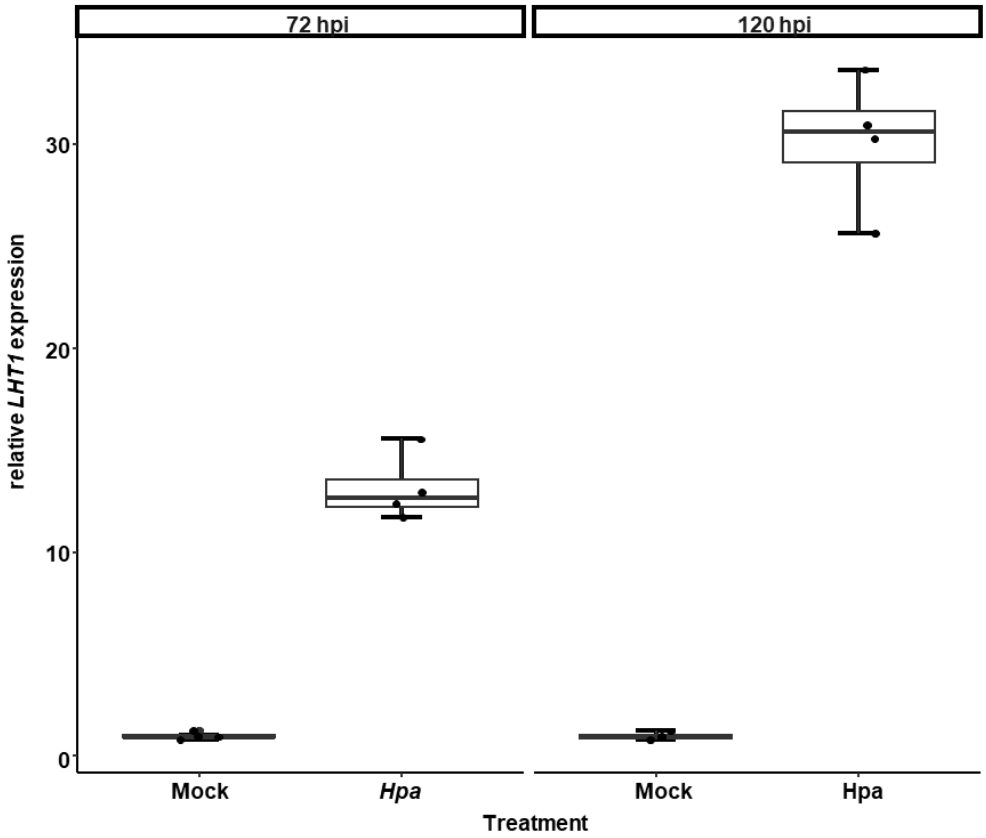

Supplemental Figure 2.10. Induction of *LHT1* expression by *Hpa* (supports Figure 2.1). RT-qPCR analysis of *LHT1* expression levels in Col-0 after *Hpa* inoculation. Two-week-old seedlings were sprayed with water (mock) or 10^5 spores/mL *Hpa.* Biologically replicated samples (n=4) were harvested at 72 and 120 hours post inoculation (hpi). Boxplots show median (middle bar), interquartile range (IQR; box), 1.5 x IQR (whiskers) and replication units (single dots) of relative expression values, normalized to the mean relative expression value of mock treatment at 72 hpi.

Supplemental Table S1. Primers used for characterization of T-DNA insertion lines.

Gene	SALK/SAIL Number[1]	*iri* Mutant	Left Primer (LP; 5' to 3')	Right Primer (RP: 5' to 3')
At5g40780	SALK_115555	*iri1-1*	ATTGATTGGGTTTACCCCATC	CCACAACTCTTCGGTTCTTTG
	SALK_036871	*iri1-2*	TGTCAGTGGGCTAAAAATGTG	CAGCTCATAACTCTTGTGCCC
At5g28150	SALK_204380	*iri2-1*	ATCGTCAAACACCCAAATCG	GCTTTCGTTGCAAACACTCTC
	SAIL_902_B08	-	ATAAAGTGGTAGGCGCTCATG	CCAAAGCAAGAAGGAAAATCC
At3g53320	SALK_118654	*iri3-1*	TGTTCTCCACAGTGCAGTCAC	CCATCCCAAATCATAATCCTTG
	SALK_078838	-	CGAGGTACTTCGTTCGAAATG	CCATCCCAAATCATAATCCTTG
At2g30680	SALK_076708	*iri4-1*	GATCCCAATGAAAATGCAGAC	ACATCCATGACGTTTTTCTGG
	SALK_046376	-	ACATCCATGACGTTTTTCTGG	GTTCGCACACGAGTAGTTTCC

[1] Genomic integration was confirmed by PCR using the gene-specific RP listed above in combination the LBb1.3 primer (5'-ATTTTGCCGATTTCGGAAC-3'; SALK lines) or the LB3 primer (5'-TAGCATCTGAATTTCATAACCAATCTCGATACAC-3'; SAIL_902_B08).
SALK_115555 (*iri1-1*) is *lht1-5*.
SALK_036871 (*iri1-2*) is *lht1-4*.

Chapter 3: The sphingolipid α-hydroxylase FAH2 interacts with the BABA receptor to regulate BABA-induced plant responses

Chia-Nan Tao[1], Roland Schwarzenbacher[1], Cornelia Herrfurth[2,3], Ivo Feussnerand[2,3,4], Jurriaan Ton[1]

[1] School of Biosciences, Institute for Sustainable Food, The University of Sheffield; Sheffield, S10 2TN; United Kingdom

[2] Department for Plant Biochemistry, Albrecht-von-Haller-Institute for Plant Sciences, University of Goettingen, Justus-von-Liebig-Weg 11, Goettingen 37077, Germany

[3] Service Unit for Metabolomics and Lipidomics, Goettingen Center for Molecular Biosciences (GZMB), University of Goettingen, Justus-von-Liebig-Weg11, Goettingen 37077, Germany

[4] Department of Plant Biochemistry, Goettingen Center for Molecular Biosciences (GZMB), University of Goettingen, Justus-von-Liebig-Weg 11, Goettingen 37077, Germany

3.1 Abstract

Sphingolipids in plants fulfil important functions in membrane integrity, development and defence. Most plant sphingolipids are hydroxylated by fatty acid α-hydroxylases. In Arabidopsis, this process is controlled by two enzymes: FATTY ACID ALPHA-HYDROXYLASE I (FAH1) and FAH2, of which the latter mainly hydroxylates the long-chain fatty acid (LCFA) of sphingolipids. This Chapter provides new evidence that the BABA receptor, IMPAIRED IN BABA-INDUCED DISEASE IMMUNITY 1 (IBI1), interacts with FAH2. Mutation of *FAH2* was found to reduce BABA-induced resistance (BABA-IR) against *Hyaloperonospora arabidopsidis* (*Hpa*) and increase sensitivity to BABA-induced stress, indicating that FAH2, like IBI1, regulates both IR and BABA tolerance. Sphingolipid profiling of wild-type, *ibi1-1* and *fah2-1* plants by ultrahigh pressure liquid chromatography coupled to triple quadrupole mass spectrometry (LC-QqQ) confirmed that FAH2 largely hydroxylates C16 long-chain fatty acids, which was unrelated to IBI1-dependent BABA responses since both BABA and the *ibi1-1* mutation did not significantly influence the accumulation of these sphingolipids. Nonetheless, statistical selection of sphingolipid species that *i*) responded to BABA/*Hpa* treatment and *ii*) were similarly affected in BABA/*Hpa* responsiveness by both the *ibi1-1* and *fah2-1* mutations, revealed a potential role for the glycosyl-inositol-phosphoryl-ceramides (GIPC) 18.0.3/24.1.1 in IBI-dependent BABA-IR. Furthermore, based on previous evidence that BABA primes the translocation of IBI1 from the ER to the cytosol during pathogen attack, the research described in this Chapter investigated whether FAH2 controls the defence-related cytosolic translocation of IBI1 during BABA-IR. Using confocal microscopy analysing IBI1::YFP subcellular in *35Spro::IBI1-YFP* and *fah2*/*35Spro::IBI1-YFP* plants, it indeed appeared as if the *fah2-1* mutation prevented cytosolic translocation of IBI1 during BABA-IR against *Hpa*. However, the experiment remained inconclusive because the overall IBI1-YFP fluorescence in *fah2*/*35Spro::IBI1-YFP* plants was strongly reduced under all experimental conditions, which correlated with reduced transcription of the 35S-driven *IBI1-YFP* transgene. In conclusion, this Chapter shows that the IBI1-interacting sphingolipid hydroxylase FAH2 contributes to both tolerance to BABA-induced phytotoxicity and BABA-IR against *Hpa*, which is associated with reduced accumulation of the hydroxylated GIPC species 18.0.3/24.1.1.

3.2 Introduction

Sphingolipids in cell membranes are essential for plant development and stress responses (Berkey et al., 2012; Huby et al., 2020). Based on their structure, plant sphingolipids can be divided into four classes: 1) free long-chain base (LCB) sphingolipids, 2) ceramides, 3) glucosyl-ceramides (GlcCer) and 4) glycosyl-inositol-phosphoryl-ceramides (GIPC; Mamode Cassim et al., 2020). The LCB forms the basic backbone of all sphingolipids, consisting of an eighteen-carbon backbone with an amino group on the second carbon and a hydroxy group on the first and third carbon. Ceramides consist of a LCB fused to a fatty acid chain via an amide bond and can be further modified into GlcCers or GIPCs by glycosylation with single or multiple sugars (Fig. 3.1; Huby et al., 2020; Mamode Cassim et al., 2020). The length of the fatty acid chain in ceramides varies between 16 (C16) and 26 (C26) carbons, which can be hydroxylated (Mamode Cassim et al., 2020). The GlcCer and GIPC of plants are predominantly α-hydroxylated at the second carbon (C2) of the fatty acid chain (Pata et al., 2010). In Arabidopsis, there are two genes encoding fatty acid hydroxylases, *FATTY ACID ALPHA-HYDROXYLASE I* (*FAH1*) and *FAH2* (Nagano et al., 2012b). Although both enzymes are highly homologous, FAH1 and FAH2 have different substrate preferences. FAH1 mainly hydroxylases very long-chain fatty acids (VLCFA; C≥20), while FAH2 use both C16 fatty acids and VLCFA as substrates (Nagano et al., 2012b; Ukawa et al., 2022). Unlike animal and yeast FAHs, Arabidopsis FAHs do not contain cytochrome *b5* (Cb5)-like domains but instead interact with Cb5s within the endoplasmic reticulum (ER) membrane to control their activities (Nagano et al., 2009; Nagano et al., 2012a).

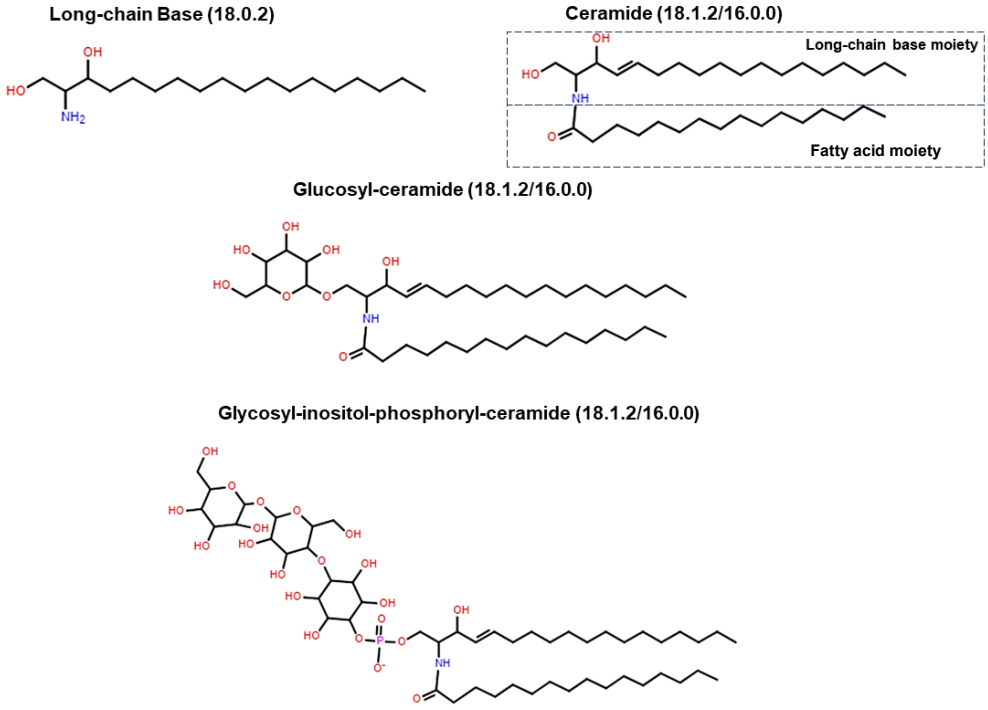

Figure 3.1. A diagram of plant sphingolipid structure. Example structures of free long-chain base (LCB) sphingolipids, ceramides, glucosyl-ceramides (GlcCer) and glycosyl-inositol-phosphoryl-ceramides. The core of ceramides, GlcCer and GIPC consist of a LCB fused to a fatty acid chain via an amide bond, and the head group at 1-position of LCB can be substituted by glucose or glycosyl-inositol-phosphate, generating GlcCer or GIPC, respectively.

Previous research has shown that both FAH1 and FAH2 are essential for cell membrane organisation and stress responses (König et al., 2012; Nagano et al., 2016; Ukawa et al., 2022). König et al. (2012) reported the *fah1fah2* double mutant accumulated sphingolipids without an α-hydroxylated fatty acid moiety, which was associated with an increased accumulation of defence-inducing salicylates. Furthermore, *FAHs* in rice and Arabidopsis have been reported to play a role in plant defence by affecting the abundance and organisation of nanodomains in the cell membrane (Nagano et al., 2016; Ukawa et al., 2022). Nanodomains are proteins and/or lipid assemblies, sized between 20 nm to 1 μm and distributed in the cell membrane with a dot-like pattern (Gronnier et al., 2018; Martinière and Zelazny, 2021). Many defence-related proteins have been found located in nanodomains, including FALGELLIN SENSITIVE 2 (FLS2), BOTRYTIS-INDUCED KINASE 1 (BIK1; Bücherl et al., 2017), and RESPIRATORY BURST OXIDASE D (RBOHD; Lherminier et al., 2009). Reduced *FAH* expression in rice affects the mobilisation of Rac/ROP small GTPase and RBOHs to nanodomains and further reduces reactive oxygen species

(ROS) production after exposure to chitin (Nagano et al., 2016). More recently, Ukawa et al. (2022) knocked out both *FAH1* and *FAH2* in Arabidopsis and revealed the importance of α-hydroxylated sphingolipids in nanodomains organisation. Significantly, their Arabidopsis *fah1cfah2* double mutant showed decreased abundance of defence-related proteins, like BRASSINOSTEROID INSENSITIVE 1-ASSOCIATED RECEPTOR KINASE 1 (BAK1), CHITIN ELICITOR RECEPTOR KINASE 1 (CERK1), and RBOHD, which was linked to impaired ROS production upon treatment with flagellin 22 or chitin (Ukawa et al., 2022). Thus, FAHs are essential regulators of plant innate immunity.

Besides the innate immune system, plants can acquire immunity upon recovery from stress, which is commonly referred to as induced resistance (IR). In addition to pests and diseases, IR can also be triggered by treatment with selected chemicals, including defence hormones, such as salicylic acid (SA) and jasmonic acid (JA), as well as other endogenous defence regulatory metabolites, such as pipecolic acid and β-aminobutyric acid (BABA), or microbe-associated molecular patterns (MAMPs). Induced resistance is often based on priming, which enables plants to ignite faster and more robust defence responses upon later stress challenges.

Chemical priming agents has potential for exploitation in plant protection purposes (Yassin et al., 2021). BABA is one of the most intensively studied priming agents. Since the discovery of BABA, its ability to trigger IR has been demonstrated in many different crop species against nearly all major phytopathogens types (Cohen et al., 2016). In Arabidopsis, BABA boosts both SA-dependent and independent defences, resulting in protection against both biotrophic and necrotrophic pathogens (Zimmerli et al. 2000; Ton and Mauch-Manio, 2004). In subsequent years, new insights were obtained about the molecular machinery of BABA-IR, including the perception of BABA and downstream defence signalling. A tRNA synthase, IMPAIRED IN BABA-INDUCED DISEASE IMMUNITY 1 (IBI1), was reported to act as a receptor of BABA by binding with the active R-enantiomer of BABA at (L)-Asp-binding domain (Luna et al., 2014; Buswell et al., 2018). This event primes the pathogen-inducible translocation of IBI1 from the ER to the cytosol (Luna et al. 2014), where it interacts with defence-regulatory VASCULAR PLANT ONE ZINC FINGER PROTEIN (VOZ) transcription factors (Schwarzenbacher et al., 2020). A recent study has revealed the BABA transporter, LHT1, which controls both BABA-IR and BABA-induced phytotoxicity (Tao et al., 2022).

These results, combined with the finding that BABA accumulates endogenously upon stress exposure, reinforce the notion that BABA functions as a natural defence signal in plants (Thevenet et al., 2017; Balmer et al., 2019).

Once BABA is perceived by IBI1, the downstream IR signal is transmitted by interacting proteins. Schwarzenbacher et al. (2020) used yeast two-hybrid analysis to screen for IBI1-interacting proteins and identified cytosol located VOZ1 and VOZ2 transcription factors. The VOZ1 and VOZ2 contribute to BABA-IR by mediating penetration resistance and simultaneously suppressing ABA-inducible abiotic stress tolerance genes (Schwarzenbacher et al., 2020). The yeast two-hybrid screen by Schwarzenbacher et al. (2020) revealed other putative interactors, including FAH2. As IBI1 and FAH2 are ER-localised proteins (Nagano et al., 2009; Luna et al., 2014), it is likely they interact *in planta*.

The study described in this Chapter has further explored the role of FAH2 in BABA signalling. The interaction between IBI1 and FAH2 was confirmed by Bimolecular Fluorescence Complementation (BiFC) and Co-immunoprecipitation (Co-IP) assays. Furthermore, testing the *fah2-1* mutant for BABA responses revealed that *FAH2* contributes to both BABA-IR and BABA-induced stress (BABA-IS). In addition, global sphingolipid profiling confirmed that mutation in *FAH2* causes a massive shift in C16 sphingolipids, which is unrelated to BABA-IR. However, one GIPC was identified, which responded to both BABA and *Hpa* treatments. Moreover, the accumulation of this sphingolipid was similarly affected by the *ibi1-1* and *fah2-1* mutations, suggesting a role in BABA-IR. Finally, this chapter has investigated whether FAH2 controls the IR-related translocation of IBI1 from the ER to the cytosol during pathogen attack by examining IBI1-YFP cellular location in *35Spro::IBI1-YFP* and *fah2/35Spro::IBI1-YFP* plants.

3.3 Results

3.3.1 FAH2 physically interacts with IBI1 *in planta*

Based on the IBI1-interacting candidates from the yeast two-hybrid screen by Schwarzenbacher et al. (2020), FAH2 was selected for further analysis, since it is expressed in leaves and localises on the ER membrane (Nagano et al., 2009). To confirm *in planta* interaction, BiFC and Co-IP was used in *Nicotiana*

benthamiana leaves upon transient expression by *Agrobacterium tumefaciens* infiltration. Co-infiltration of leaves with *A. tumefaciens* expressing complementary IBI1-YFP and FAH2-YFP constructs resulted in clear YFP fluorescence, which was apparent for both reciprocal combinations (IBI1-YFP-C versus FAH2-YFP-N and IBI1-YFP-N versus FAH2-YFP-C), while IBI1 co-expressed with the empty vector or OUTGROWTH-ASSOCIATED PROTEIN KINASE (OAK) failed to cause YFP fluorescence (Fig. 3.2A). Confocal scanning microscopy of the BiFC signal upon co-infiltration with the IBI1-YFP-N and FAH2-YFP-C IP analysis revealed a subcellular fluorescence pattern that is characteristic for the ER (Fig. 3.2B), suggesting that the IBI-FAH2 interaction likely occurs at the ER. Co-IP was performed on leaves that had been co-infiltrated with IBI1-YFP and FAH2-FLAG constructs, using an anti-FLAG antibody for immunoprecipitation and an anti-GFP antibody for detection of IBI1-YFP. Based on the previously reported autointeraction of IBI1 (Schwarzenbacher et al., 2020), the combination of IBI1-FLAG and IBI-YFP was included as a positive control. As is shown in Fig. 3.2C, IBI1 was detected by anti-GFP upon immuno-precipitation with anti-FLAG when the IBI1-YFP construct was co-expressed with FAH2-FLAG or IBI1-FLAG (control), thereby confirming the *in planta* interaction between FAH2 and IBI1.

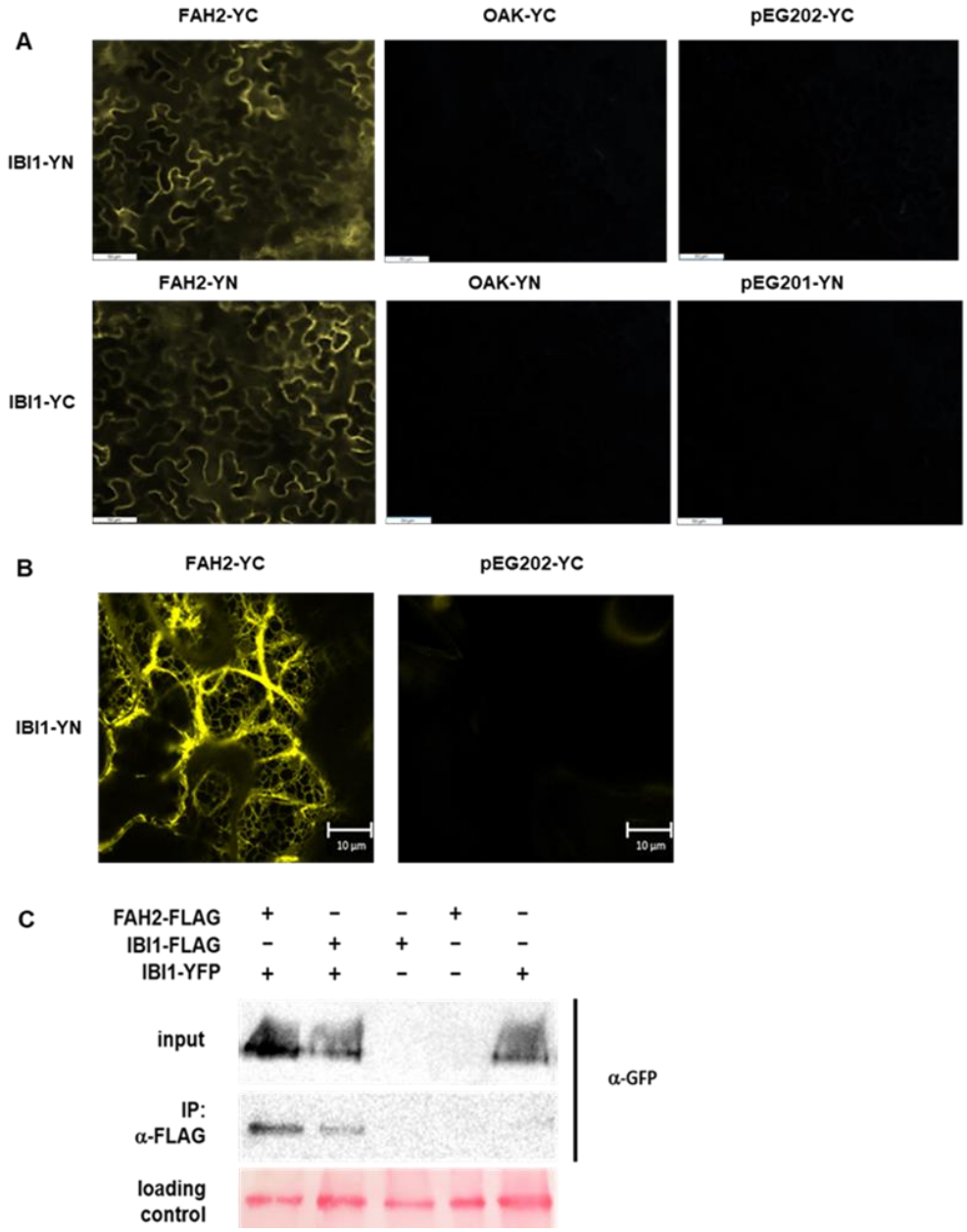

Figure 3.2. The fatty acid hydroxylase FAH2 interacts with the BABA receptor IBI1. The interaction between FAH2 and IBI1 was confirmed by bimolecular fluorescence complementation (BiFC; **A** - **B**) and co-immunoprecipitation (CoIP; **C**). For BiFC analysis, the amino-terminal (-YN) or carboxyl-terminal (-YC) half of Yellow fluorescent protein (YFP) were reciprocally fused to the C-terminal end of the interacting proteins. BiFC analysis was performed by co-infiltrating *Nicotiana benthamiana* leaves with *Agrobacterium tumefaciens* strains carrying the indicated BiFC constructs (2 days after infiltration). Yellow fluorescence was observed using epifluorescence microscopy **(A)** or confocal microscopy **(B)**. Co-infiltration of *IBI1-YN/YC* with *OUTGROWTH-ASSOCIATED PROTEIN KINASE* (*OAK*)-*YN/YC* or empty vectors (pEG202-YC, pEG201-YN) were used as a negative controls. For the CoIP assay **(C)**, *N. benthamiana* leaves co-infiltrated with *Agrobacterium tumefaciens* strains carrying the *FAH2-FLAG* and *IBI1-YFP* constructs (lane 1), *IBI1-FLAG* and *IBI1-YFP* constructs (lane 2), the *IBI1-FLAG* construct (lane 3), the *FAH2-FLAG* construct (lane 4) and the *IBI1-YFP* construct (lane 5). Samples for CoIP was collected at 3 days post infiltration (dpi). Total proteins were extracted from the leaves and incubated with anti-FLAG antibody for immunoprecipitation. Anti-GFP antibody was used for immunoblot detection of YFP-tagged proteins, and ponceau staining was used as a loading control for total proteins**.** Both experiments have been repeated once with similar results.

3.3.2 FAH2 regulates both BABA-IR and BABA-IS

To examine the role of FAH2 in plant responses to BABA, the effects of BABA on IR and IS were compared between wild-type and *fah2-1* plants (SALK_011293; Nagano et al., 2012b). Soil-drench treatment of Col-0 seedlings resulted in near-complete levels of BABA-IR against *Hpa* (Fig. 3.3A). Although similar treatment of *fah2* seedlings still resulted in a reduction of *Hpa* colonisation, this BABA-IR was strongly attenuated in comparison to Col-0 plants (Fig. 3.3A), which indicates that FAH2 has a contribution to BABA-IR. The stress response to BABA was examined by comparing growth phenotypes of Col-0, *ibi1-1* and *fah2-1* seedlings grown on ½-strength MS agar supplemented with 0mM or 5 mM BABA. Although previous research reported that the *fah2-1* mutation does not lead to an obvious growth phenotype (Nagano et al., 2012b), *fah2-1* seedlings developed marginally smaller leaf areas compared to Col-0 and *ibi1-1* plants when cultivated on control plates without BABA under our growth conditions (Fig. 3.3B and Supplemental Fig. 3.1A). Cultivation of seedlings on agar plates supplemented with 5 mM BABA revealed a complete lack of growth by the *ibi1-1* mutant (Fig. 3.3B and Supplemental Fig. 3.1B), confirming the previously reported hypersensitivity of this mutant to BABA (Luna et al. 2014). Furthermore, in comparison to Col-0, *fah2-1* seedlings on BABA medium showed less green leaf area (Fig. 3.3B and Supplemental Fig. 3.1B). To determine in how far this reduced growth is caused by increased sensitivity to BABA-IS, the reduction in green leaf area by BABA was calculated relative to the control conditions (i.e. *fah2-1* seedlings grown on medium without BABA). This analysis confirmed that the *fah2-1* mutant is more sensitive to BABA-induced growth reduction than the Col-0 wild-type (Fig. 3.3C). Hence, FAH2 has a quantitative contribution to both BABA-IR and BABA-IS.

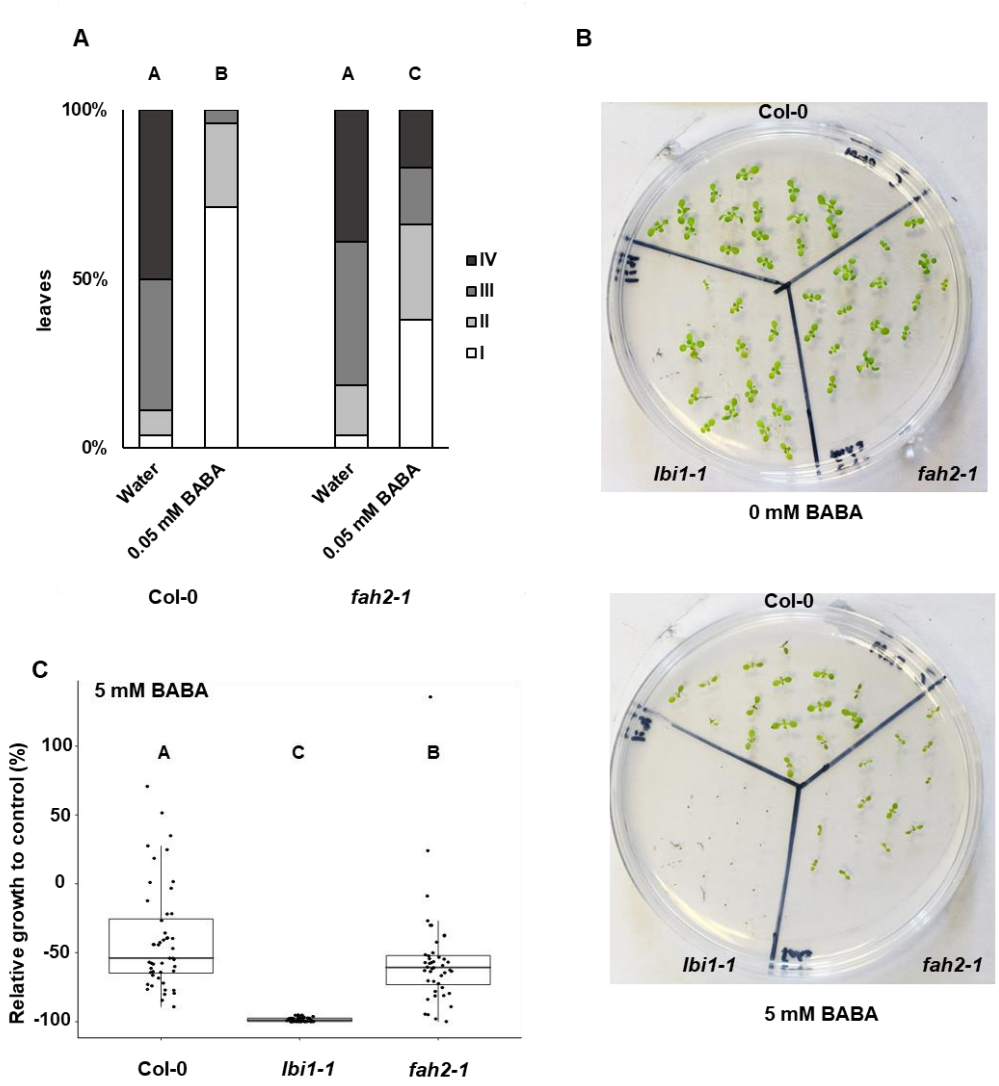

Figure 3.3. FAH2 controls both BABA-induced resistance and stress. (A) BABA-IR in Col-0 and the *fah2-1* mutant of Arabidopsis. Two-week-old seedlings were treatment with water (control) or 0.05 mM BABA by soil-drenching and challenged 2 days later by spraying with *Hpa* conidiospores solution. *Hpa* colonisation of leaves was examined at 6 days post inoculation (dpi) by assigning trypan blue-stained leaves to 4 different *Hpa* colonisation classes using a dissection microscope: (I) healthy, no colonisation, (II) hyphae colonisation with less than 10 conidiophores, (III) extensive hyphae colonisation with equal or more than 10 conidiophores, (IV) extensive hyphae colonisation with the presence of both conidiophores and sexual oospores. Shown are the relative frequency distributions. Different letters indicate statistically significant differences in class distribution between treatment/genotype combinations (Fisher's exact tests+ Bonferonni correction; $p < 0.05$; n=50-60 leaves; the experiment has been repeated once with similar results). **(B)** BABA reduces plant growth of Col-0, *ibi1-1* and *fah2-1* plants. Shown are 12-day-old seedlings of Col-0 (top), *ibi1-1* (bottom left) and *fah2-1* (bottom right) grown on ½ MS agar plates, supplemented with 0 (water) or 5 mM BABA **(C)** Relative growth reduction of 12-day-old Col-0, *ibi1-1* and *fah2-1* seedlings on BABA-containing ½ MS medium, relative to plants growing on ½ MS plate without BABA (control). Relative growth (%) was calculated by dividing individual green leaf areas on BABA-containing medium by the average green leaf area of the control from each genotype. Different letters indicate statistically significant differences in growth reduction (Kruskal-Wallis test followed by Wilcoxon signed-rank test; $p < 0.05$; n=39-48 seedlings; the experiment has been repeated once with similar results).

3.3.3 Role of FAH2 and IBI1 in global sphingolipid profiles upon BABA and *Hpa* treatment

FAH2 is a fatty acid α-hydroxylase, which targets the fatty acid chain of sphingolipids (König et al., 2012; Nagano et al., 2012b). To investigate whether FAH2-dependent changes in the sphingolipid profile play a role in the IBI1-dependent plant responses to BABA, ultrahigh pressure liquid chromatography (UPLC) coupled to triple quadrupole mass spectrometry (ULPC-QqQ) analysis was conducted of shoot samples from Col-0, *ibi1-1* and *fah2-1* upon BABA and/or *Hpa* treatment. Principal component analysis of all sphingolipid species revealed a clear separation of *fah2-1* from the other two genotypes (Col-0 and *ibi1-1*; Fig. 3.4A). Plotting sphingolipid quantities grouped by length of fatty acid moiety (LCFA < C20 versus VLCFA ≥ C20) and hydroxylation status of the second carbon atom in the fatty acid chain revealed that the *fah2-1* mutation drastically reduces hydroxylated LCFA sphingolipid content, while it increases the pool of un-hydroxylated LCFA sphingolipids (Supplemental Fig. 3.2A, B), thereby supporting previous reports (König et al., 2012; Nagano et al., 2012b; Ukawa et al., 2022). Interestingly, *fah2-1* plants also contained higher quantifies of VLCFA sphingolipids in both hydroxylated and non-hydroxylated forms (Supplemental Fig. 3.2C, D). In addition, the *ibi1-1* mutant, like *fah2-1*, appeared to have a higher content of sphingolipids with hydroxylated VLCFA (Supplemental Fig. 3.2D). To obtain a more detailed impression of the FAH2- and IBI1-dependent changes in sphingolipid species during BABA-IR, hierarchical clustering analysis (HCA) was performed on the log(x+1)-transformed values for each genotype-treatment combination. Since α-hydroxylation occurs downstream of ceramide formation (Pata et al., 2010), HCA was performed for ceramides, GlcCers and GIPCs separately (Fig. 3.4B-D). The *ibi1-1* mutant showed a strong increase in selected ceramide species after BABA only treatment, which was responsible for the separate clustering of BABA-treated *ibi1-1* samples (Fig. 3.4B). Since the *ibi1-1* mutant is hypersensitive to BABA-IS (Luna et al. 2014; Figs. 3.3B, C), it is likely that this response is associated with BABA-IS. Indeed, a similar, albeit weaker, increase in these ceramide species was observed upon BABA treatment of *fah2-1* plants (Fig. 3.4B). By contrast, *Hpa* repressed ceramide concentrations in untreated (susceptible) Col-0 but not in the more resistant BABA-treated Col-0 plants, suggesting that *Hpa* reduces ceramide content as a possible virulence strategy (Fig. 3.4B). Finally, as expected by the finding that α-hydroxylation occurs downstream of ceramide formation (Pata et al. 2010), HCA of both GlcCers

and GIPCs revealed a dominant effect by the *fah2-1* mutation. The distinct clustering of all *fah2-1* samples relative to all Col-0 and *ibi1-1* samples (Fig. 3.4C, D) was largely driven by the FAH2-dependent differences in LCFA GlcCers and GIPCs. However, the abundance of these FAH2-controlled sphingolipid species was not affected by the *ibi1-1* mutation, nor was it influenced by BABA and/or *Hpa* treatment (Fig. 3.4C, D). This indicates that the α-hydroxylation of LCFA GlcCers and GIPCs by FAH2 is unrelated to BABA-IR.

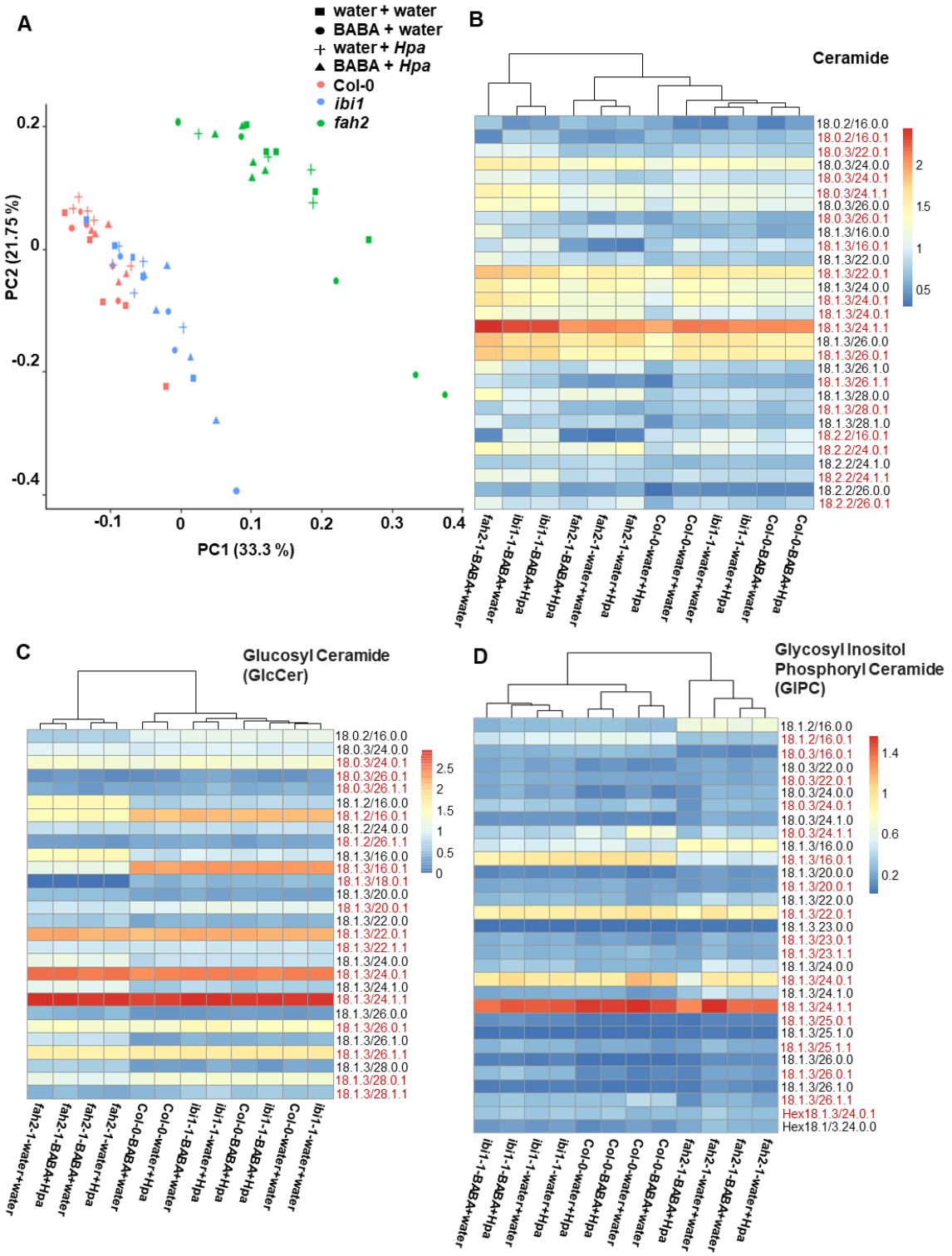

Figure 3.4. Impacts of FAH2 and IBI1 on the global sphingolipid profiles of Arabidopsis. Three-week-old plants were treated with water (control) or BABA (0.05 mM) and 2 days later challenged by spraying with mock solution (water) or *Hpa* conidiospores (10^5 spores/mL). Leaves of seedlings were collected for sphingolipids profiling by ULPC-QoQ mass spectrometry at 3 days post inoculation (dpi). **(A)** Principal Component Analysis (PCA) on all 60 samples collected for profiling. Ceramides **(B)**, glucosylceramides **(C)** and glycosyl inositol phosphoceramides **(D)** heatmaps project mean values (n=5) of sphingolipid species after log(x+1)-transformed (pmol/mg d.w.); red letter font indicates the 2C-hydroxylated sphingolipid species. Hierarchical clustering was based on complete-linkage by Euclidean distance.

3.3.4 Identification of a FAH2- and IBI1-dependent VLCFA GIPC that is responsive to BABA and *Hpa* treatments

Although the main α-hydroxylation activity by FAH2 on LCFA GlcCers and GIPCs appeared to be unrelated to IBI1-dependent BABA-IR, it is still possible that FAH2 has secondary activities related to BABA-IR. To identify the corresponding FAH2- and IBI1-dependent sphingolipids, two-way ANOVA was performed on each sphingolipid species, which allowed for the selection for sphingolipid species that are statistically influenced by both genotype and BABA/*Hpa* treatment (Supplemental Fig. 3.3). The analysis identified the α-hydroxylated VLCFA GIPC 18.0.3/24.1.1, which displayed a statistically significant response to genotype and treatment, as well as a statistically significant genotype x treatment interaction (Fig. 3.5A and Supplemental Fig. 3.3). Plotting the concentration values of this GIPC species revealed that un-treated *ibi1-1* and *fah2-1* contain reduced basal levels compared to un-treated Col-0 plants (Fig. 3.5A). Furthermore, GIPC 18.0.3/24.1.1 was responsive to BABA/*Hpa* in Col-0 but not *ibi1-1* and *fah2-1*. Single treatment of Col-0 plants with BABA or *Hpa* induced a weak and variable reduction in GIPC 18.0.3/24.1.1, respectively, while this reduction was far more pronounced upon BABA treatment and subsequent *Hpa* challenge, reaching concentrations that were statistically similar to the reduced concentrations in *ibi1-1* and *fah2-1* (Fig. 3.5A). Hence, GIPC 18.0.3/24.1.1 is produced in a IBI1- and FAH2-dependent manner and BABA augments the *Hpa*-inducible breakdown of this sphingolipid. To determine in how far this pattern is due to α-hydroxylation by FAH2, the non-hydroxylated counter-species, GIPC 18.0.3/24.1.0, was plotted (Fig. 3.5B). Although the concentrations of non-hydroxylated GIPC 18.0.3/24.1.0 were an order of lower than the α-hydroxylated GIPC 18.0.3/24.1.1, their patterns generally mirrored each other (Figs. 3.5A, B). These results suggest that IBI1 facilitates FAH2-dependent production of GIPC 18.0.3/24.1.1, which acts as the pre-cursor of an *Hpa*-inducible defence signal, whose GIPC 18.0.3/24.1.1-dependent production is primed by BABA.

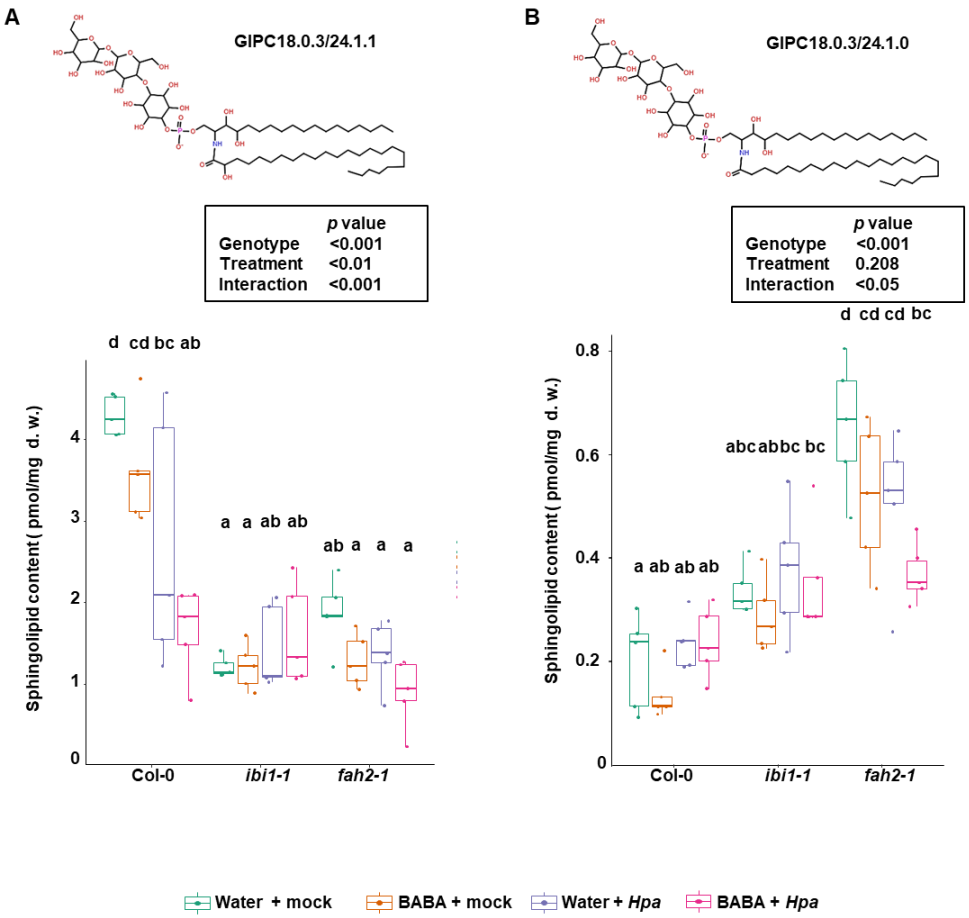

Figure 3.5. Genotype- and treatment-dependent accumulation of GIPC18.0/3.24.1.0 and GIPC18.0/3.24.1.1. Concentrations of **(A)** GIPC18.0.3/24.1.1 and **(B)** 18.0.3/24.1.0 in leaves of 3-week-old Col-0, *ibi1-1* and *fah2-1* after soil-drench treatment with water (control) or 0.05 mM BABA and subsequent spray inoculation with mock solution or *Hpa* conidiospores at 2 days after water/BABA treatment. Tissues were harvested at 3 days post inoculation (dpi). Insets show statistically significant effects on GIPC18.03/24.1.1 by genotype, treatment and interaction and GIPC18.0.3/24.1.0 by genotype and interaction (two-way ANOVA). Different letters indicate significant differences between samples (Tukey's post hoc test; $p < 0.05$, n=5).

3.3.5 Role of FAH2 in the BABA-induced priming of pathogen-induced translocation of IBI1 from the ER to the cytosol

Dysfunctional α-hydroxylase activity by FAH enzymes disturbs membrane integrity and affects protein distribution and exchange between membrane fractions (Nagano et al., 2016; Ukawa et al., 2022). Previously, Luna et al. (2014) demonstrated that BABA primes the release of IBI1 from the ER membrane to cytosol upon *Hpa* inoculation. To examine whether this BABA-induced priming is controlled by FAH2, the *35Spro::IBI1-YFP* was introgressed into the background of *fah2-1* mutation line and

examined by confocal scanning microscopy under control and BABA-primed conditions following mock and *Hpa* inoculation. As reported before, a clear mobilisation of IBI1 from the ER to cytosol was observed in BABA-treated *35Spro::IBI1-YFP* after *Hpa* inoculation (Fig. 3.6A ; Luna et al., 2014). Interestingly, BABA-treated *fah2/35Spro::IBI1-YFP* plants failed to show a clear cytosolic translocation of IBI1-YFP upon subsequent *Hpa* inoculation (Fig. 3.6A). However, the YFP fluorescence intensity in *fah2/35Spro::IBI1-YFP* plants was reduced across all treatments in comparison to *35Spro::IBI1-YFP* plants, which may have confounded the detection of the cytosolic translocation by IBI1-YFP (Fig. 3.6A). To verify that the reduced quantities of IBI1:YFP in *fah2/35Spro::IBI1-YFP* are due to post-transcriptional/translational processes, the levels of *IBI1*:*YFP* transcription were quantified by RT-qPCR, using primers against the *IBI1* and *YFP* sequences. Surprisingly, this assay revealed significant reductions in the relative quantities of *IBI1* and *YFP* mRNA in *fah2/35Spro::IBI1-YFP* plants relative to *35Sprop::IBI1-YFP* plants. Hence, the reduced presence of YFP fluorescence signals observed by confocal microscopy are likely caused by reduced transcription of the *IBI1-YFP* transgene in *fah2/35Spro::IBI1-YFP* (Fig. 3.6B and Supplemental Fig. 3.4).

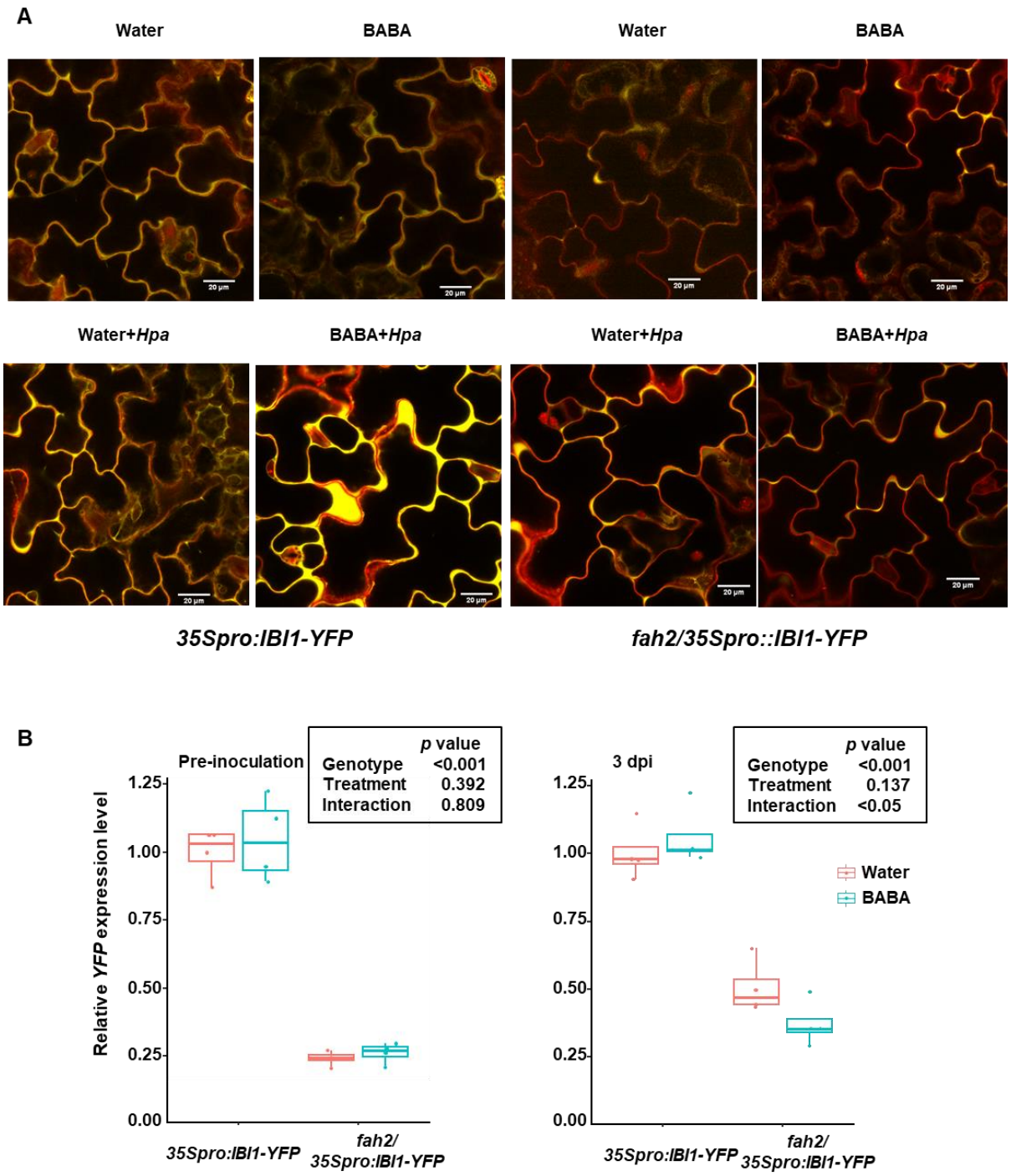

Figure 3.6. Effects of the *fah2-1* mutation on the subcellular localisation of IBI1-YFP and transcription of the *35Spro::IBI1-YFP* cassette. (A) Confocal microscopy photos of IBI1-YFP in water- or BABA-treated *35Spro::IBI1-YFP* and *fah2/35Spro::IBI1-YFP* before and after *Hpa* inoculation (3 dpi). White bars in the photos represent scale bar (20 µm). **(B)** Relative *YFP* expression level in water- or BABA-treated *35Spro::IBI1-YFP* and *fah2/35Spro::IBI1-YFP* before and after *Hpa* inoculation (3 dpi). Insets show statistically significant effects on *YFP* expression by genotype before inoculation and by genotype and interaction after inoculation (3 dpi; two-way ANOVA). Both experiments have been repeated once with similar results.

3.4 Discussion

3.4.1 FAH2, a interactor of IBI1 and a regulator of BABA-induced signalling

The results presented in this Chapter provide evidence that the fatty acid hydroxylase FAH2 is a regulator of both BABA-IR and BABA-IS. In addition to the physical interaction between IBI1 and FAH2 (Fig. 3.2), mutation of the *FAH2* gene reduced BABA-IR against *Hpa* and makes Arabidopsis more sensitive toward BABA-IS. Hence, the *fah2-1* mutation weakly mimics the phenotype of the *ibi1-1* mutant (Fig. 3.3; Luna et al., 2014). Sphingolipid profiling by UPLC-QqQ analysis furthermore revealed a major shift in the sphingolipid composition by the *fah2-1* mutation, which was largely driven α-hydroxylation of LCFA GlcCers and GIPCs (Fig. 3.4A, and 3.4C, D). However, this primary FAH2 activity appeared unrelated to BABA-IR, since the concentrations of FAH2-dependent C16 sphingolipids were not affected by BABA/*Hpa* treatment or the *ibi1-1* mutation (Fig. 3.4C, D). Nevertheless, the profiling also detected secondary activities by FAH2. For instance, both *ibi1-1* and *fah2-1* plants showed similar shifts in ceramide profiles upon BABA treatment (Fig. 3.4B), suggesting that this response is linked to the increased sensitivity to BABA-IS of these mutants (Fig 3.4 and Supplemental Fig 3.2). It remains, however, unclear how α-hydroxylation by FAH2 affects the ceramide concentrations, since this activity is suggested to occur downstream of ceramide formation (Pata et al., 2010). Furthermore, statistical selection of sphingolipid species displaying a statistically significant change in response to both BABA/*Hpa* treatment and genotype revealed the GIPC 18.0.3/24.1.1, whose content changes differently in Col-0 when compared to the other two genotypes (Supplemental Fig. 3.3). Moreover, this α-hydroxylated VLCFA GIPC showed a pattern that is consistent with a mechanism by which IBI1 facilitates GIPC 18.0.3/24.1.1 production, which acts as a negative regulator of BABA-IR (Fig. 3.7). In this scenario, the IBI1-FAH2 interaction induces production of GIPC 18.0.3/24.1.1, which generate ER nanodomains that retain IBI1 to the ER membrane. BABA treatment then reduces the physical interaction of BABA-bound IBI1 with FAH2, which affects FAH2 activity and/or diffuses GIPC 18.0.3/24.1.1 in IBI1-retaining nanodomains, thereby loosening the anchorage of IBI1 to the ER membrane. Subsequent *Hpa* challenge results in ER stress that is known to cause ER autophagy (ER-Phagy; Park and Park, 2020), during which GIPC 18.0.3/24.1.1 is broken down. This *Hpa*-induced reduction in GIPC 18.0.3/24.1.1 in the ER membrane enables the primed release of loosened BABA-IBI1

from the ER to the cytosol, where it interacts with defence signalling proteins, such as VOZ1/2, and mediate augmented defence (Schwarzenbacher et al. 2020; Fig. 3.7). Support for this hypothesis comes from a previous findings that sphingolipids contribute to stress regulation directly or through their catabolites (Huby et al., 2020). For example, GIPC sphingolipids act as receptor for a group of pathogens toxins, necrosis and ethylene-inducing peptide 1-like proteins (NLPs) in eudicots (Lenarčič et al., 2017). Furthermore, a sphingolipid derivative, phytosphingosine-1-phosphate, can regulate stomata response, which associates with pathogens entering the plants (Coursol et al., 2005).

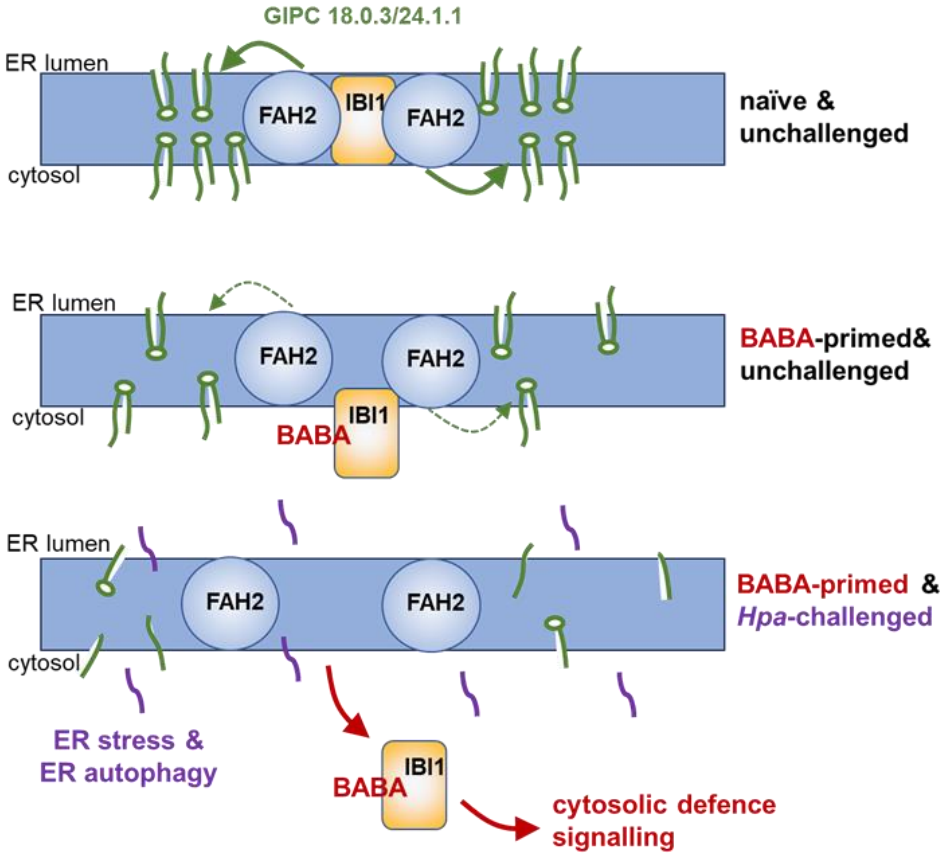

Figure 3.7. Model of the IBI1- and FAH2-dependent role of the GIPC 18.0.3/24.1.1 in BABA-IR against *Hpa*. In naive un-challenged plants, the interaction between FAH2 and IBI1 stimulates GIPC 18.0.3/24.1.1 deposition in ER nanodomains, which keep IBI1 firmly anchored to the ER. Priming with BABA affects the physical interaction between IBI1 with FAH2, which reduces FAH2 activity and/or diffuses GIPC 18.0.3/24.1.1 in the IBI1-retaining nanodomains, resulting in a weakened anchorage of IBI1 to the ER membrane (Luna et al. 2014). *Hpa* challenge results in ER stress and ER autophagy, causing degradation of GIPC 18.0.3/24.1.1 (purple lines) and the release of IBI1 to the cytosol, where it interacts with defence-inducing signalling proteins (Schwarzenbacher et al. 2020). Because BABA had already reduced the anchoring of IBI1 to the ER membrane, this defence response is augmented in BABA-primed cells.

3.4.2 How can FAH2 regulate BABA-induced stress responses

The phytotoxicity of BABA is a major barrier against commercial exploitation of the compound in crop protection. This BABA-IS, which includes growth reduction and anthocyanin accumulation, is the result of non-canonical binding of R-BABA to the aspartic acid-binding pocket of IBI1 (Wu et al., 2009; Luna et al., 2014). As an aspartyl-tRNA synthetase, IBI1 primarily binds to L-aspartic acid (L-Asp) to charge cognate tRNAs (Gomez and Ibba, 2020). In the presence of BABA, BABA physically interacts with IBI1 and interferes with the tRNA synthetase activity (Luna et al., 2014). The hyperaccumulation of uncharged tRNA is sensed by the protein kinase GCN2, which in turn phosphorylates the eukaryotic translation initiation factor 2 (eIF2-α) to repress/alter gene translation, resulting in an amino acid starvation response (Luna et al., 2014). Challenging *gcn2-1* mutant plants with BABA showed reduced phytotoxicity responses under high concentration but intact BABA-IR (Luna et al. 2014), indicating that the undesirable BABA-IS response is linked to the GCN2 pathway and distinct from the regulation of BABA-IR. In this Chapter, *FAH2* was found to be essential for both processes, meaning it acts upstream of the bifurcation in the BABA-induced pathways controlling IR and IS respectively (Fig. 3.3).

Since FAH2 interacts physically with IBI1 at the ER (Fig. 3.2B), our results indicate that it might act as an anchor to stabilise IBI1 at the ER membrane. Alternatively, since both FAH1 and FAH2 contribute to membrane nanodomain formation, it is possible that FAH2-dependent sphingolipids create nanodomains in the ER membrane that favour the interaction and retainment of ER-associated proteins, such as IBI1 (Nagano et al., 2016; Ukawa et al., 2022; Fig. 3.7). In both scenarios, the *fah2-1* mutation would reduce level of free IBI1 that can bind to BABA, thereby lowering the BABA threshold concentration to cause phytotoxicity. Previously, BABA-IR was found to not only depend on the expression of *IBI1* (Luna et al. 2014), but also by its ability to interact with downstream regulators (Schwarzenbacher et al., 2020) and the ability of the plant to take up BABA (Chapter 2; Tao et al. 2022). Ukawa et al. (2022) recently reported that cell membrane nanodomains were severely reduced in the *fah1c fah2* double mutant, causing a major reduction in the abundance of cell membrane-located proteins. Since the membrane-located amino acid transporter, LHT1, acts as the BABA transporter, it is possible that FAH2 indirectly affects the cellular uptake of BABA (Tao et al., 2022).

3.4.3 Will FAH1, a FAH2 homolog, also interact with IBI1 and contribute in BABA-induced signalling?

The two FAHs in Arabidopsis, FAH1 and FAH2, are highly homologous, yet act on different substrates (Nagano et al., 2012b; Nagano et al., 2012a; Ukawa et al., 2022). Nagano et al. (2012b) demonstrated that both proteins interact with BAX INHIBITOR 1 (BI-1) through Cb_5, with FAH1 having stronger affinity to BI-1 than FAH2. Although FAH1 was not identified as a potential interactor with IBI1 (Schwarzenbacher et al., 2020), the high degree of homology between FAH1 and FAH2 makes it possible that FAH1 also interacts with IBI1, albeit with lower affinity. Like FAH2, FAH1 could contribute to BABA-IR by participating in nanodomain formation. In addition, FAH1 and BI-1 complexes primarily suppress cell death, which is an effective means to limit colonisation by biotrophic pathogens (Nagano et al., 2012b). If IBI1 also interacts with FAH1, it is plausible that BABA treatment can enforce the interaction, leading to competition between IBI1 and BI-1 and, as a result, lifting the suppression force on cell death. Further analysis of the IBI1-FAH1 interaction in the presence and absence of BABA, as well as further characterisation of the BABA-IR phenotype *fah1* single mutant and *fah1 fah2* double mutant would be required to validate this hypothesis further.

3.4.4 FAH2 might control IBI1 translocation

Finally, it remains highly plausible that FAH2 activity controls the defence-related translocation of IBI1 from the ER membrane to the cytosol during BABA-IR. Indeed, confocal microscopy analysis of *fah2/35Spro::IBI1-YFP* revealed lack of cytosolic translocation of IBI1-YFP during BABA-IR against *Hpa* (Fig. 3.6A). However, the reduced YFP signal in the *fah2* background due to repressed IBI1-YFP transcription was a confounding factor for this experiment (Fig. 3.6B and Supplemental Fig. 3.5). While it remains difficult to explain how reduced sphingolipid hydroxylation by FAH2 influences 35S-driven transcription of *IBI1-YFP*, quantification of cytosolic YFP fluorescence in replicated samples from water/BABA-treated plants upon mock/*Hpa* challenge would be required to confirm that FAH2 indeed controls the defence-related release of IBI1 from the ER to the cytosol during BABA-IR.

3.5 Methods

3.5.1 Biological material

All *Arabidopsis thaliana* lines used in this study are in the Col-0 background and characterised previously: *ibi1-1, 35Spro::IBI1-YFP* (Luna et al., 2014) and *fah2-1* (Nagano et al., 2012b). The *fah2/35Spro::IBI1-YFP* was generated by crossing *fah2-1* with *35Spro::IBI1-YFP*. Plants homozygous both the *fah2-1* mutation and *35Spro::IBI1-YFP* were identified by PCR-based genotyping, using gene-specific primers and the left border T-DNA primer listed in Supplemental Table 1, and segregation analysis of YFP-fluorescence, respectively. *Hyaloperonospora arabidopsidis* strain WACO9 (*Hpa*) was kept under the asexual cycle by alternatively propagating on Col-0 and Ws *NahG* plants via conidiospore inoculations.

3.5.2 Plant growth conditions

Arabidopsis seeds were stratified in 0.18% agar at 4℃ in the dark for 2-3 days before planting. Seeds were sown on a mix of 2:1 (v/v) Levington M3 soil: sand. Plants for BABA-IR assays, confocal microscopy imaging, and lipid profiling were cultivated under in environment conditions under short-day conditions (8.5 hours light/day; 150 µmol/m^2/s, at 21°C and 15.5 hours dark/day at 18°C) with 60% relative humidity (RH). *Nicotiana benthamiana* were cultivated under long-day conditions (16 hours light/day; 150 µmol/m^2/s at 21°C and 8 hours dark at 18 °C) at 60% RH in a controlled growth chamber. For agar plate assays to quantify BABA-IS, Arabidopsis seeds were vapour-sterilized with chlorine gas (Lindsey III et al., 2017) and planted onto ½-strength Murashige & Skoog (MS) agar plates containing 1% sucrose. Plates were kept in the dark at 4 ℃ for 2-3 days to stratify and then transferred to similar long-day similar conditions as detailed above.

3.5.3 BABA-induced resistance assay

The BABA-IR assay was conducted as described by Schwarzenbacher et al. (2020). Two-week-old seedlings in 60 mL pots were soil-drenched with water or BABA at the indicated final concentrations. Two days after application, plants were spray-inoculated with *Hpa* conidiospores (10^5 spores/mL) and kept at 100% RH to facilitate

infection. Six days post-inoculation, seedlings were collected for trypan blue staining to visualise and quantify *Hpa* colonisation under a dissecting microscope. Leaves were categorised into four *Hpa* colonisation classes, ranging from healthy leaf (I) to heavily colonised leaf (IV), as detailed by Schwarzenbacher et al. (2020) and Tao et al. (2022; Chapter 2). Statistical differences in *Hpa* colonisation were analysed by pairwise Fisher's exact tests with Bonferroni multiple correction, using the package 'fifer' (fifer_1.1.tar.gz) in R software (v 3.5.1).

3.5.4 BABA-induced stress assay

Vapour-sterilised seeds were grown on ½-strength MS agar plates for 12 days. Photos were taken after 12 days of growth using a Nikon D5300 camera, and the green leaf area (GLA) was quantified from the photos using Fiji/ImageJ software (Rueden et al., 2017). To quantify the relative contribution of BABA to plant growth repression, GLA from individual plants on plates supplemented with 5 mM were divided by the average GLA of plants grown on the control plate without BABA. Statistical differences in GLA and growth changes were determined by Kruskal-Wallis test, followed by Wilcoxon signed-rank test, using R software (v 3.5.1).

3.5.5 Subcellular localisation of IBI1-YFP

Plants were grown and treated with BABA and *Hpa,* as described above. To study the subcellular localisation of IBI1-YFP, samples were harvested either 2 days after water/BABA treatment, or 3 days after challenge with mock/*Hpa*, as described previously (Luna et al. 2014). To examine the subcellular localisation of IBI1-YFP, 6 plants were collected per treatment and vacuum-infiltrated with propidium iodide (100 µg/mL; Sigma-Aldrich, #P4170) to stain the cell walls. The subcellular localisation was observed and imaged by confocal scanning microscopy (Nikon A1) using a Plan Fluor 40× oil immersion object lens (numerical aperture=1.3). YFP was excited at 488 nm, and emission was collected at 500-550 nm. Propidium iodide was excited at 562 nm, and emission was collected at 570-620 nm.

3.5.6 Real-time quantitative PCR analysis

To quantify *IBI1-YFP* expression, four seedlings were pooled into one biological replicate and -frozen in liquid N_2. A total of 4 biological replicates/per treatment were collected for RT-qPCR analysis. Tissues were homogenised and total RNA was extracted using the RNeasy Plant Mini Kit (Qiagen, cat. no. 74904). The Maxima First Strand cDNA Synthesis Kit (Thermo Fisher, cat. no. K1641) was used to synthesise cDNA from 800 ng RNA. All qPCR reactions were carried out with ten times diluted cDNA and 250 nM primer concentration in a Rotor-Gene Q real-time PCR cycler (Qiagen, Q-Rex v1.0), using the Rotor-Gene SYBR Green PCR Kit (Qiagen, cat. no. 204074). The qPCR amplification of *YFP*, *IBI1,* and two housekeeping genes (*At2g28390* and *At5g25760*) was performed with gene-specific primers (Supplemental Table 3.1). The expression of *YFP* and *IBI1* was normalised to the expression level of two housekeeping genes, as detailed in Schwarzenbacher et al. (2020). Statistical differences in expression level were determined by two-way ANOVA, using R software (v 3.5.1).

3.5.7 Bimolecular fluorescence complementation assay

Assays were performed as described previously (Schwarzenbacher et al., 2020). In short, coding sequences (without out stop codon) of target genes were amplified by Phusion High-Fidelity DNA Polymerase (New England Biolabs, #M0530L) from Arabidopsis cDNA. After amplification, sequences were cloned into pENTR plasmids. Gateway cloning was conducted to ligate the coding sequences into pEarleygate201-YN (pEG201-YN) and pEarleygate202-YC (pEG202-YC) vectors for generating BiFC expression vectors. Four to six-week-old *N. benthamiana* plant leaves were infiltrated with *Agrobacterium tumefaciens* (strain GV3101::pMP90) transformed with the appropriate constructs. YFP fluorescence was observed three days after injection by using Leica DM6B upright microscope (excitation filter: 460-490 nm, emission filter: 510-550 nm, dichromatic filter: 505 nm) and Zeiss LSM880 confocal microscope (excitation:514 nm, emission: 526-560 nm).

3.5.8 Co-immunoprecipitation assay

Genes were cloned as described above for the BiFC assays. The FLAG- and YFP-tagged coding sequences were cloned into pGW512 and pEarleygate101, respectively.

Leaf infiltration was performed with four- to six-week-old *N. benthamiana* plants. Three days post infiltration, leaf samples were collected for protein extraction. Protein extraction and immunoprecipitation were conducted as described by Luna et al. (2014). Briefly, total proteins were extracted from one gram of leaf sample with 2.4 ml protein extraction buffer (50 mM Tris-HCl, pH 7.5, 150 mM NaCl, 10% (v/v) glycerol, 0.1% (v/v) Nonidet P-40, 1mM PMSF, and 10u/ml Sigma protease inhibitor cocktail) by using pestle and mortar. Samples were centrifuged at 12,000g for 10 min at 4°C twice, and supernatant was collected and combined after each centrifugation. Protein concentration was quantified by using Bradford assay (Sigma, #B6916), adjusted to 2.1mg/ml for each sample and incubated with anti-flag magnetic beads (Sigma, #M8823) at 4°C overnight. Beads were pelleted by using magnetic rack and washed with washing buffer (50 mM Tris-HCl, pH 7.5, 150 mM NaCl, 10% glycerol, 0.1% Nonidet P-40) twice, then boiled 5 mins in protein loading buffer (0.25 M Tris-HCl, pH 6.8, 2.2% (w/v) SDS, 10% (v/v) glycerol, 2.5% (v/v) 2-mercaptoethanol, 1 mg/ mL bromophenol blue). Proteins were separated on 8 - 16% Mini-PROTEAN TGX Precast Protein gels (Bio-Rad #4561104) and transferred to PVDF membrane using Bio-Rad Mini Protean 3 system, following manufacturer instruction. Ponceau staining was conduct by using Ponceau S solution (Sigma, #P7170). Detection of YFP fusion proteins was performed by immunoblotting with an anti-GFP (Abcam, #ab290) primary antibody and anti-rabbit IgG (Cell Signalling, #7074) secondary antibody in 1:5000 and 1:20000 dilution, respectively. Chemiluminescent detection was performed with Amerhsam ECL Prime Western Blotting Detection Reagent (GE Healthcare, #RPN2232) and Syngene G:Box Chemi XRQ system (Syngene, UK).

3.5.9 Sphingolipid profiling

Three-week-old seedlings were used for sphingolipid profiling. Plants were treated with water or BABA, as described above, and inoculated with mock or *Hpa* (10^5 spores/mL) 2 days later. Plants were kept in 100% RH condition to promote infection. Three days after inoculation, 25 seedlings were pooled into one biological replicate, and a total of five biological replicates were collected per genotype/treatment combination. Samples were frozen in liquid nitrogen. A total of 100 mg of homogenised tissue was used for sphingolipid extraction. Sphingolipid extraction and analysis were performed as described previously (Zienkiewicz et al., 2020). Briefly, frozen

homogenised tissue was resuspended in isopropyl alcohol/hexane/water (60:26:14,v/v/v) and incubated at 60℃ for 30 mins, then centrifuged at 635 g for 20 mins. Supernatant was collected after centrifugation and dried under nitrogen stream. Extracts were dissolved in methanol/tetrahydrofuran/water (4/4/1, v/v/v). Sphingolipid extracts were first reversed-phase-separated with ACQUITY UPLC HSS T3 column (100 mm x 1 mm, 1.8 µm) in ACQYITY UPLC system (Waters Crop, USA) and analysed by nano ESI (Advion BioSceinces, USA) equipped with a 6500 QTRAP tandem mass spectrometer (AB Sciex, USA). Data was processed and analysed as described by (Tarazona et al., 2015). Heatmaps of sphingolipid content were generated by using pheatmap package (Kolde and Kolde, 2015) in R software (v 3.5.1). Statistical differences in individual sphingolipid content were determined by two-way ANOVA following by Bonferroni multiple correction, using R software (v 3.5.1).

3.6 Acknowledgements

We thank the technical support from the Wolfson Light Microscopy Facility. Imaging work was performed at the Wolfson Light Microscopy Facility, using the Nikon A1 and Zeiss LSM880 confocal microscopes. This work was supported by a grant from the European Research Council (ERC; no. 309944 "*Prime-A-Plant*") to J.T., two BBSRC-IPA grants to J.T. (BB/P006698/1 and BB/W015250/1) and supplementary grant from Enza Zaden to J.T., and a ERC-PoC grant to JT (no. 824985 "*ChemPrime"*).

3.7 Author Contributions

J.T. and R.S. conceived the research; C.-N.T, R.S., and J.T. designed the experiments; C.-N.T (Figs. 3.1, 3.2, 3.3, 3.4, 3.5, Supplemental Figs. 3.1, 3.2, 3.3, 3.4), R.S. (Figs. 3.1, 3.2, 3.3, 3.4, Supplemental Figs. 3.2, 3.3), and C.H. (Figs. 3.3, 3.4, Supplemental Figs.3.2, 3.3) conducted the experiments; C.-N.T, R.S., C.H., I.F. and J.T. analyzed the data; C.-N.T, and J.T. wrote the paper.

3.8 References

Balmer, A., Glauser, G., Mauch-Mani, B., and Baccelli, I. (2019). Accumulation patterns of endogenous β-aminobutyric acid during plant development and defence in *Arabidopsis thaliana*. Plant Biology 21, 318-325.

Berkey, R., Bendigeri, D., and Xiao, S. (2012). Sphingolipids and plant defense/disease: the "death" connection and beyond. Frontiers in Plant Science 3, 68.

Bücherl, C.A., Jarsch, I.K., Schudoma, C., Segonzac, C., Mbengue, M., Robatzek, S., MacLean, D., Ott, T., and Zipfel, C. (2017). Plant immune and growth receptors share common signalling components but localise to distinct plasma membrane nanodomains. eLife 6, e25114.

Buswell, W., Schwarzenbacher, R.E., Luna, E., Sellwood, M., Chen, B., Flors, V., Pétriacq, P., and Ton, J. (2018). Chemical priming of immunity without costs to plant growth. New Phytologist 218, 1205-1216.

Cohen, Y., Vaknin, M., and Mauch-Mani, B. (2016). BABA-induced resistance: milestones along a 55-year journey. Phytoparasitica 44, 513-538.

Coursol, S., Le Stunff, H., Lynch, D.V., Gilroy, S., Assmann, S.M., and Spiegel, S. (2005). Arabidopsis sphingosine kinase and the effects of phytosphingosine-1-phosphate on stomatal aperture. Plant Physiology 137, 724-737.

Gomez, M.A.R., and Ibba, M.J.R. (2020). Aminoacyl-tRNA synthetases 26, 910-936.

Gronnier, J., Gerbeau-Pissot, P., Germain, V., Mongrand, S., and Simon-Plas, F. (2018). Divide and Rule: Plant Plasma Membrane Organization. Trends in Plant Science 23, 899-917.

Huby, E., Napier, J.A., Baillieul, F., Michaelson, L.V., and Dhondt-Cordelier, S. (2020). Sphingolipids: towards an integrated view of metabolism during the plant stress response. New Phytologist 225, 659-670.

Kolde, R., and Kolde, M.R.J.R.p. (2015). Package 'pheatmap' 1, 790.

König, S., Feussner, K., Schwarz, M., Kaever, A., Iven, T., Landesfeind, M., Ternes, P., Karlovsky, P., Lipka, V., and Feussner, I. (2012). Arabidopsis mutants of sphingolipid fatty acid α-hydroxylases accumulate ceramides and salicylates. New Phytologist 196, 1086-1097.

Lenarčič, T., Albert, I., Böhm, H., Hodnik, V., Pirc, K., Zavec, A.B., Podobnik, M., Pahovnik, D., Žagar, E., Pruitt, R., Greimel, P., Yamaji-Hasegawa, A., Kobayashi, T., Zienkiewicz, A., Gömann, J., Mortimer, J.C., Fang, L., Mamode-Cassim, A., Deleu, M., Lins, L., Oecking, C., Feussner, I., Mongrand, S., Anderluh, G., and Nürnberger, T. (2017). Eudicot plant-specific sphingolipids determine host selectivity of microbial NLP cytolysins. Science 358, 1431-1434.

Lherminier, J., Elmayan, T., Fromentin, J., Elaraqui, K.T., Vesa, S., Morel, J., Verrier, J.L., Cailleteau, B., Blein, J.P., and Simon-Plas, F. (2009). NADPH oxidase-mediated reactive oxygen species production: subcellular localization and reassessment of its role in plant defense. Molecular Plant-Microbe Interactions 22, 868-881.

Lindsey III, B.E., Rivero, L., Calhoun, C.S., Grotewold, E., and Brkljacic, J. (2017). Standardized method for high-throughput sterilization of Arabidopsis seeds. JoVE, e56587.

Luna, E., van Hulten, M., Zhang, Y., Berkowitz, O., López, A., Pétriacq, P., Sellwood, M.A., Chen, B., Burrell, M., van de Meene, A., Pieterse, C.M.J., Flors, V., and Ton, J. (2014). Plant perception of β-aminobutyric acid is mediated by an aspartyl-tRNA synthetase. Nature Chemical Biology 10, 450-456.

Mamode Cassim, A., Grison, M., Ito, Y., Simon-Plas, F., Mongrand, S., and Boutté, Y. (2020). Sphingolipids in plants: a guidebook on their function in membrane architecture, cellular processes, and environmental or developmental responses. FEBS 594, 3719-3738.

Martinière, A., and Zelazny, E. (2021). Membrane nanodomains and transport functions in plant. Plant Physiology 187, 1839-1855.

Nagano, M., Uchimiya, H., and Kawai-Yamada, M. (2012a). Plant sphingolipid fatty acid 2-hydroxylases have unique characters unlike their animal and fungus counterparts. Plant Signaling & Behavior 7, 1388-1392.

Nagano, M., Takahara, K., Fujimoto, M., Tsutsumi, N., Uchimiya, H., and Kawai-Yamada, M. (2012b). Arabidopsis sphingolipid Fatty Acid 2-Hydroxylases (AtFAH1 and AtFAH2) are functionally differentiated in fatty acid 2-hydroxylation and stress responses. Plant Physiology 159, 1138-1148.

Nagano, M., Ishikawa, T., Fujiwara, M., Fukao, Y., Kawano, Y., Kawai-Yamada, M., and Shimamoto, K. (2016). Plasma membrane microdomains are essential for Rac1-RbohB/H-mediated immunity in rice. The Plant cell 28, 1966-1983.

Nagano, M., Ihara-Ohori, Y., Imai, H., Inada, N., Fujimoto, M., Tsutsumi, N., Uchimiya, H., and Kawai-Yamada, M. (2009). Functional association of cell death suppressor, Arabidopsis Bax inhibitor-1, with fatty acid 2-hydroxylation through cytochrome b5. The Plant Journal 58, 122-134.

Park, W.J., and Park, J.W. (2020). The role of sphingolipids in endoplasmic reticulum stress. FEBS letters 594, 3632-3651.

Pata, M.O., Hannun, Y.A., and Ng, C.K.-Y. (2010). Plant sphingolipids: decoding the enigma of the Sphinx. New Phytologist 185, 611-630.

Rueden, C.T., Schindelin, J., Hiner, M.C., DeZonia, B.E., Walter, A.E., Arena, E.T., and Eliceiri, K.W. (2017). ImageJ2: ImageJ for the next generation of scientific image data. BMC Bioinformatics 18, 1-26.

Schwarzenbacher, R. (2017). Signalling mechanisms by which the aspartyl-tRNA synthetase IBI1 controls broad-spectrum induced resistance in Arabidopsis thaliana (University of Sheffield).

Schwarzenbacher, R.E., Wardell, G., Stassen, J., Guest, E., Zhang, P., Luna, E., and Ton, J. (2020). The IBI1 receptor of β-aminobutyric acid interacts with voz transcription factors to regulate abscisic acid signaling and callose-associated defense. Molecular Plant 13, 1455-1469.

Tao C-N, Buswell W, Zhang P, Walker H, Johnson I, Field K, Schwarzenbacher R, Ton J (2022) A single amino acid transporter controls the uptake of priming-inducing beta-amino acids and the associated tradeoff between induced resistance and plant growth. The Plant Cell 34: 4840-4856

Tarazona, P., Feussner, K., and Feussner, I. (2015). An enhanced plant lipidomics method based on multiplexed liquid chromatography–mass spectrometry reveals additional insights into cold- and drought-induced membrane remodeling 84, 621-633.

Thevenet, D., Pastor, V., Baccelli, I., Balmer, A., Vallat, A., Neier, R., Glauser, G., and Mauch-Mani, B. (2017). The priming molecule β-aminobutyric acid is naturally present in plants and is induced by stress. New Phytologist 213, 552-559.

Ukawa, T., Banno, F., Ishikawa, T., Kasahara, K., Nishina, Y., Inoue, R., Tsujii, K., Yamaguchi, M., Takahashi, T., Fukao, Y., Kawai-Yamada, M., and Nagano, M. (2022). Sphingolipids with 2-hydroxy fatty acids aid in plasma membrane nanodomain organization and oxidative burst. Plant Physiology 189, 839-857.

Wu, C.-C., Singh, P., Chen, M.-C., and Zimmerli, L. (2009). L-Glutamine inhibits beta-aminobutyric acid-induced stress resistance and priming in Arabidopsis. Journal of Experimental Botany 61, 995-1002.

Yassin, M., Ton, J., Rolfe, S.A., Valentine, T.A., Cromey, M., Holden, N., and Newton, A.C. (2021). The rise, fall and resurrection of chemical-induced resistance agents. Pest Management Science 77, 3900-3909.

Zienkiewicz, A., Gömann, J., König, S., Herrfurth, C., Liu, Y.-T., Meldau, D., and Feussner, I. (2020). Disruption of Arabidopsis neutral ceramidases 1 and 2 results in specific sphingolipid imbalances triggering different phytohormone-dependent plant cell death programmes. New Phytologist 226, 170-188.

3.9 Supplemental Material

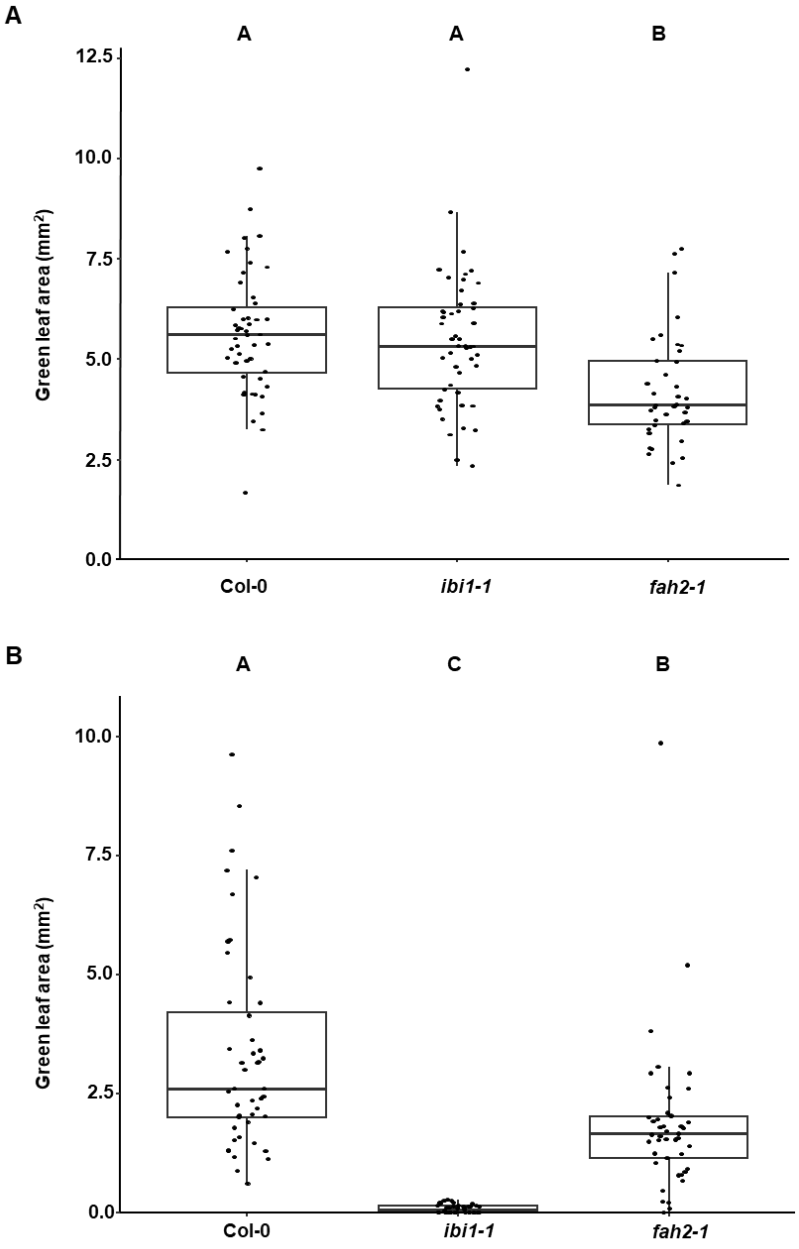

Supplemental Figure 3.1. Green leaf area is reduced in *fah2-1* plants (Supports Figure 3.2). Green leaf area of 12-day-old Col-0, *ibi1-1* and *fah2-1* seedlings, which were grown on ½ MS plates **(A)** or ½ MS plates supplied with 5 mM BABA **(B)**. Different letters indicate significant differences in plant size (Kruskal-Wallis test followed by Wilcoxon signed-rank test; $p<0.05$; n= 39-49 seedlings; the experiment has been repeated once with similar results).

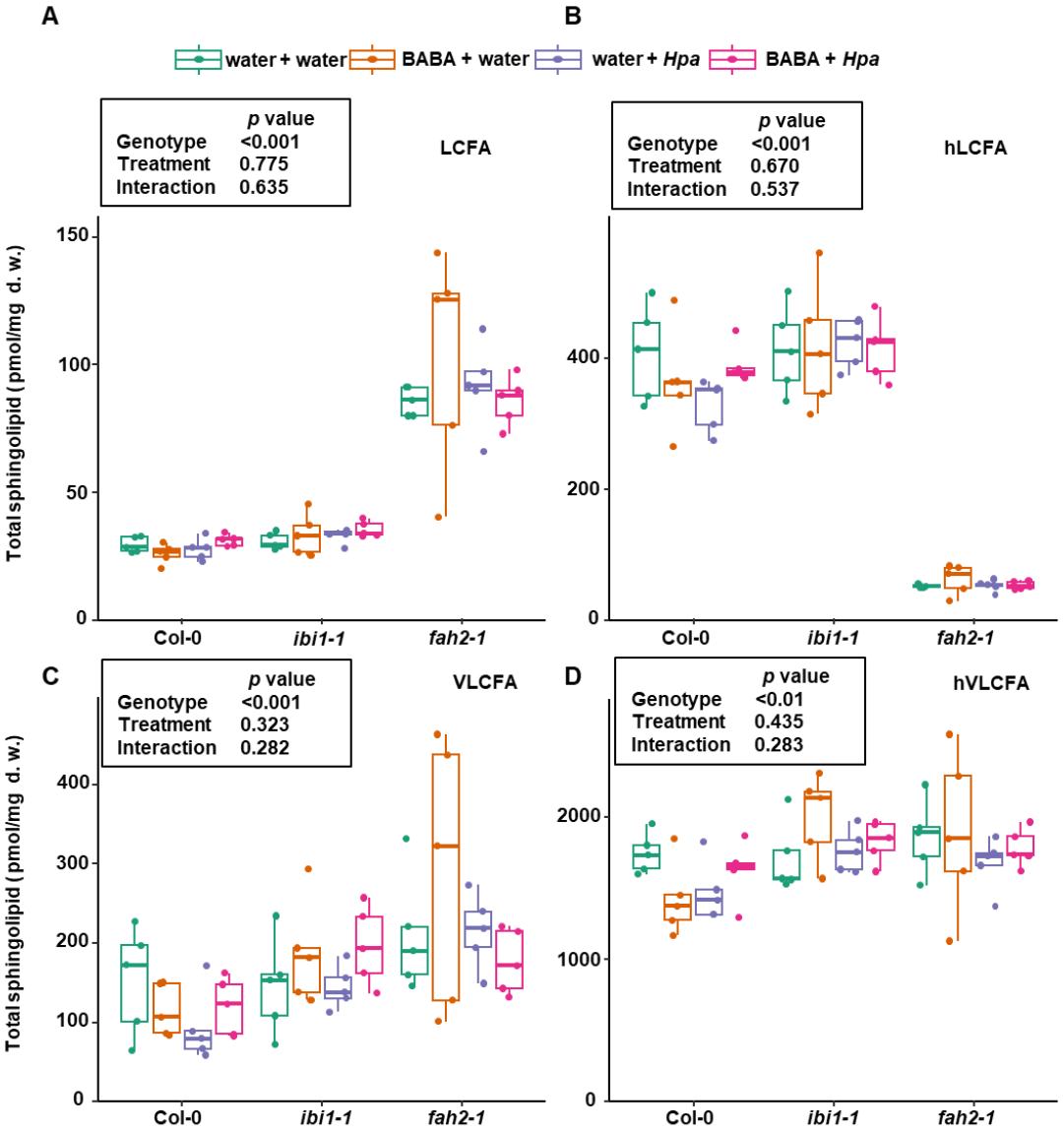

Supplemental Figure 3.2. Sphingolipid composition is genotype-dependent (Supports Figure 3.3). Sphingolipid analysis on Col-0, *ibi1-1* and *fah2-1* plants after treatments. Three-week-old plants were exposed to water (mock) or 0.05 mM BABA by soil application and sprayed with mock solution (water) or *Hpa* conidiospores two days after water/BABA treatment. Seedlings were harvested 3 days post-inoculation (dpi). Total sphingolipid (ceramides, glucosylceramides and glycosyl inositol phosphoceramides) content was shown and separated into **(A)** LCFA (sphingolipid with less than C20 fatty acid moiety), **(B)** hLCFA (sphingolipid with less than C20 α-hydroxylated fatty acid moiety), **(C)** VLCFA (sphingolipid with C20 or more fatty acid moiety) and **(D)** hVLCFA(sphingolipid with C20 or more α-hydroxylated fatty acid moiety). Insets show statistically significant effects on sphingolipid content by genotype (two-way ANOVA).

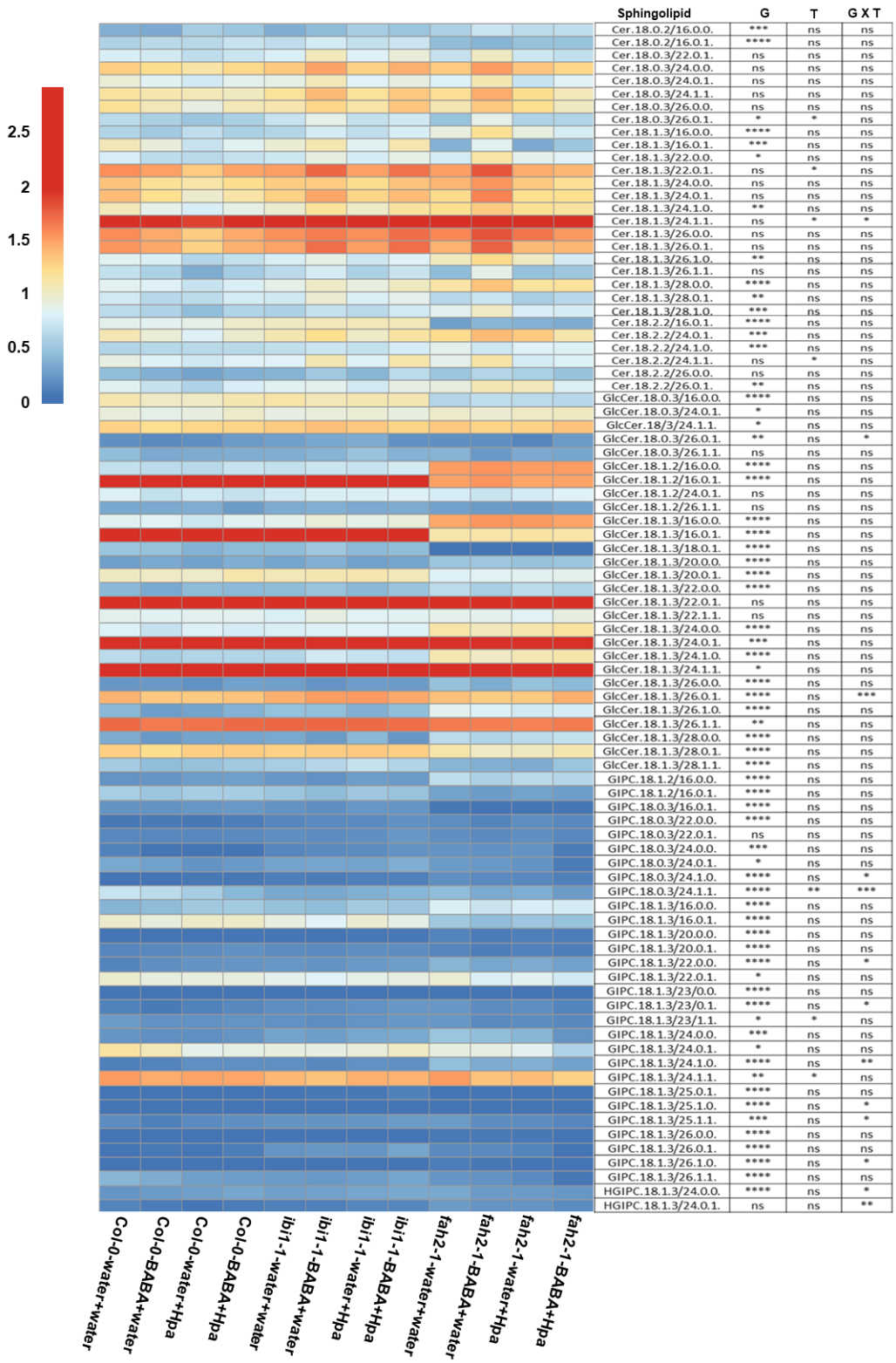

Sphingolipid	G	T	G X T
Cer.18.0.2/16.0.0.	***	ns	ns
Cer.18.0.2/16.0.1.	****	ns	ns
Cer.18.0.3/22.0.1.	ns	ns	ns
Cer.18.0.3/24.0.0.	ns	ns	ns
Cer.18.0.3/24.0.1.	ns	ns	ns
Cer.18.0.3/24.1.1.	ns	ns	ns
Cer.18.0.3/26.0.0.	ns	ns	ns
Cer.18.0.3/26.0.1.	*	*	ns
Cer.18.1.3/16.0.0.	****	ns	ns
Cer.18.1.3/16.0.1.	***	ns	ns
Cer.18.1.3/22.0.0.	*	ns	ns
Cer.18.1.3/22.0.1.	ns	*	ns
Cer.18.1.3/24.0.0.	ns	ns	ns
Cer.18.1.3/24.0.1.	ns	ns	ns
Cer.18.1.3/24.1.0.	**	ns	ns
Cer.18.1.3/24.1.1.	ns	*	*
Cer.18.1.3/26.0.0.	ns	ns	ns
Cer.18.1.3/26.0.1.	ns	ns	ns
Cer.18.1.3/26.1.0.	**	ns	ns
Cer.18.1.3/26.1.1.	ns	ns	ns
Cer.18.1.3/28.0.0.	****	ns	ns
Cer.18.1.3/28.0.1.	**	ns	ns
Cer.18.1.3/28.1.0.	***	ns	ns
Cer.18.2.2/16.0.1.	****	ns	ns
Cer.18.2.2/24.0.1.	***	ns	ns
Cer.18.2.2/24.1.0.	***	ns	ns
Cer.18.2.2/24.1.1.	ns	*	ns
Cer.18.2.2/26.0.0.	ns	ns	ns
Cer.18.2.2/26.0.1.	**	ns	ns
GlcCer.18.0.3/16.0.0.	****	ns	ns
GlcCer.18.0.3/24.0.1.	*	ns	ns
GlcCer.18/3/24.1.1.	*	ns	ns
GlcCer.18.0.3/26.0.1.	**	ns	*
GlcCer.18.0.3/26.1.1.	ns	ns	ns
GlcCer.18.1.2/16.0.0.	****	ns	ns
GlcCer.18.1.2/16.0.1.	****	ns	ns
GlcCer.18.1.2/24.0.1.	ns	ns	ns
GlcCer.18.1.2/26.1.1.	ns	ns	ns
GlcCer.18.1.3/16.0.0.	****	ns	ns
GlcCer.18.1.3/16.0.1.	****	ns	ns
GlcCer.18.1.3/18.0.1.	****	ns	ns
GlcCer.18.1.3/20.0.0.	****	ns	ns
GlcCer.18.1.3/20.0.1.	****	ns	ns
GlcCer.18.1.3/22.0.0.	****	ns	ns
GlcCer.18.1.3/22.0.1.	ns	ns	ns
GlcCer.18.1.3/22.1.1.	ns	ns	ns
GlcCer.18.1.3/24.0.0.	****	ns	ns
GlcCer.18.1.3/24.0.1.	***	ns	ns
GlcCer.18.1.3/24.1.0.	****	ns	ns
GlcCer.18.1.3/24.1.1.	*	ns	ns
GlcCer.18.1.3/26.0.0.	****	ns	ns
GlcCer.18.1.3/26.0.1.	****	ns	***
GlcCer.18.1.3/26.1.0.	****	ns	ns
GlcCer.18.1.3/26.1.1.	**	ns	ns
GlcCer.18.1.3/28.0.0.	****	ns	ns
GlcCer.18.1.3/28.0.1.	****	ns	ns
GlcCer.18.1.3/28.1.1.	****	ns	ns
GIPC.18.1.2/16.0.0.	****	ns	ns
GIPC.18.1.2/16.0.1.	****	ns	ns
GIPC.18.0.3/16.0.1.	****	ns	ns
GIPC.18.0.3/22.0.0.	****	ns	ns
GIPC.18.0.3/22.0.1.	ns	ns	ns
GIPC.18.0.3/24.0.0.	***	ns	ns
GIPC.18.0.3/24.0.1.	*	ns	ns
GIPC.18.0.3/24.1.0.	****	ns	*
GIPC.18.0.3/24.1.1.	****	**	***
GIPC.18.1.3/16.0.0.	****	ns	ns
GIPC.18.1.3/16.0.1.	****	ns	ns
GIPC.18.1.3/20.0.0.	****	ns	ns
GIPC.18.1.3/20.0.1.	****	ns	ns
GIPC.18.1.3/22.0.0.	****	ns	*
GIPC.18.1.3/22.0.1.	*	ns	ns
GIPC.18.1.3/23/0.0.	****	ns	ns
GIPC.18.1.3/23/0.1.	****	ns	*
GIPC.18.1.3/23/1.1.	*	*	ns
GIPC.18.1.3/24.0.0.	***	ns	ns
GIPC.18.1.3/24.0.1.	*	ns	ns
GIPC.18.1.3/24.1.0.	****	ns	**
GIPC.18.1.3/24.1.1.	**	*	ns
GIPC.18.1.3/25.0.1.	****	ns	ns
GIPC.18.1.3/25.1.0.	****	ns	*
GIPC.18.1.3/25.1.1.	***	ns	*
GIPC.18.1.3/26.0.0.	****	ns	ns
GIPC.18.1.3/26.0.1.	****	ns	ns
GIPC.18.1.3/26.1.0.	****	ns	*
GIPC.18.1.3/26.1.1.	****	ns	ns
HGIPC.18.1.3/24.0.0.	****	ns	*
HGIPC.18.1.3/24.0.1.	ns	ns	**

Supplemental Figure 3.3. Two-way ANOVA analysis on individual sphingolipids content (Supports Figure 3.4). Three-week-old plants were treated with water (control) or BABA (0.05 mM) and 2 days later challenged by spraying with mock solution (water) or *Hpa* conidiospores. Leaves of seedlings were collected for sphingolipids profiling by ULPC-QoQ mass spectrometry at 3 dpi. Heatmap on the left projects the mean value (n=5) of each sphingolipid species after log(x+1)-transformed (pmol/mg d.w.). The results from two-way ANOVA analysis on individual sphingolipid content are shown in the right. G, T and G x T in the figure mean genotype, treatment and genotype x treatment, respectively. Asterisk indicates significant effect on sphingolipid content (Two-way ANOVA with Bonferroni correction; ****: p<0.00001; ***: p<0.0001; **: p<0.001; *: 0.001<p<0.05).

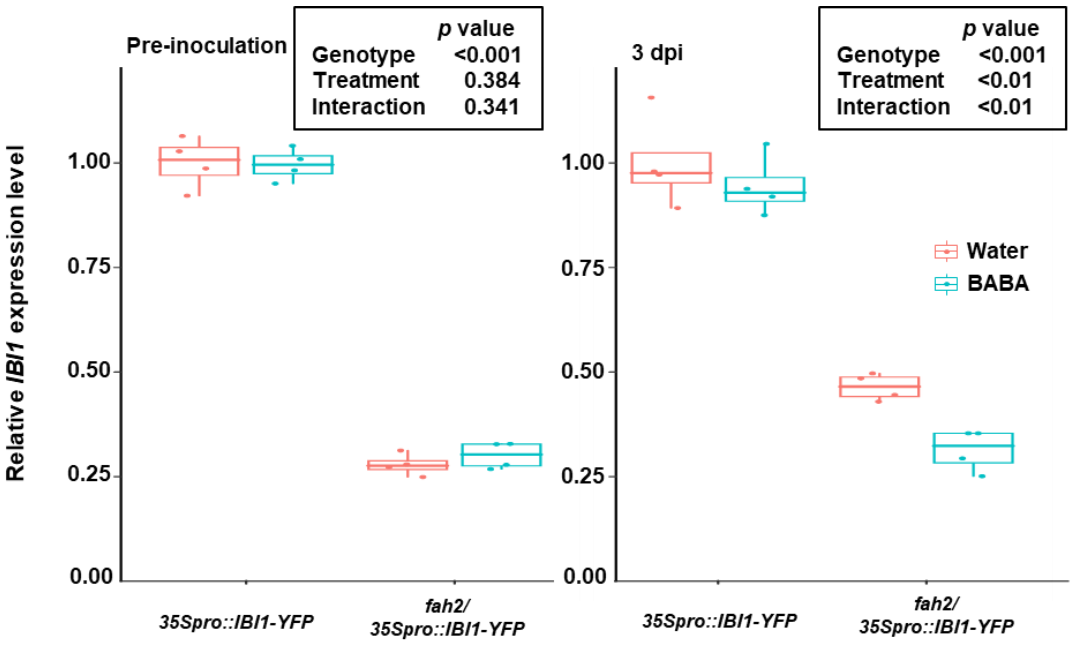

Supplemental Figure 3.4. *IBI1* expressed less in *fah2/35Spro::IBI1-YFP* (Supports Figure 3.5). Relative *IBI1* expression level in water- or BABA-treated *35Spro::IBI1-YFP* and *fah2/35Spro::IBI1-YFP* before and after *Hpa* inoculation (3 dpi). Insets show statistically significant effects on *IBI1* expression by genotype before inoculation and by genotype, treatment and interaction after inoculation (3 dpi; two-way ANOVA; the experiment has been repeated once with similar results).

Supplemental Table 3.1. Primers used in this study and their sequences.

Primer name	Usage	Primer sequence (5' to 3')
fah2-1LP	genotyping *fah2-1*	CTCCAAGAATAGCAGGTGCTG
fah2-1RP	genotyping *fah2-1*	ATGAGCAGAATTTTGCAGCAC
LBb1.3	genotyping *fah2-1*	ATTTTGCCGATTTCGGAAC
UBC qPCR Fwd	qRT-PCR	CTGCGACTCAGGGAATCTTCTAA
UBC qPCR Rev	qRT-PCR	TTGTGCCATTGAATTGAACCC
SAND qPCR Fwd	qRT-PCR	AACTCTATGCAGCATTTGATCCACT
SAND qPCR Rev	qRT-PCR	TGATTGCATATCTTTATCGCCATC
IBI1 qPCR Fwd	qRT-PCR	GAGCGAGTGGTCATGCTTTTC
IBI1 qPCR Rev	qRT-PCR	CGAGGGAAGAGGGATGTTTTC
YFP qPCR Fwd	qRT-PCR	ACCCTGAAGCTGATCTGCAC
YFP qPCR Rev	qRT-PCR	GGTCTTGTAGTTGCCGTCGT

Chapter 4: A new player in the priming of cell wall defence by β-aminobutyric acid

Chia-Nan Tao[1] and Jurriaan Ton[1 *]

[1] School of Biosciences, Institute for Sustainable Food, The University of Sheffield; Sheffield, S10 2TN; United Kingdom

4.1 Abstract

β-aminobutyric acid (BABA) and R-β-homoserine (RBH) prime early deposition of pathogen-arresting callose papillae at the cell wall. The machinery enabling this penetration resistance remains largely unknown. We have investigated the subcellular structure and machinery driving RBH- and BABA-induced penetration resistance against the downy mildew pathogen *Hyaloperonospora arabidopsidis* (*Hpa*) in Arabidopsis. Although three-dimensional reconstruction of *Hpa*-arresting papillae revealed no discernible morphological differences, RBH- and BABA-induced penetration resistance differed in their requirement for the callose synthase POWDERY MILDEW RESISTANT4. Furthermore, BABA-induced penetration resistance was strongly attenuated by a triple mutation in PLASMODESMATA LOCATED PROTEINS (PDLPs), while *PDLP1* over-expression mimicked primed penetration resistance against *Hpa*. Analysis of the translational marker line *PDLP1pro::PDLP-GFP* revealed that BABA primes early mobilisation of PDLP1 to germinating *Hpa* spores prior to callose deposition. Our study shows that RBH- and BABA-induced penetration resistance operate through distinct mechanisms and uncovers a novel role for PLDPs in BABA-primed cell wall immunity.

4.2 Introduction

Plants lack specialised immune cells to acquire immunity yet can acquire resistance after recovery from pests or diseases. This so-called induced resistance (IR) can be long-lasting and is often based on immune priming, which enables a faster and/or stronger immune reaction to future challenges by pests or diseases (Wilkinson et al., 2019; De Kesel et al., 2021). In addition to biological elicitors, such as pathogens, herbivores and rhizosphere-colonising microbes, there are many chemicals that can mimic biological IR, including damage- and microbe-associated molecular patterns and plant-endogenous stress signalling compounds, such as salicylic acid (SA), jasmonic acid (JA) and β-aminobutyric acid (BABA). Of these, BABA offers protection across a range of taxonomically unrelated plant species against a broad spectrum of environmental stresses, including biotrophic pathogens, necrotrophic pathogens, insect herbivores and abiotic stresses (Cohen et al., 2016). BABA is produced by plants under conditions of (a)biotic stress (Thevenet et al., 2017) and is perceived by

the aspartyl-tRNA synthetase IMPAIRED IN BABA-INDUCED DISEASE IMMUNITY 1 (IBI1; Luna et al., 2014; Buswell et al., 2018; Schwarzenbacher et al., 2020). When applied at higher doses, BABA is phytotoxic and represses plant growth (Wu et al., 2010; Luna et al., 2014). This undesirable effect is caused by the inhibitory binding of the active R-enantiomer of BABA to the L-aspartic acid-binding pocket of IBI1 (Buswell et al. 2018), resulting in uncharged $tRNA^{Asp}$ accumulation and GENERAL CONTROL NONDEREPRESSIBLE2 (GCN2)-dependent inhibition of gene translation (Luna et al., 2014).

A screen of β-amino acids that are structurally related to BABA and induce resistance against the downy mildew pathogen *Hyaloperonospora arabidopsidis* (*Hpa*) without concomitant growth repression led to the discovery of R-β-homoserine (RBH; Buswell et al., 2018). Despite the structural similarity between RBH and BABA, they induce resistance via different pathways. While both chemicals use the same transporter to enter the cells (LYSINE HISTIDINE TRANSPORTER 1; LHT1; Tao et al., 2022), RBH is not perceived by the IBI1 receptor (Buswell et al., 2018). Furthermore, unlike BABA, RBH primes jasmonic acid (JA)- and ethylene (ET)- dependent defences against the necrotrophic fungus *Plectosphaerella cucumerina* (Buswell et al., 2018). On the other hand, RBH and BABA both prime the deposition of callose papillae, which arrests early colonisation by *Hpa* (Ton et al., 2005; Buswell et al., 2018). Although this penetration resistance is highly effective against filamentous pathogens, little is known about the mechanisms by which RBH and BABA prime this defence layer.

Callose is a (1,3)-β-polyglucan in cell walls with numerous functions, including pollen development, regulation of plasmodesmata permeability, and plant defence (Ellinger and Voigt, 2014). Twelve *CALLOSE SYNTHASE* (*CalS*) genes have been identified in the Arabidopsis genome (Richmond and Somerville, 2000), of which *CalS12,* also known as *POWDERY MILDEW RESISTANT 4* (*PMR4*)*,* is the dominant CalS for pathogen-induced callose (Jacobs et al., 2003; Nishimura et al., 2003). PMR4-dependent callose is induced by damage- and microbe-associated molecular patterns and contributes to penetration resistance via different mechanisms (Jacobs et al., 2003; Kim et al., 2005; Luna et al., 2011; Ellinger and Voigt, 2014). Apart from reinforcing the primary cell wall to resist intercellular colonisation and cellular parasitisation, callose is thought to form a matrix in which antimicrobial metabolites and defence-related proteins can be deposited (Luna et al., 2011; Ellinger et al., 2013).

Here, we have investigated the role of resistance-enhancing callose depositions during RBH- and BABA-IR against *Hpa*. Although both IR responses involve multiple defence layers, they share the characteristic that they prime the deposition of *Hpa*-arresting papillae. However, the regulatory mechanisms controlling this induced penetration resistance remain largely unknown. Using a combination of microscopy approaches and genetic resources, we show that RBH- and BABA-induced penetration resistance differ in their requirement of PMR4, despite similar ultrastructural morphologies of the *Hpa*-arresting callose papillae. We furthermore show that BABA primes the mobilisation of PLASMODESMATA LOCATED PROTEIN 1 (PDLP1) at *Hpa* conidiospores to mediate primed callose deposition.

4.3 Results

4.3.1 Morphology of primed callose papillae arresting early *Hpa* colonisation

Although BABA is more effective than RBH in IR against *Hpa*, both chemicals prime the deposition of *Hpa*-arresting callose papillae in Arabidopsis (Ton et al., 2005; Buswell et al., 2018). To compare the priming of this defence layer by RBH and BABA, we soil-drenched 2-week-old Arabidopsis seedlings with 1.5 mM RBH or 0.1 mM BABA to obtain similar levels of IR against *Hpa* (Fig. 4.1A). Epifluorescence microscopy analysis of aniline-blue/calcofluor-stained leaves at 3 dpi confirmed that the percentage of callose papillae arresting early *Hpa* colonisation was statistically increased in RBH- and BABA-primed plants compared to control plants (Fig. 4.1B, C). To obtain a subcellular impression of these *Hpa*-arresting papillae, leaves were analysed by confocal scanning laser microscopy after double-staining with aniline blue (to visualise callose) and direct red-23 (to visualise the cell walls of *Hpa* and the plant cell). Reconstruction of three-dimensional (3D) models from z-stacked scans revealed that the callose within *Hpa*-arresting papillae was deposited underneath the spore to encapsulate the emerging germ tube (Fig. 4.1D). However, apart from the enhanced frequency of *Hpa*-arresting papillae in RBH- and BABA-primed plants, we observed no obvious morphological differences between *Hpa*-arresting papillae in water-, RBH- and BABA-treated plants.

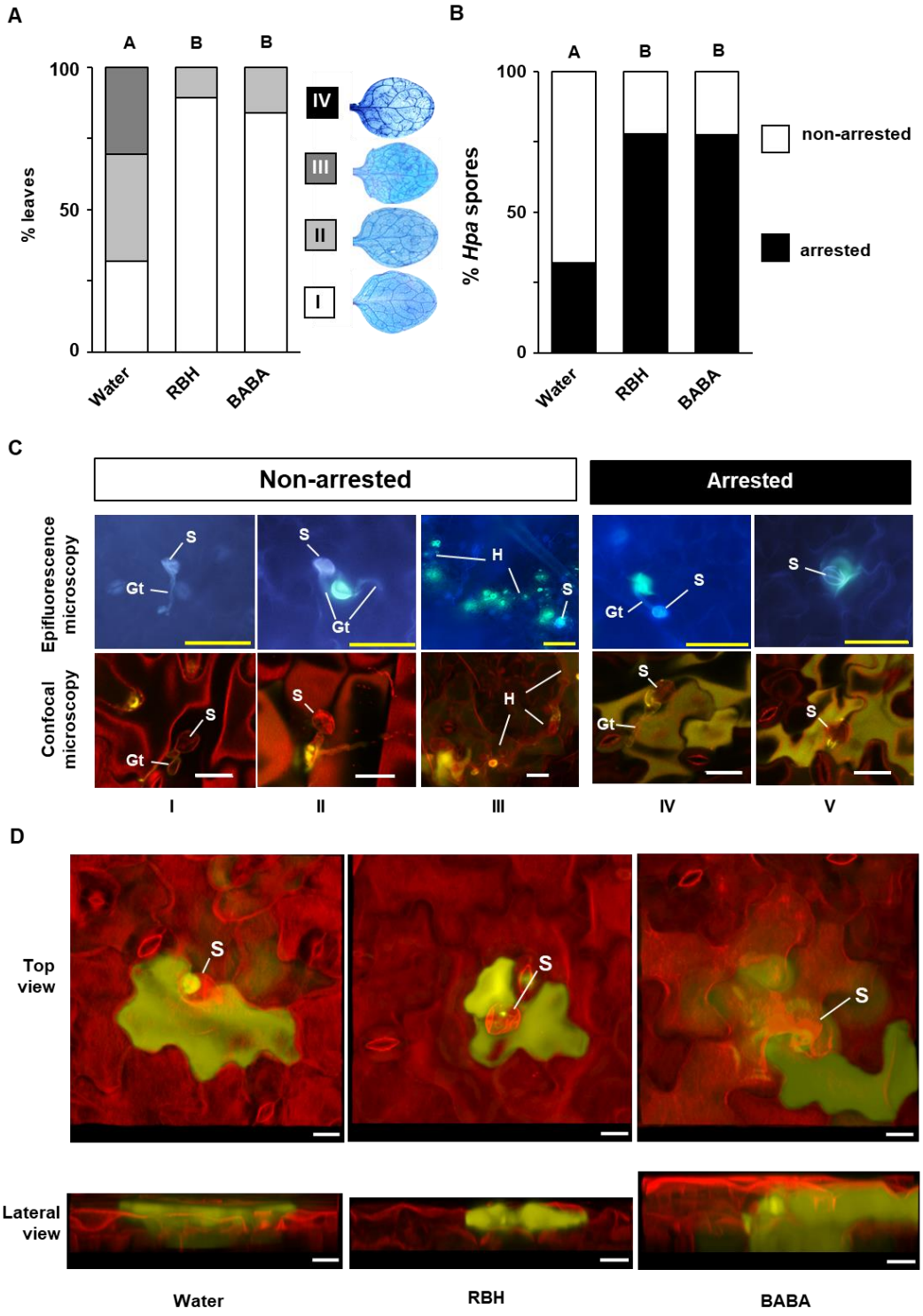

Figure 4.1. β-amino acid-induced resistance against *Hyaloperonospora arabidopsidis*. **(A)** Colonisation of Arabidopsis leaves (Col-0) by downy mildew pathogen *Hyaloperonospora arabidopsidis* WACO9 (*Hpa*) after treatment of the soil with 1.5 mM R-β-homoserine (RBH) or 0.1 mM β–aminobutyric acid (BABA). Seedlings were challenged with *Hpa* conidiospores at 2 days after soil treatment. Resistance was quantified at 6 days post inoculation (dpi) by assigning trypan-blue stained leaves to four *Hpa* colonisation classes (Schwarzenbacher et al. 2020): healthy leaves (I), leaves showing hyphal colonisation with < 10 conidiophores/leaf (II), extensive hyphal colonisation with ≥10 conidiophores/leaf (III), extensive hyphal growth with conidiospores and sexual oospores (IV).

(Continued on the following page.)

(Continued from the preceding page)

Shown are relative frequency distributions across the *Hpa* colonisation classes. Different letters indicate statistically significant differences between treatments (Fisher's exact tests+ Bonferonni correction; $p<0.05$; n=70-80 leaves; the experiment has been repeated once with similar results). (**B**) Quantification of penetration resistance in water-, RBH-, and BABA-treated Arabidopsis at the stage of spore germination and early hyphal colonisation (3 dpi). Leaves were double-stained by aniline blue and calcofluor, and analysed by epifluorescence microscopy. Shown are percentages of callose-arrested and non-arrested conidiospores, as detailed in Fig. 4.1C. Different letters indicate statistically significant differences in frequency distribution between treatments (Fisher's exact tests+ Bonferonni correction; $p<0.05$; n>100 conidiospores; the experiment has been repeated once with similar results). (**C**) Germinated conidiospores were categorised as 'non-arrested' if no callose was deposited at the germinated spore (I), or if the germ tube/expanding hyphae penetrated through the callose (II and III). Conidiospores were categorised as 'arrested' if the callose encapsulated the tip of the germ tube (IV) or the adhesion site spore (V). Shown are representative examples by epifluorescence microscopy (upper panel) and confocal laser scanner microscopy (lower panel) after double-staining with aniline blue/calcofluor or aniline blue/direct red 23, respectively. Conidiospores, germ tubes and expanding hyphae are indicated by S, Gt, and H, respectively. Callose fluorescence is indicated by yellow/green. Yellow and white bars at the bottom of each photo represent scale bars 50 µm and 20 µm, respectively. (**D**) Top and lateral views of *Hpa*-arresting callose papillae in water-, RBH- or BABA-treated plants after 3-dimensional reconstruction of z-stacked images using Morphographx software. White bar in each of photo represents 10 µm.

4.3.2 Role of PMR4 in BABA-and RBH-IR against Hpa

Although RBH and BABA both prime formation of *Hpa*-arresting callose papillae (Fig. 4.1B), the contribution of the pathogen-responsive callose synthase PMR4 in RBH- and BABA-IR against *Hpa* has never been investigated. To address this question, *Hpa* colonisation was compared at 6 dpi between wild-type (Col-0) and *pmr4-1* plants after pre-treatment of the roots with water (control) or increasing concentrations of RBH or BABA. Water-treated *pmr4-1* showed enhanced basal resistance compared to water-treated Col-0, supporting previous reports that the *pmr4-1* mutation increases SA-dependent resistance to biotrophic pathogens (Fig. 4.2A; Nishimura et al.. 2003; Flors et al. 2008). Secondly, all RBH and BABA concentrations statistically reduced *Hpa* colonisation compared to the water-treated controls, which was apparent in both Col-0 and *pmr4-1* (Fig. 4.2A). Hence, PMR4 is not critical for either IR response. However, despite the elevated basal resistance of *pmr4-1*, BABA-treated *pmr4-1* plants still allowed for hyphal colonisation by *Hpa* and failed to reach the near-complete levels of BABA-IR observed in wild-type plants. Thus, PMR4 has a quantitative contribution to BABA-IR against *Hpa* (Fig. 4.2A).

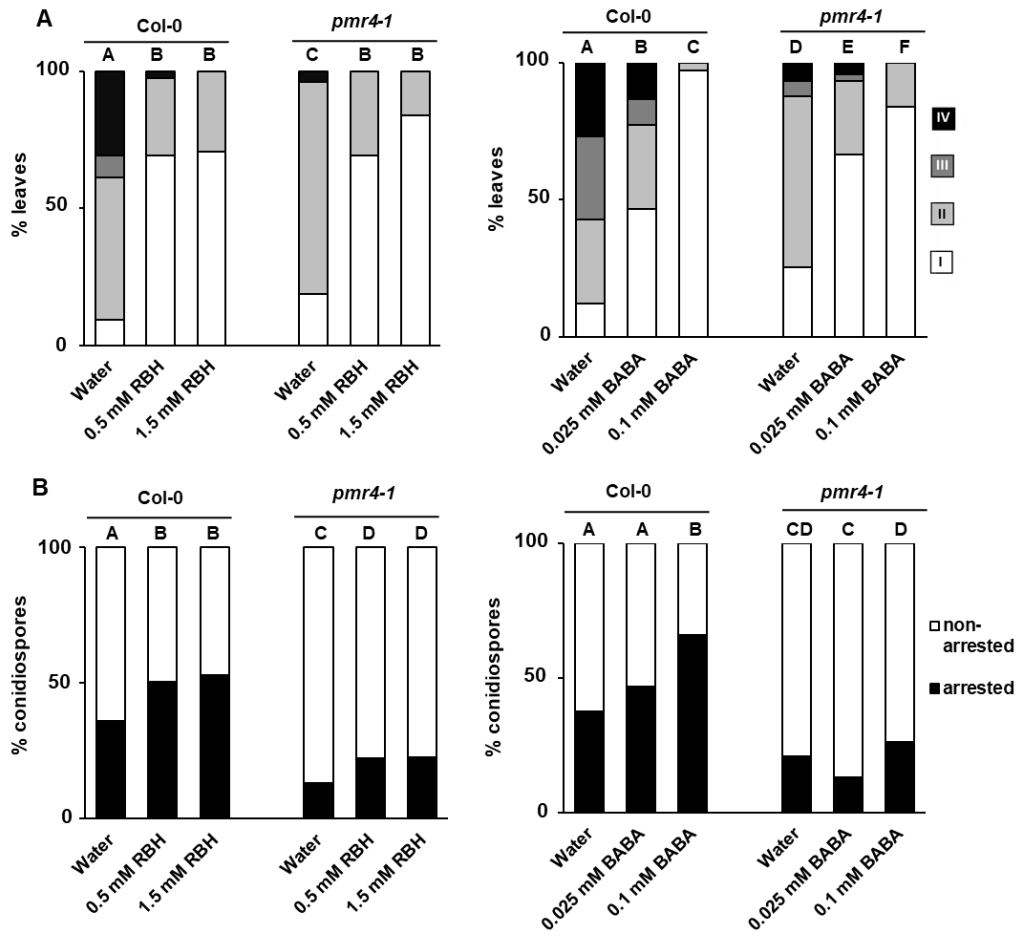

Figure 4.2. Role of the callose synthase PMR4 in RBH- and BABA-induced penetration resistance. (A) *Hpa* colonisation in leaves of Col-0 and *pmr4-1* at 6 dpi after pre-treatment with water (control) or increasing concentrations of RBH or BABA. For details, see legend of Fig. 4.1A. Different letters indicate statistically significant differences between treatments (Fisher's exact tests+ Bonferonni correction; $p< 0.05$; n=70-80 leaves). **(B)** Penetration resistance by callose papillae in leaves of Col-0 and *pmr4-1* seedlings at 3 dpi after pre-treatment with water (control) or increasing concentrations of RBH or BABA. For details, see legends of Fig. 4.1B and C. Different letters indicate statistically significant differences between arrested and non-arrested *Hpa* (Fisher's exact tests+ Bonferonni correction; $p<0.05$; n>100 conidiospores). All experiments have been repeated once with similar results.

4.3.3 Role of PMR4 in RBH- and BABA-induced penetration resistance

Since IR is a form of quantitative resistance that is the results of multiple defence layers (Wilkinson et al. 2019, Cooper & Ton, 2022), it is possible that the contribution of PMR4-dependent callose is masked by other, later-acting, defence layers. To test this hypothesis, the frequency of *Hpa*-arresting callose papillae was compared between water, RBH- and BABA-treated Col-0 and *pmr4-1* at the relatively early stage of 3 dpi. (Fig. 4.2B and Supplemental Fig. 4.1). As observed previously, both IR chemicals enhanced the deposition of *Hpa*-arresting callose papillae even though the

enhancement in 0.025 mM BABA was not significant (p=0.0646; Fig. 4.2B). Although the intensity and efficiency of *Hpa*-induced callose were dramatically reduced in *pmr4-1* compared to Col-0, there was still a residual level of *Hpa*-induced callose in *pmr4-1* supporting earlier reports of *PMR4*-independent callose deposition (Dong et al., 2008; Luna et al., 2011; Caillaud et al., 2014). Interestingly, while BABA failed to enhance penetration resistance in *pmr4-1*, RBH still enhanced the frequency of pathogen-arresting callose papillae in *pmr4-1* (Fig. 4.2B). Therefore, RBH- and BABA-induced penetration resistance differ in their requirement for PMR4.

4.3.4 Role of PDLP proteins in RBH- and BABA-induced penetration resistance

Caillaud et al. (2014) reported that the PDLP triple mutant *pdlp123* is affected in callose deposition around *Hpa* haustoria and that PDLP1 locates to the extrahaustorial membrane before callose formation. Hence, PDLP proteins orchestrate callose deposition to prevent functional haustoria at advanced stages of the Arabidopsis-*Hpa* interaction. To investigate whether PDLPs also contribute to RBH- and BABA-induced penetration resistance at earlier stages of the interaction, we quantified *Hpa*-arresting callose papillae in Col-0 and *pdlp123* plants after pre-treatment with increasing concentrations of RBH or BABA (Fig. 4.3A). A significant increase of *Hpa*-arresting callose papillae was observed in 0.025 mM BABA treated Col-0 in this experiment (Fig. 4.3A). Noticeably, the ratio of *Hpa*-arresting callose in water treated Col-0 was much lower in this experiment, comparing with the same treatment in Fig. 4.2B (19.1% vs 37.5%), which might be the cause of discrepancy in significance of 0.025 mM BABA treatment between these two experiments. The BABA-induced penetration resistance was abolished in the *pdlp123* mutant after treatment with 0.025 mM BABA and strongly reduced after treatment with 0.1 mM BABA (Fig. 4.3A). By contrast, RBH-induced penetration resistance was unaffected in *pdlp123* plants compared to wild-type plants, and even appeared more pronounced after treatment with the relatively low dose of 0.5 mM RBH (Fig. 4.3A). Hence, PDLP proteins contribute to BABA-induced penetration resistance, not RBH-induced penetration resistance, supporting our notion that priming of early cell wall defences by RBH and BABA are controlled by different pathways. To study the behaviour of PDLP1 in penetration resistance, we quantified *Hpa*-arresting callose papillae and *Hpa* colonisation in *35Spro::PDLP1-GFP* over-expression plants and Col-0. The *35Spro::PDLP1-GFP* line showed strongly

enhanced penetration resistance by callose papillae at 3 dpi (Fig. 4.3B), resulting in reduced *Hpa* colonisation by 6 dpi (Fig. 4.3C). Hence, increased expression of *PDLP1* mimics BABA-induced penetration resistance against *Hpa*.

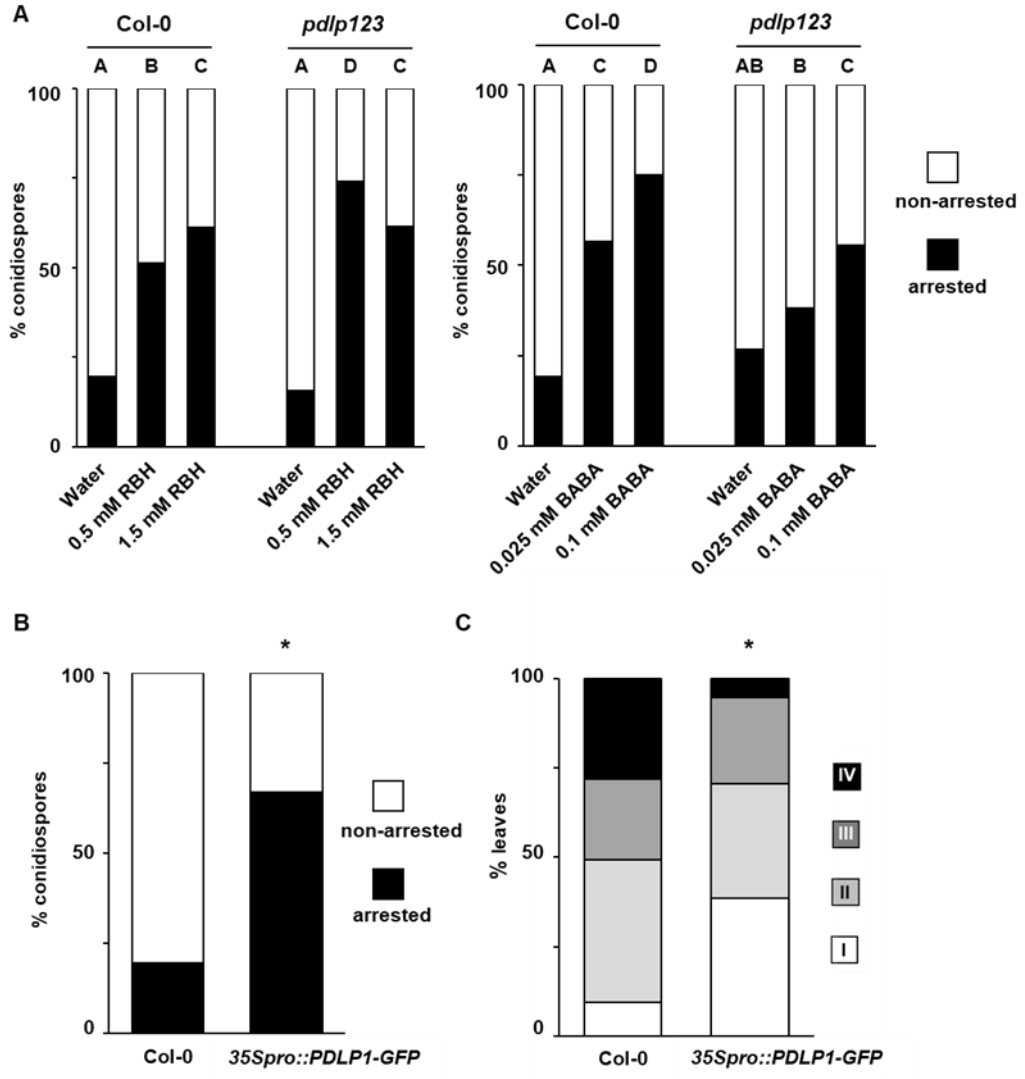

Figure 4.3. role of PDLPs in RBH- and BABA-induced penetration resistance against *Hpa*.
(A) Penetration resistance by callose papillae in leaves of Col-0 and *pdlp123* at 3 dpi after pre-treatment of the soil with water (control) or increasing concentrations of RBH or BABA. For details, see the legend to Figures 4.1B and C. Different letters indicate statistically significant frequency differences between treatments (Fisher's exact tests+ Bonferonni correction; $p<0.05$; n>100 conidiospores). **(B)** Penetration resistance by callose papillae in leaves of Col-0 and *35Spro::PDLP1-GFP* at 3 dpi. For details, see legends to Figures 4.1B and C. Asterisk indicates statistically significant differences in the frequency of arrested and non-arrested *Hpa* (Fisher's exact tests+ Bonferonni correction; $p<0.05$; n>100 conidiospores). **(C)** *Hpa* colonisation at 6 dpi in leaves of Col-0 and *35Spro::PDLP1-GFP*. For details, see legend to Figure 4.1A. Asterisk indicates statistically significant frequency differences from Col-0 (Fisher's exact tests+ Bonferonni correction; $p< 0.05$; n=70-80 leaves). All experiment have been repeated once with similar results.

4.3.5 BABA mobilises PDLP1 to germinating *Hpa* spores

To further investigate the role of PDLP1 in BABA-induced penetration resistance, we employed laser scanning confocal microscopy to determine the subcellular localisation of PDLP1 in water- and BABA-treated *PDLP1pro::PDLP1-GFP* plants. This analysis was performed at 1 dpi to capture the early signalling events preceding the deposition of augmented callose deposition in BABA-primed plants (2-3 dpi). Pre-treatment with 0.1 mM BABA not only increased the co-localisation of Hpa spores with PDLP1-GFP (Fig. 4.4B), but also intensified the PLDP1-GFP signal at *Hpa* spores (Fig. 4.4C). Hence, BABA primes the mobilisation of PDLP1 to *Hpa* spores during the onset of BABA-induced penetration resistance (Fig. 4.4 and Supplemental Fig. 4.2;). Interestingly, no increased co-localisation of PDLP1-GFP with *Hpa* spores was observed in RBH-primed plants following *Hpa* inoculation (Supplemental Fig. 4.3), confirming our conclusion that RBH- and BABA-induced penetration resistance are regulated by different pathways.

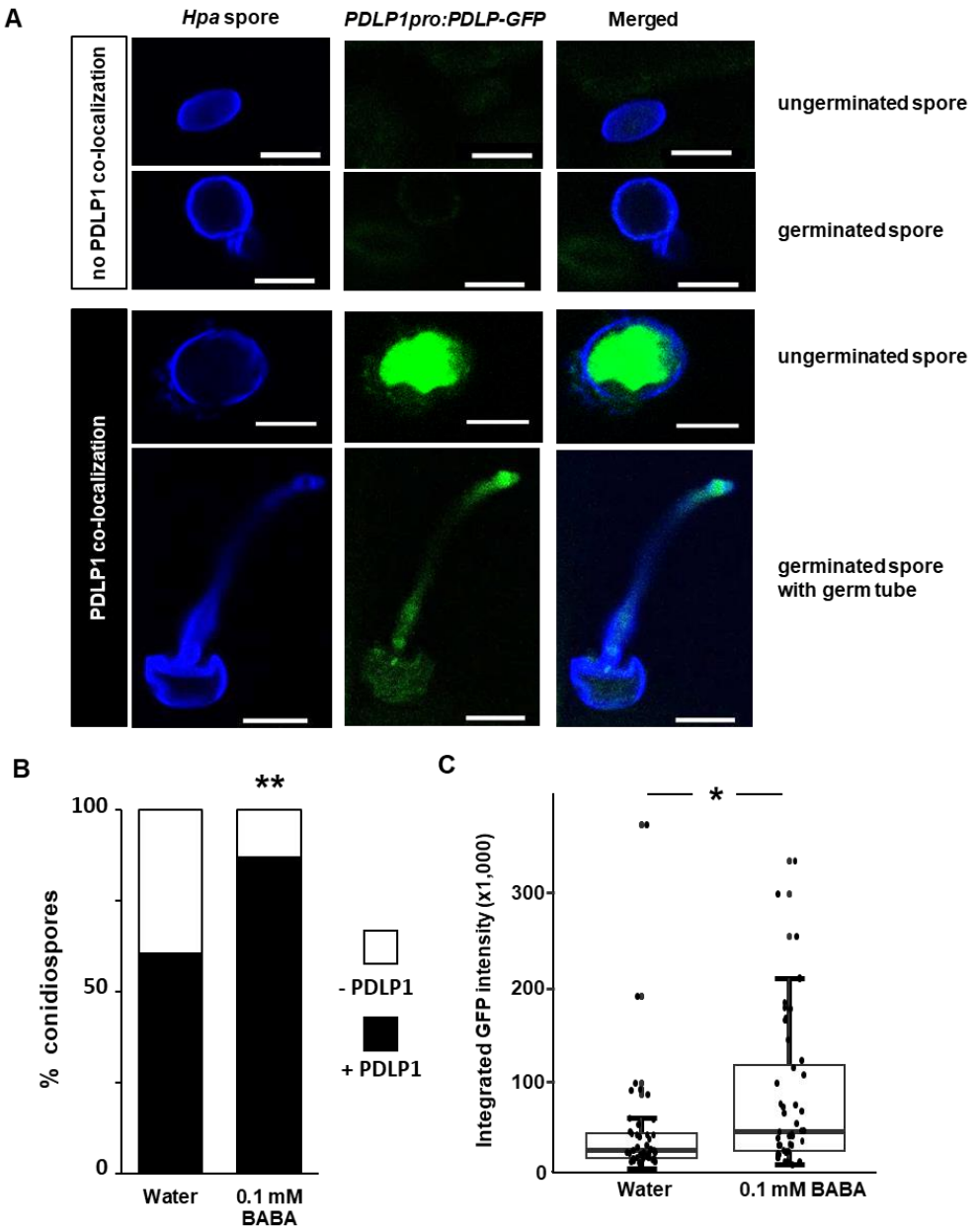

Figure 4.4. BABA primes early translocation of PDLP1 to germinating *Hpa* conidiospores.
(A) Representative examples of PDLP1-GFP in leaves of *PDLP1pro::PDLP1-GFP* plants relative to *Hpa* conidiospores at 1 dpi. Leaves were stained with calcofluor and imaged by confocal microscopy. Calcofluor-stained spores and germ tubes are shown in blue; PDLP1-GFP is shown in green. White bars represent scale bars (10 µm).
(B) Co-localisation of PDLP1-GFP with *Hpa* conidiospores in leaves of water- and BABA-treated *PDLP1pro::PDLP-GFP* plants. Shown are frequency distributions of PDLP1-GFP that co-localised (+PDLP1) or did not co-localise (-PDLP1) with *Hpa* conidiospores at 1 dpi, as illustrated in Fig. 4.4A. Asterisks indicate a statistically significant difference to the water treatment (Fisher's exact test, **:p<0.01, n=40-50 conidiospores; the experiment has been repeated once with similar results).
(C) Quantification of PDLP1-GPP signal intensity at *Hpa* spores. Shown are integrated fluorescence intensities of GFP co-localizing with *Hpa* spores. Asterisk indicates a statistically significant difference in the *Hpa* co-localising GFP signal between water- and BABA-treated plants (Welch t-test, *:p<0.05, n=40-50 spores; the experiment has been repeated once with similar results).

4.4 Discussion

4.4.1 Penetration resistance against *Hpa*: a multifaceted immune response controls diverse signalling pathways

Despite the differences in perception and priming for phytohormone-dependent defences (Buswell et al. 2018), RBH and BABA both prime early-acting cell wall defence against *Hpa*. Here, we have shown that the induced penetration resistance by RBH and BABA manifests itself as increased deposition of *Hpa*-arresting callose papillae, which are similar in ultrastructural morphology (Fig. 4.1B, C), but controlled by different pathways (Fig. 4.2-4.4). Buswell et al. (2018) reported that RBH-IR against *Hpa* is associated with augmented induction of the tryptophan-derived phytoalexin camalexin and that the camalexin-deficient *pad3-1* mutant shows attenuated levels of RBH-IR to *Hpa*. Interestingly, previous studies have demonstrated signalling activity by tryptophan-derived secondary metabolites during penetration resistance against filamentous pathogens, such as PEN2/GSTU13-dependent products of 4-methoxy-indole-3-ylmethylglucosinolate (4MI3G), indole-3-carboxylic acid (I3CA), benzoxazinoids (BXs) and camalexin accordingly (Clay et al., 2009; Ahmad et al., 2011; Piślewska-Bednarek et al., 2017; Gamir et al., 2018). In this context, we propose that this diversity in tryptophan-derived metabolites plays a role in the differential regulation of RBH- and BABA-induced penetration resistance against *Hpa*.

4.4.2 The contribution of PMR4 to penetration resistance

Previous experiments with the chemical callose synthesis inhibitor 2-deoxy-D-glucose (2-DDG) indicated an important role for callose in IR (Ton and Mauch-Mani, 2004; Sanmartin et al., 2020; Yang et al., 2022). However, despite the dominant role of the callose synthase PMR4 in pathogen-induced immune responses, the *pmr4-1* loss-of-function mutation had no effect on RBH-IR against *Hpa* and only weakly affected BABA-IR against *Hpa* colonisation at 6 dpi (Fig. 4.2A). The latter finding suggests a quantitative contribution of PMR4 to BABA-IR against *Hpa*, supporting earlier reports that BABA-IR against this pathogen involves priming of differentially regulated defence layers (Ton et al. 2005, Schwarzenbacher et al. 2020). The *pmr4-1* mutant showed smaller *Hpa*-inducible callose papillae and compromised penetration resistance (Fig. 4.2B and Supplemental Fig. 4.1), confirming the dominant role of PMR4 in pathogen-induced callose and penetration resistance. Moreover, while *pmr4-1* failed to express

BABA-induced penetration resistance to *Hpa*, RBH still displayed a statistically significant increase in the frequency of *Hpa*-arresting callose papillae (Fig. 4.2B). Thus, while BABA-induced penetration resistance to *Hpa* is fully dependent on PMR4, RBH-induced penetration resistance against this pathogen involves activity by other callose synthases. Defence-related callose has previously been reported in the *pmr4-1* mutant upon treatment with chitosan and during infection by *Hpa* (Dong et al., 2008; Luna et al., 2011; Caillaud et al., 2014). Dong et al. (2008) showed that besides *PMR4* (*CalS12*), the expression of *CalS1* is also induced by both SA and *Hpa* in an NPR1-dependent manner. Furthermore, both CalS1 and CalS8 have been implicated in ROS-dependent callose deposition at plasmodesmata (Cui and Lee, 2016), making these callose synthetases plausible candidates to contribute to RBH-induced penetration resistance against *Hpa*.

4.4.3 The contribution of PDLPs to penetration resistance

PDLPs are conserved receptor-like proteins with transmembrane helix domain and two extracellular DUF26 domains that show similarity to carbohydrate-binding proteins (Vaattovaara et al., 2019). PDLPs have been implicated in the regulation of plasmodesmata callose deposition and permeability (Thomas et al., 2008; Lee et al., 2011; Li et al., 2022). Moreover, PDLP1 has been reported to co-localise with *Hpa* haustoria to mediate PMR4-dependent callose deposition during the relatively advanced stages of the interaction (Caillaud et al., 2014). Here, we have shown that the *pdlp123* mutant is strongly attenuated in BABA-induced penetration resistance against *Hpa* (Fig. 4.3A) and that genetic over-expression of *PDLP1* mimics this priming of early-acting penetration defence (Fig. 4.3B, C). Together with our finding that BABA primes the co-localisation of PDLP1 at *Hpa* spores during the onset of BABA-induced penetration resistance (Fig. 4.4B, C), we conclude that PDLP1 regulates the augmented induction of PMR4-dependent penetration during BABA-IR. Interestingly, PDLP1 and PDLP5 have recently been shown to be part of a protein complex with the immune regulatory protein NDR1/HIN1-LIKE 3 (NHL3), which mediates CalS1-dependent callose and defence-related plasmodesmatal closure (Tee et al., 2023). However, PDLP5, unlike PDLP1, did not co-localise with *Hpa* haustoria, while NHL3 was not identified as a direct interactor with PDLP1, suggesting that PDLP1 acts through a different signalling complex to regulate *Hpa*-induced callose (Caillaud et al.,

2014). Our finding that BABA primes PDLP1 mobilisation during the onset of PMR4-dependent penetration resistance provides further evidence for a specific defence regulatory role of this protein in the Arabidopsis-*Hpa* interaction.

4.5 Materials and Methods

4.5.1 Biological material and cultivation

All *Arabidopsis thaliana* lines used in this research are in the genetic background of the Columbia (Col-0) accession. The *pmr4-1* mutant was identified and characterised by Nishimura et al. (2003), while the *pdlp123*, *35Spro::PDLP1-GFP* and *PDLP1pro::PDLP-GFP* lines have been described and characterised by Caillaud et al. (2014). Arabidopsis seeds were suspended in 0.18% agar, stratified for 2-3 days in the dark at 4℃, and planted onto 2:1 (v/v) Scott's Levington M3 compost/sand mixture. Plants (~20-25 per 70-mL pot) were then cultivated in a climate chamber containing Valoya NS1 LED lights at 150 µmol/m^2/s, using a 8.5h light (21℃)/15.5h dark (18℃) cycle at ~60% relative humidity. *Hyaloperonospora arabidopsidis* (*Hpa*) strain WACO9 was kept in its asexual cycle by alternately inoculating Col-0 and Ws NahG with *Hpa* conidiospores.

4.5.2 Induced resistance bioassays

Two-week-old seedlings were treated with BABA (Sigma-Aldrich, #A44207) or RBH (Ark Pharm; #AK-23884) by saturating soil media with chemical solutions at indicated concentrations, as described previously (Buswell et al. 2018). Two days after chemical treatment, plants were spray-inoculated with *Hpa* conidiospores (10^5 spores/mL) and kept in sealed containers at 100% RH to promote infection. For quantification of callose-associated penetration resistance, leaves were harvested at 3 dpi and double-stained with aniline blue (Sigma-Aldrich, #4415049) and calcofluor white (Sigma-Aldrich, #F3543), as described by Ton et al. (2005). Ten leaves from each genotype/treatment combination were analysed by epifluorescence microscopy (Leica DM6B; light source: CoolLED pE-2; 365 nm excitation filter, L 425 nm emission filter, 400 nm dichroic filter). Germinated conidiospores from ten leaves were categorised into ‘arrested’ (spore adhesion site or tip of germination tubes fully encased in callose)

or ‘non-arrested’ (no callose or callose deposited alongside germination tubes/hyphae) as further detailed and illustrated in Fig. 1C. Total levels of IR were based on lactophenol trypan blue-stained leaves at 6-7 dpi (Koch and Slusarenko, 1990). *Hpa* colonisation was quantified by categorising leaves into four distinct classes (I-IV), ranking from no hyphal colonisation (I) to major hyphal colonisation with deposition of conidiospores and oospores (IV), as detailed previously (Schwarzenbacher et al., 2020). Statistical differences in penetration resistance and *Hpa* colonisation between treatments and genotypes were based on pairwise Fisher's exact tests with a Bonferroni false-discovery rate correction, using R software (v 3.5.1), package 'fifer' (fifer_1.1.tar.gz).

4.5.3 Three dimensional imaging of callose papillae by confocal microscopy

Three days after *Hpa* inoculation, seedlings were collected and detained overnight (ON) in 100% ethanol. Samples were then washed twice in dH_2O for 15 mins and stained ON with 1:1 mixture of 0.05% aniline blue (Sigma-Aldrich, #4415049) in 0.07M phosphate buffer and 0.2% direct red 23 (Scientific Laboratory Supplies, #CHE1866). Seedlings were imaged with a Nikon A1 confocal scanning microscope, using Plan Fluor 40× oil immersion object lens (numerical aperture=1.3). Aniline blue was excited at 405 nm and emission was collected at 425-475 nm; direct red 23 was excited at 562 nm and emission was collected at 570-620 nm. Three dimensional models were constructed from z-stacked images using MorphoGraphX software (Barbier de Reuille et al., 2015).

4.5.4 Quantification of co-localisation between PDLP1-GFP and *Hpa* conidiospores

One day after *Hpa* inoculation, *PDLP1pro::PDLP-GFP* seedlings were collected and vacuum-infiltrated with calcofluor white (1.25µg/mL; Sigma-Aldrich, #F3543) to stain *Hpa* conidiospores and germination tubes. Co-localisation between spores and PDLP1-GFP was analysed and imaged by confocal scanning microscopy (Nikon A1) using a Plan Fluor 40× oil immersion object lens (numerical aperture=1.3). Calcofluor white was excited at 405 nm and emission was collected at 425-475 nm; GFP was excited at 488 nm and emission was collected at 500-550 nm. MorphoGraphX was

used to reconstruct 3D models from z-stacked images. Integrated fluorescence intensity was quantified by Fiji/ImageJ software (Rueden et al., 2017). Statistically significant differences in PDLP-GFP co-localisation and intensity were assessed with R software (v 3.5.1), using a Fisher's exact test (package 'fifer'; fifer_1.1.tar.gz) and a Welch' t-test, respectively.

4.6 Acknowledgements

We thank Dr. Christine Faulkner for providing the seeds of the *pdlp123*, *35Spro::PDLP1-GFP* and *PDLP1pro::PDLP-GFP* lines, and Dr. Matthew Wilson for advicing 3D model reconstruction. We gratefully acknowlege PhD student support from Ministry of Education Republic of China (Taiwan). Imaging work was performed at the Wolfson Light Microscopy Facility, using the Nikon A1 confocal microscope This work was supported by a grant from the European Research Council (ERC; no. 309944 "*Prime-A-Plant*") to J.T., two BBSRC-IPA grants to J.T. (BB/P006698/1 and BB/W015250/1) and supplementary grant from Enza Zaden to J.T., and a ERC-PoC grant to JT (no. 824985 "*ChemPrime"*).

4.7 Author Contributions

J.T. conceived the research; C.-N.T and J.T. designed the experiments; C.-N.T conducted the experiments; C.-N.T analysed the data; C.-N.T and J.T. wrote the paper.

4.8 References

Ahmad S, Veyrat N, Gordon-Weeks R, Zhang Y, Martin J, Smart L, Glauser G, Erb M, Flors V, Frey M, Ton J (2011) Benzoxazinoid metabolites regulate innate immunity against aphids and fungi in maize. Plant Physiology 157, 317-327

Barbier de Reuille P, Routier-Kierzkowska A-L, Kierzkowski D, Bassel GW, Schüpbach T, Tauriello G, Bajpai N, Strauss S, Weber A, Kiss A, Burian A, Hofhuis H, Sapala A, Lipowczan M, Heimlicher MB, Robinson S, Bayer EM, Basler K, Koumoutsakos P, Roeder AHK, Aegerter-Wilmsen T, Nakayama N, Tsiantis M, Hay A, Kwiatkowska D,

Xenarios I, Kuhlemeier C, Smith RS (2015) MorphoGraphX: A platform for quantifying morphogenesis in 4D. eLife 4, e05864

Bigeard J, Colcombet J, Hirt H (2015) Signaling mechanisms in pattern-triggered immunity (PTI). Molecular Plant 8, 521-539

Buswell W, Schwarzenbacher RE, Luna E, Sellwood M, Chen B, Flors V, Pétriacq P, Ton J (2018) Chemical priming of immunity without costs to plant growth. New Phytologist 218, 1205-1216

Caillaud M-C, Wirthmueller L, Sklenar J, Findlay K, Piquerez SJM, Jones AME, Robatzek S, Jones JDG, Faulkner C (2014) The plasmodesmal protein PDLP1 localises to haustoria-associated membranes during downy mildew infection and regulates callose deposition. PLoS Pathogens 10, e1004496.

Chisholm ST, Coaker G, Day B, Staskawicz BJ (2006) Host-microbe interactions: shaping the evolution of the plant immune response. Cell 124, 803-814

Choi HW, Klessig DF (2016) DAMPs, MAMPs, and NAMPs in plant innate immunity. BMC Plant Biology 16, 232

Clay NK, Adio AM, Denoux C, Jander G, Ausubel FM (2009) Glucosinolate metabolites required for an arabidopsis innate immune response. Science 323, 95-101

Cohen Y, Vaknin M, Mauch-Mani B (2016) BABA-induced resistance: milestones along a 55-year journey. Phytoparasitica 44, 513-538

Cui H, Tsuda K, Parker JE (2015) Effector-triggered immunity: from pathogen perception to robust defense. Annunal Review Plant Biology 66, 487-511

Cui W, Lee JY (2016) Arabidopsis callose synthases CalS1/8 regulate plasmodesmal permeability during stress. Nature Plants 2, 16034

De Kesel J, Conrath U, Flors V, Luna E, Mageroy MH, Mauch-Mani B, Pastor V, Pozo MJ, Pieterse CMJ, Ton J, Kyndt T (2021) The induced resistance lexicon: do's and don'ts. Trends Plant Science 26, 685-691

Desmedt W, Kudjordjie EN, Chavan SN, Desmet S, Nicolaisen M, Vanholme B, Vestergård M, Kyndt T (2022) Distinct chemical resistance-inducing stimuli result in common transcriptional, metabolic, and nematode community signatures in rice root and rhizosphere. Journal of Experimental Botany 73, 7564-7581.

Diao M, Ren S, Wang Q, Qian L, Shen J, Liu Y, Huang S (2018) Arabidopsis formin 2 regulates cell-to-cell trafficking by capping and stabilizing actin filaments at plasmodesmata. eLife 7, e36316

Dong X, Hong Z, Chatterjee J, Kim S, Verma DPS (2008) Expression of callose synthase genes and its connection with NPR1 signaling pathway during pathogen infection. Planta 229, 87-98

Ellinger D, Naumann M, Falter C, Zwikowics C, Jamrow T, Manisseri C, Somerville SC, Voigt CA (2013) Elevated early callose deposition results in complete penetration resistance to powdery mildew in Arabidopsis. Plant Physiology 161, 1433-1444

Ellinger D, Voigt CA (2014) Callose biosynthesis in arabidopsis with a focus on pathogen response: what we have learned within the last decade. Annunal Botany 114, 1349-1358

Gamir J, Pastor V, Sánchez-Bel P, Agut B, Mateu D, García-Andrade J, Flors V (2018) Starch degradation, abscisic acid and vesicular trafficking are important elements in callose priming by indole-3-carboxylic acid in response to *Plectosphaerella cucumerina* infection. 96, 518-531

Jacobs AK, Lipka V, Burton RA, Panstruga R, Strizhov N, Schulze-Lefert P, Fincher GB (2003) An Arabidopsis callose synthase, GSL5, is required for wound and papillary callose formation. The Plant Cell 15, 2503-2513

Jones JDG, Dangl JL (2006) The plant immune system. Nature 444, 323-329

Kim MG, da Cunha L, McFall AJ, Belkhadir Y, DebRoy S, Dangl JL, Mackey D (2005) Two *Pseudomonas syringae* Type III effectors inhibit RIN4-regulated basal defense in Arabidopsis. Cell 121, 749-759

Koch E, Slusarenko A (1990) Arabidopsis is susceptible to infection by a downy mildew fungus. The Plant Cell 2, 437-445

Lee J-Y, Wang X, Cui W, Sager R, Modla S, Czymmek K, Zybaliov B, van Wijk K, Zhang C, Lu H, Lakshmanan V (2011) A plasmodesmata-localized protein mediates crosstalk between cell-to-cell communication and innate immunity in Arabidopsis. The Plant Cell 23, 3353-3373

Li Z, Liu S-L, Montes-Serey C, Walley JW, Aung K (2022) Plasmodesmata-located proteins regulate plasmodesmal function at specific cell interfaces in Arabidopsis. bioRxiv, 502996

Luna E, Pastor V, Robert J, Flors V, Mauch-Mani B, Ton J (2011) Callose deposition: a multifaceted plant defense response. Molecular Plant Microbe Interaction 24, 183-193

Luna E, van Hulten M, Zhang Y, Berkowitz O, López A, Pétriacq P, Sellwood MA, Chen B, Burrell M, van de Meene A, Pieterse CMJ, Flors V, Ton J (2014) Plant perception of β-aminobutyric acid is mediated by an aspartyl-tRNA synthetase. Nature Chemical Biology 10, 450-456

Mauch-Mani B, Baccelli I, Luna E, Flors V (2017) Defense Priming: An adaptive part of induced resistance. Annunal Review Plant Biology 68, 485-512

Nishimura MT, Stein M, Hou B-H, Vogel JP, Edwards H, Somerville SC (2003) Loss of a callose synthase results in salicylic acid-dependent disease resistance. Science 301, 969-972

Piślewska-Bednarek M, Nakano RT, Hiruma K, Pastorczyk M, Sanchez-Vallet A, Singkaravanit-Ogawa S, Ciesiołka D, Takano Y, Molina A, Schulze-Lefert P, Bednarek P (2017) Glutathione transferase U13 functions in pathogen-triggered glucosinolate metabolism. Plant Physiology 176, 538-551

Richmond TA, Somerville CR (2000) The cellulose synthase superfamily. Plant Physiol 124, 495-498

Rueden CT, Schindelin J, Hiner MC, DeZonia BE, Walter AE, Arena ET, Eliceiri KW (2017) ImageJ2: ImageJ for the next generation of scientific image data. BMC Bioinformatics 18, 1-26.

Sanmartin N, Pastor V, Pastor-Fernandez J, Flors V, Jose Pozo M, Sanchez-Bel P (2020) Role and mechanisms of callose priming in mycorrhiza-induced resistance. Journal of Experimental Botany 71, 2769-2781

Schwarzenbacher RE, Wardell G, Stassen J, Guest E, Zhang P, Luna E, Ton J (2020) The IBI1 receptor of β-aminobutyric acid interacts with voz transcription factors to regulate abscisic acid signaling and callose-associated defense. Molecular Plant 13, 1455-1469

Tao C-N, Buswell W, Zhang P, Walker H, Johnson I, Field K, Schwarzenbacher R, Ton J (2022) A single amino acid transporter controls the uptake of priming-inducing beta-amino acids and the associated tradeoff between induced resistance and plant growth. The Plant Cell 34, 4840-4856

Tee Estee E, Johnston Matthew G, Papp D, Faulkner C (2023) A PDLP-NHL3 complex integrates plasmodesmal immune signaling cascades. Proceedings of the National Academy of Sciences of the United States of America 120, e2216397120

Thevenet D, Pastor V, Baccelli I, Balmer A, Vallat A, Neier R, Glauser G, Mauch-Mani B (2017) The priming molecule β-aminobutyric acid is naturally present in plants and is induced by stress. New Phytologist 213, 552-559

Thomas CL, Bayer EM, Ritzenthaler C, Fernandez-Calvino L, Maule AJ (2008) Specific Targeting of a plasmodesmal protein affecting cell-to-cell communication. PLOS Biology 6, e7

Ton J, Jakab G, Toquin V, Flors V, Iavicoli A, Maeder MN, Métraux J-P, Mauch-Mani BJTPC (2005) Dissecting the β-aminobutyric acid–induced priming phenomenon in Arabidopsis. The Plant Cell 17, 987-999

Ton J, Mauch-Mani B (2004) β-amino-butyric acid-induced resistance against necrotrophic pathogens is based on ABA-dependent priming for callose. The Plant Journal 38, 119-130

Vaattovaara A, Brandt B, Rajaraman S, Safronov O, Veidenberg A, Luklová M, Kangasjärvi J, Löytynoja A, Hothorn M, Salojärvi J, Wrzaczek M (2019) Mechanistic insights into the evolution of DUF26-containing proteins in land plants. Communications Biology 2, 56

Wilkinson SW, Magerøy MH, Sánchez AL, Smith LM, Furci L, Cotton TEA, Krokene P, Ton J (2019) Surviving in a Hostile World: Plant Strategies to Resist Pests and Diseases. Annual Review Phytopathology 57, 505-529

Wu CC, Singh P, Chen MC, Zimmerli L (2010) L-Glutamine inhibits beta-aminobutyric acid-induced stress resistance and priming in Arabidopsis. Journal of Experimental Botany 61, 995-1002

Yang F, Zhang X, Xue H, Tian T, Tong H, Hu J, Zhang R, Tang J, Su Q (2022) (Z)-3-hexenol primes callose deposition against whitefly-mediated begomovirus infection in tomato. The Plant Journal 112, 694-708

Zimmerli L, Jakab G, Métraux J-P, Mauch-Mani B (2000) Potentiation of pathogen-specific defense mechanisms in Arabidopsis by beta-aminobutyric acid. Proceedings of the National Academy of Sciences of the United States of America 97: 12920-12925

4.9 Supplemental Material

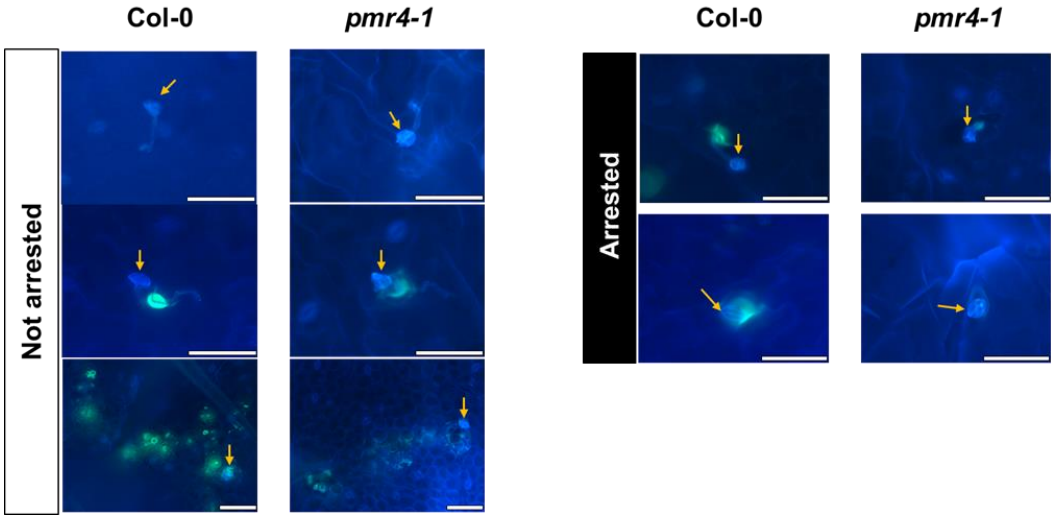

Supplemental Figure 4.1. *Hpa*-induced callose depositions in Col-0 and *pmr4-1* (Supports Figure 4.2). Shown are representative photos from epifluorescence microscopy analysis of germinating *Hpa* conidiospores and callose papillae in aniline blue/calcofluor-stained leaves at 3 dpi. Germinating *Hpa* conidiospores (orange arrows) were categorised as either 'non-arrested' or 'arrested', as detailed and illustrated in Fig. 4.1C. The example images for Col-0 are reused from Fig. 4.1C. The calcofluor signal from *Hpa* is light blue; the aniline blue signal from callose depositions is yellow/green. White bars indicate scale bars (50 µm).

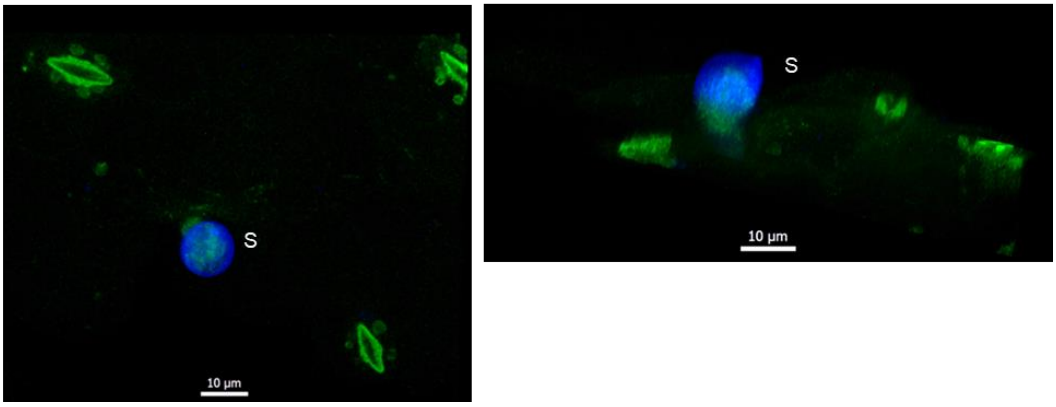

Supplemental Figure 4.2. Co-localisation of PDLP1-GFP with *Hpa* (Supports Figure 4.4). Shown are representative top (right) and lateral (left) views of PDLP-GFP co-localising with a germinating conidiospore of *Hpa*. Z-stack images were taken from a calcofluor-stained *PDLP1pro::PDLP1-GFP* leaf at 1 dpi with *Hpa*. The *Hpa* spore is indicated by S.

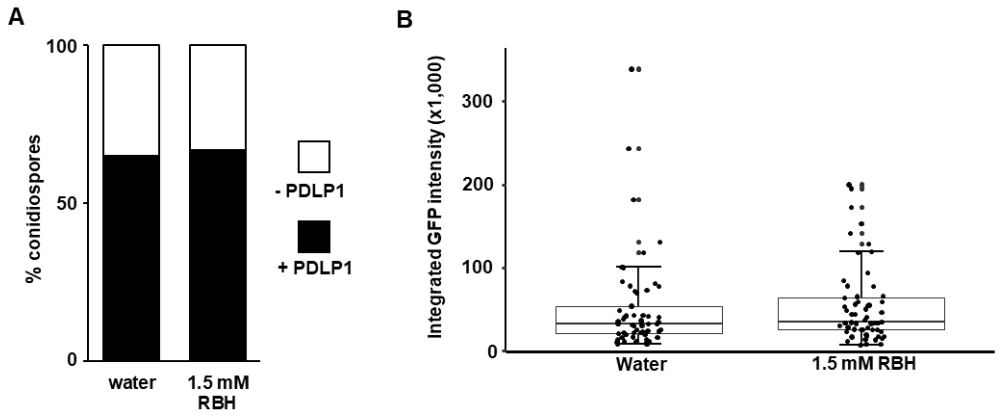

Supplemental Figure 4.3. RBH does not prime early translocation of PDLP1 to germinating *Hpa* conidiospores (Supports Figure 4.4). (A) Co-localization frequency of PDLP1-GFP with *Hpa* conidiospores. Two-week-old *PDLP1pro::PDLP-GFP* seedlings were treated with water or 1.5 mM RBH and inoculated with *Hpa* 2 days later. Shown are frequency distributions of PDLP1-GFP that co-localised (+PDLP1) or did not co-localise (-PDLP1) with *Hpa* conidiospores at 1 dpi, as illustrated in Fig. 4A (n=57 spores; the experiment has been repeated once with similar results). **(B)** PDLP1-GFP signal intensity at *Hpa* conidiospores. Shown are integrated fluorescence intensities of GFP co-localizing with *Hpa* spores. No statistically significant difference was detected in the *Hpa* co-localising GFP signal between water- and RBH-treated plants (Welch t-test, p>0.05, n=57 spores; the experiment has been repeated once with similar results).

Chapter 5: General Discussion

5.1 RBH and BABA share the same cellular transporter but prime different defence pathways

This thesis aimed to improve our understanding of the molecular pathways driving (R)-β-homoserine (RBH)- and β-aminobutyric acid (BABA)-induced resistance (IR). The work described in this thesis has generated new insights into the cellular uptake of resistance-inducing β-amino acids (Chapter 2), the mechanisms contributing to the establishment of the priming (Chapter 3) and the mechanisms underpinning the augmented defence response upon pathogen attack (Chapter 4).

The forward genetic screen in Chapter 2 was designed to select for Arabidopsis T-DNA insertion mutants that are *impaired in RBH-induced immunity* (*iri*) against downy mildew and yielded 108 putative mutants, of which four were completely impaired in RBH-IR (Fig. 2.1A and Supplemental Fig. S1.1B). Of these, only one mutant phenotype could be confirmed in an independent T-DNA insertion line (Fig. 2.1C, D and Supplemental Fig. S2B, C). The affected gene in these allelic *iri* mutants encodes the amino acid transporter LHT1. Subsequent experiments revealed that this transporter is not only essential for the uptake of RBH from the soil, but also responsible for the uptake of BABA (Fig. 2.2 A and Fig. 2.4A). Interestingly, it was previously reported that the BABA receptor IBI1 is not necessary for RBH-IR (Buswell et al., 2018). Thus, while both β-amino acids share the same transporter, they are not perceived by the same receptor (Fig. 5.1).

Chapter 3 revealed that the fatty acid hydroxylase FAH2 interacts *in planta* with the BABA receptor IBI1. Further characterisation of the *fah2-1* mutant showed that FAH2, like IBI1, functions as a regulator of both BABA-IR and BABA-induced stress (Fig. 3.2A, B and C). Since FAH2 is an ER-localised enzyme (Nagano et al., 2012) and IBI1 moves to the cytoplasm during the BABA-potentiated defence response after pathogen attacks (Luna et al. 2014), it follows that FAH2 acts at the initial perception of BABA leading to the establishment of priming.

Finally, Chapter 4 focused on the mechanisms controlling the augmented defence response of primed plants to pathogen challenge. Previous studies reported that RBH and BABA both augment callose-related penetration defence at the cell wall, suggesting a convergence in the pathways controlling RBH- and BABA-IR (Ton et al., 2005; Buswell et al., 2018). However, the results in this chapter suggest otherwise:

BABA-primed callose defence against the downy mildew pathogen *Hyloperonospora arabidopsidis* (*Hpa*) entirely depended on the callose synthase PMR4, whereas RBH-induced penetration resistance against *Hpa* could operate independently of PMR4, suggesting an involvement of an additional, yet unknow, callose synthase (Fig. 4.2B). A similar difference was found for callose-regulating PDLP proteins: the *pdlp123* mutations only affected BABA-induced penetration resistance and not RBH-induced penetration resistance (Fig 4.3B). These results strongly suggest that the pathways controlling BABA- and RBH-IR diverge after LHT1-dependent uptake (Fig. 5.1), despite the phenotypic similarities in terms of callose-associated defence.

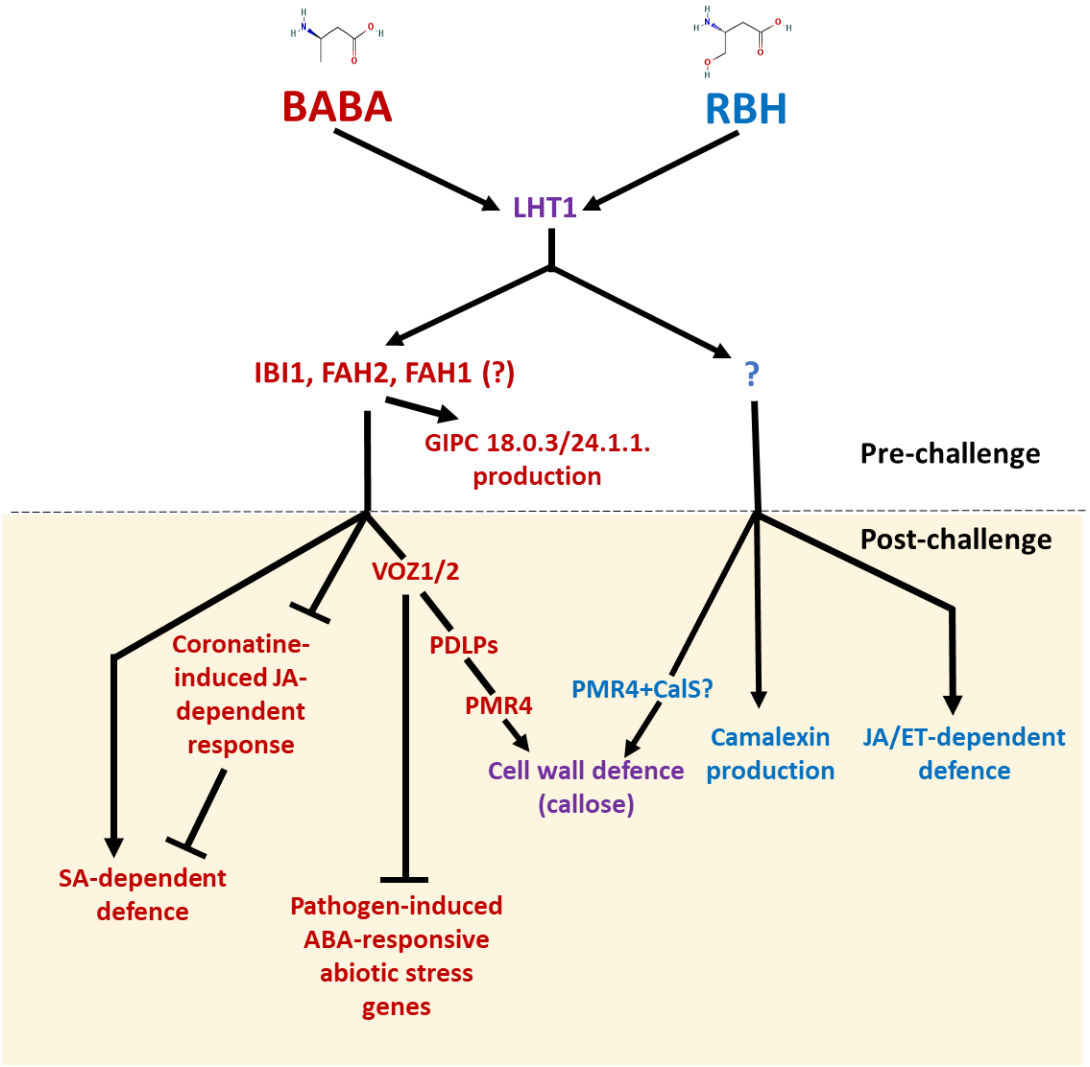

Figure 5.1. Molecular mechanism of R-β-homoserine (RBH)- and β-aminobutyric acid (BABA)-induced resistance (IR) in Arabidopsis. The mechanisms can be divided into two sectors: pre-challenge and post-challenge. In the pre-challenge phase, RBH and BABA enter the cell through the transporter LHT1. After entering the cell, BABA binds to the receptor IBI1, while the receptor for RBH is still unknown. FAH2, possibly acting with FAH1, coordinates and passes the signal from IBI1. IBI1 and FAH2 also regulate the production of GIPC 18.0.3/24.1.1, which likely contributes to anchoring IBI1 on ER membrane. After the pathogen challenge, BABA primes salicylic acid (SA)-dependent defence and suppresses coronatine-induced jasmonic acid (JA)-dependent response, which can antagonise SA-dependent defence. The IBI1 interactors, VASCULAR PLANT ONE ZINC FINGER PROTEIN (VOZ) 1 and VOZ2 inhibit the expression of pathogen-inducing abscisic acid (ABA)-responsive abiotic stress genes and regulate the primed cell wall defence, callose, generated by PMR4 under the regulation of PDLPs. As for RBH, it enhances camalexin production and JA/ethylene (ET) dependent defence. RBH also enhances callose deposition, but unlike BABA, the augmented callose is generated by PMR4 with other callose synthases.

5.2 The molecular mechanisms and biological relevance of RBH-induced resistance: a known unknown

The genetic screen in Chapter 2 yielded 108 putative mutants that are affected in RBH-IR against *Hpa*, of which only four were completely impaired in RBH-IR, while the remaining 104 mutants were partially impaired in RBH-IR (Fig. 2.1A and Supplemental Fig. 2.1B). This finding supports the notion that IR is a highly quantitative resistance response that involves a multitude of genes, pathways and mechanisms (Balmer et al., 2015; Desmedt et al., 2022). This multi-layered aspect of IR is illustrated by the results in Chapter 4. Mutation in *PMR4* blocked the first layer of BABA-primed penetration defence (Fig. 4.2B), even though the total level of disease protection by BABA was only mildly affected due to the activity of later-acting defence barriers in the BABA-IR response. Furthermore, the *pmr4-1* mutation only partially affected the potentiated callose barrier in RBH-primed plants (Fig. 4.2B), suggesting complementary action by an additional callose synthase during RBH-induced penetration resistance.

Cohen and Gisi (1994) reported that the uptake and distribution of BABA in tomato is causally related to BABA-IR. Chapter 2 showed a similar relationship for RBH, BABA and IR: the loss of LHT1 function impaired both the uptake and IR by RBH and BABA, which suggested that the contribution of LHT1 to RBH-IR is based on uptake. This hypothesis was corroborated by the biochemical uptake experiments with LHT1-expressing yeast cells (Fig. 2.6C and E), demonstrating that LHT1 acts as a medium- to high-affinity transporter of RBH. Nevertheless, it remains possible that LHT1 has a dual function: apart from its activity of a transporter, it may simultaneously also act as a receptor of RBH. This hypothesis gained traction by the observation that *LHT1* over-expressing plants displayed statistically increased levels of RBH-IR at relatively low doses of RBH, even though there was no increase in RBH content in the leaves at these concentrations (Fig 2.2A and B). This could be explained by a mechanism in which the IR pathway is elicited at low concentrations by high-affinity binding of RBH to LHT1 before the medium- to high-affinity transportation activity of the protein becomes activated. However, it is also possible that the mass spectrometry quantification of RBH in the leaves was not sufficiently sensitive to pick up subtle increases in response to relatively low doses of RBH applied to the roots. Thus, it remains equally possible that LHT1 merely serves as a cellular transporter of RBH, in

which case the chemical must be perceived inside plant cell by a yet unknown intracellular receptor. While it is possible that RBH binds and acts through another aminoacyl tRNA synthetase than IBI1, the receptor of RBH remains to be identified.

BABA has been reported to accumulate as an endogenous plant metabolite in stress plant tissues (Thevenet et al., 2017; Balmer et al., 2019) suggesting it acts as an endogenous defence signalling molecule, but the biological relevance of RBH remains unknown. It is possible that RBH mimics other IR signals, for example, the IR-eliciting determinants that are produced by plant growth-promoting rhizobacteria (PGPR) in the rhizosphere, such as N-acyl-homoserine lactones (Fig. 5.2). Indeed, applying N-acyl-homoserine lactones to plants has been reported to induced system resistance (ISR) against biotrophic and hemi-biotrophic pathogens (Schikora et al., 2011). Buswell et al. (2018) furthermore reported that RBH-IR against necrotrophic fungus *Plectosphaerella cucumerina* relies on JA and ET signalling pathways, which are known to control ISR in Arabidopsis (Pieterse et al., 2014). In addition, fully functional ISR depends on Fe homeostasis (Pieterse et al., 2014; Zhu et al., 2022). Interestingly, the *iri* mutant screen identified a T-DNA insertion mutant in *FERRIC REDUCTASE DEFECTIVE 3* (*FRD3*), showing reduced RBH-IR compared to the Col-0 wild-type (Supplemental Fig. 2.1B and Supplemental Data set 2.1). Mutation of *FRD3* has been reported to disturb Fe distribution and homeostasis, causing increased Fe accumulation in the root and reduced Fe content in the aboveground tissues, which results in smaller rosettes, chlorotic leaves, and a Fe-deficiency response (Rogers and Guerinot, 2002; Roschzttardtz et al., 2011). Thus, Fe homeostasis, which is a key component of ISR regulation (Pieterse et al., 2014; Zhu et al., 2022), may also be important for RBH-IR.

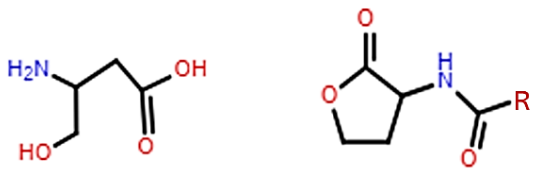

R-β-homoserine (RBH) **N-acyl-homoserine lactone**

Figure 5.2. Chemical structure of RBH and N-acyl-homoserine lactone. Shown are chemical structure of RBH (left) and N-acyl-homoserine lactone (right). R stands for any functional group.

There are yet many unanswered questions about RBH-IR. For instance, why did plants evolve a cellular transporter for RBH-IR? Is it this merely due to the non-specific nature of the LHT1 transporter or is there a biological function to the high-affinity uptake of RBH by roots? The similarity in signalling between RBH-IR and ISR hints towards the possibility that RBH acts as, or mimics, an ISR-eliciting rhizosphere signalling, but there is currently no further evidence to support this hypothesis. In addition to profiling the rhizosphere of ISR-expressing plants for RBH, or RBH-related molecules, it would be interesting to examine whether RBH has autoinduction activity in rhizosphere bacteria. Furthermore, besides augmented callose and camalexin production reported by Buswell et al. (2018), much of the defence pathways and mechanisms contributing to RBH-IR remain unknown and a further characterisation of the spectrum of effectiveness of RBH-IR against different microbial pathogens, herbivores, viruses and abiotic stresses would be informative. Moreover, although 3 of the 4 complete *iri* mutants isolated in Chapter 2 could not be confirmed in independent T-DNA insertion lines, the phenotype of these mutant lines was consistent and reproducible, indicating that their *iri* mutant phenotype is caused by a secondary T-DNA insertion or related mutation. A mapping-based approach to identify the genes affected by these *iri* mutations would generate valuable new insight and, giving their complete *iri* phenotypes, potentially reveal the RBH receptor. A better understanding of the biological context and molecular mechanism controlling RBH-IR will not only increase our understanding of the plant immune system but also but also facilitate the adoption of RBH as a future crop protection agent. The full list of *iri* mutations and associated candidate genes presented in Chapter 2, including the *iri* mutation that only partially affect RBH-IR, can be a helpful resource to being answering these questions.

5.3 BABA: a natural defence priming hormone?

BABA was been shown to accumulate naturally in leaves of stressed plants (Thevenet et al., 2017; Balmer et al., 2019). This discovery provided a first biological context for the phenomenon of BABA-IR. Although the BABA concentrations under these conditions were several orders of magnitude lower than those necessary to induced resistance, it is possible that only a minority of pathogen-interacting cells in the challenged tissues produce sufficient BABA to induce priming, rendering the BABA

concentration in whole shoot tissues well below the IR-eliciting threshold. Interestingly, BABA was found to accumulate at relatively late stages of pathogen infection, for example, at 5 dpi of *Hyaloperonospora arabidopsidis* (*Hpa*) NOCO inoculation or 24 hours of *Pseudomonas syringae* pv. *tomato* (*Pst*) DC3000 inoculation (Thevenet et al., 2017). This relatively slow response makes it unlikely that pathogen-inducible BABA functions as an early defence signal. Given the role of LHT1 in the uptake and distribution of BABA, it appears more likely that the relatively late induction of BABA during pathogen infection acts as a signal to prime neighbouring cells for defence. However, induced BABA production was only found in locally infected tissue (Balmer et al., 2019). Hence, naturally induced accumulation of BABA during pathogen infection likely acts as a localised immune signal that primes the cells neighbouring pathogen-attacked cells for enhanced defence (Baccelli and Mauch-Mani, 2017).

In most experimental settings, BABA is applied exogenously. The finding in Chapter 2 that LHT1 acts as a plasma membrane-localised transporter of BABA provides an answer to the question of how exogenously applied BABA can be perceived at the endoplasmic reticulum (ER) inside the cell. Once inside the cell, cell-to-cell transport of BABA can occur through plasmodesmata and induce priming in neighbouring cells. After binding to IBI1, BABA not only primes defences, resulting in BABA-IR, but also induces GCN2-dependent phosphorylation of the eukaryotic translation initiation factor eIF-α, resulting in BABA-induced stress (BABA-IS; Luna et al 2014; Fig 1.2).

Chapter 3 has shown that both BABA-IR and BABA-IS are regulated by the ER-localised IBI1 interactor, FAH2 (Fig. 3.2A, B and C), indicating that FAH2 acts at an early stage in the BABA response pathway, before the split in the pathway towards IR and IS (Fig. 5.1). The demonstration that a fatty acid α-hydroxylase interacts with the BABA receptor strongly points to a regulatory role of fatty acid homeostasis in BABA-IR. In particular, plant responses to pathogen infection have been associated with changes in sphingolipid metabolism. For instance, ceramide and LCB content have been reported to increase after *Pst* and *Botrytis cinerea* infection (Magnin-Robert et al., 2015; Zeng et al., 2021). The enhanced ceramide content after *B. cinerea* inoculation correlated with higher cell death and disease severity, suggesting a linkage among ceramide content. plant cell death and pathogenicity (Zeng et al., 2021).

The sphingolipid profiling of *Hpa*-inoculated plants in Chapter 3 revealed a downregulation in ceramides, which was antagonised by BABA pre-treatment. Accordingly, *Hpa* may suppress ceramide-dependent induction of defence-related cell death to allow for successful colonisation, which is prevented by BABA-IR (Fig 5.3B). The lipid profiling also revealed an IBI1- and FAH2-dependent response of GIPC 18.0.3/24.1.1 to *Hpa* infection and BABA priming. A statistically significant, albeit variable, reduction in leaf concentration of this GIPC was observed in naïve plants after *Hpa* infection, which was stronger and far more consistent in BABA-primed plants (Fig. 3.4). The fact that this *Hpa*- and BABA-regulated response was similarly affected by the *ibi1-1* and *fah2-1* mutation demonstrates involvement of this GIPC in BABA-induced priming.

Based on its treatment- and genotype-dependent profile, Chapter 3 proposed a model in which the IBI1/FAH2-dependent production of GIPC 18.0.3/24.1.1 acts a negative regulator of BABA-IR by creating ER nanodomains in which IBI1 remains firmly anchored to the ER membrane (Fig. 3.6). BABA priming treatment reduces the physical interaction of IBI1 with FAH2, thereby reducing FAH2 activity and/or diffusing GIPC 18.0.3/24.1.1 in IBI1-retaining nanodomains. Subsequent *Hpa* challenge results in ER stress and ER autophagy (ER-Phagy**;** Park and Park, 2020). This process causes breakdown of GIPC 18.0.3/24.1.1 within the membrane system (Fig. 3.4A), which enables the release of IBI1 to the cytosol, where it interacts with defence signalling proteins, such as VOZ1/2 (Schwarzenbacher et al. 2020), to mediate augmented defence expression (Fig. 3.6). Further research into the role of ER stress in BABA-induced plant responses, as well as the dynamics of the FAH2-IBI1 interaction during BABA-induced priming in relation to ER stress, could help shed new light on the mechanisms proposed in this model.

Although *FAH2* regulates both defence and stress pathways, the *fah2-1* single mutant still retains partial BABA-IR and BABA tolerance, indicating the existence of functionally redundant genes. It is therefore possible that FAH1, a highly homologous fatty acid α-hydroxylase localising to the ER membrane, acts together with FAH2 to control BABA signalling (Nagano et al., 2012). It was initially suggested that FAH1 and FAH2 have distinct substrate specificity. However, recent work by Ukawa et al. (2022) demonstrated that both enzymes can hydroxylate very long-chain fatty acids (VLCFA). This not only supports our finding that FAH2 acts on the VLCFA in GIPC 18.0.3/24.1.0

(Fig. 3.4), but also reinforces the notion that FAH1 and FAH2 might act redundantly on BABA-induced plant responses.

The BABA-IR and BABA-IS pathways likely diverge after the function of FAH2 in early BABA perception. The defence signal is possibly transmitted and amplified by other IBI1 interactors, for example, VOZ1 and VOZ2 (Schwarzenbacher et al., 2020). The VOZ transcriptional factors mediate BABA-primed callose, produced solely by PMR4, as shown in the Chapter 4 (Fig. 4.2B; Schwarzenbacher et al., 2020). To reach the full potential of augmented callose, co-localisation between spores and PDLP proteins is essential (Fig. 4.3B and 4.4B and C). It is still largely unclear how PDLPs coordinate callose deposition. However, recent work reported that two plasmodesmata located Class 1 formins, FORMIN HOMOLOGY (FH) 1 and 2, aggregate towards fungal penetration sites and participate in penetration resistance (Qin et al., 2021). As reported for the BABA-primed early translocation of PDLP1-GFP to germinating *Hpa* spores (Fig. 4.4B and C), it is plausible that PDLPs act with FH1 and FH2 to contribute to the BABA-induced priming of penetration resistance.

5.4 RBH- and BABA-induced stress responses

Although the molecular mechanisms driving β-amino acid-plant stress might be a less appealing subject to study than β-amino acid-IR, a better understanding of how and why β-amino acids induce plant stress will be critical for their exploitation as crop protection agents. After all, we can only avoid these unwanted phenotypes if we understand how they are generated in the first place. For BABA-IS, some studies have revealed mechanisms (Wu et al., 2010; Luna et al., 2014; Buswell et al., 2018; Singh et al., 2023). By contrast, the underlying causes of RBH-induced stress (RBH-IS) in plants remain largely unknown. Chapter 2 showed that RBH-IS in *35SPro:LHT1* plants is directly linked to the RBH concentration (Fig 2.3A and B). Luna et al. (2014) demonstrated that BABA causes growth reduction due to GCN2-mediated translation inhibition through the blocking of Asprtyl tRNA synthetase activity and a resulting accumulation of uncharged tRNA accumulation. Although there is currently no evidence for a mechanism underpinning RBH-IS, it is clear that the similar concentrations of BABA have a more potent stress effect than RBH (Supplemental Fig. 2.5A and B). RBH-IS is triggered by a 10-fold higher dosage than BABA-IS

(Supplemental Fig. 2.5A and B), making it unlikely that RBH-IS is controlled by the exact same mechanism as BABA-IS.

Besides GCN2 activation, the sphingolipid profiling in Chapter 3 revealed a general increase in ceramide content during conditions of BABA-IS (Fig. 3.3B). Whether the increase is linked to GCN2 regulating translation inhibition remains unclear, but a change in ceramide content could lead to cell death, as has been suggested by previous research (Shi et al., 2007; Huby et al., 2020; Zienkiewicz et al., 2020). Thus, in addition to global translation inhibition, high cell ceramide levels might have a further contribution to BABA-IS. Furthermore, sphingolipids and metabolism are involved in endoplasmic reticulum (ER) stress in humans and yeast (Kajiwara et al., 2012; Park and Park, 2020). In response to ER stress-inducing conditions, cells initiate the unfolded protein response (UPR), which involves regulation by GCN2 to maintain homeostasis in the ER. Thus, it is very plausible the BABA-induced changes in ceramides may be functionally linked to GCN2-dependent stress (Afrin et al., 2019).

5.5 Future exploitation of RBH and BABA in crop protection through dual application protocols.

The work presented in this PhD thesis has demonstrated that RBH-IR and BABA-IR are distinctly different IR responses. Accordingly, co-application of low (non-phytotoxic) doses of RBH and BABA might have additive or synergistic effects on crop protection. Indeed, application of BABA and Acibenzolar-S-methyl at half of the recommended dose is more effective in reducing grape downy mildew severity (Reuveni et al., 2001). Using reduced RBH and BABA doses would also result in less growth inhibition as the corresponding IS responses are dose-dependent (Supplemental Fig. 2.5A and B). On the other hand, LHT1 has been identified as the transporter of both RBH and BABA, so there is a possibility that both agents compete for uptake. This potential issue can be avoided by applying RBH and BABA sequentially rather than a mixture. Therefore, it is worth re-examining and defining the effective IR-mediating doses of both chemicals and establishing a new dual application protocol that is optimised for different crop species and diseases.

The link between *LHT1* expression and activity opens a new route for manipulating IR and avoiding growth costs. Breeders can select lines with higher *LHT1* expression

levels in the species that are less sensitive to RBH or BABA. By contrast, cultivars with lower *LHT1* gene expression can be bred to reduce the uptake of both chemicals to stress-inducing concentrations. This optimisation of genotype-treatment combination can be applied in a wider integrated pest management program (IPM) with other crop protection strategies (Yassin et al., 2021). High solubility in water makes RBH and BABA particularly suitable to apply as root drenches in combination with other water-soluble agrochemicals, such as fertiliser solutions. Indeed, root application was recently reported to induce stronger levels of BABA-IR against tomato root-knot nematode than foliar spray (Singh et al., 2023). Thus, the application of RBH and BABA seems particularly suitable for hydroponically grown crops: carefully controlled application of combinations of low RBH/BABA doses into the nutrient supply stream of hydroponically grown crops could provide a safe and effective means of disease protection without side effects and/or long-lasting chemical residues in crop products.

A major challenge of current agriculture is to replace pesticides with sustainable alternatives, while maintaining (or improving) crop production. Combining β-amino acids with other chemical control methods has great potential to help addressing this challenge and reduce the need for high pesticide usage. Integrated use of BABA with fungicide Fluazinam in controlling potato late blight allowed for a 20-25% reduction in Fluazinam usage without compromising protection (Liljeroth et al., 2010). Furthermore, using BABA and the fungicide mancozeb provided better control of *Phytophthora infestans* in potato and tomato and *Pseudoperonospora cubensis* in cucumber than using each chemical alone (Baider and Cohen, 2003). Thus, the fundamental research described in this PhD thesis offers new opportunities to direct further translational research towards the safe and effective exploitation of β-amino acids in crop protection.

5.6 References

Afrin, T., Diwan, D., Sahawneh, K., and Pajerowska-Mukhtar, K. (2019). Multilevel regulation of endoplasmic reticulum stress responses in plants: where old roads and new paths meet. Journal of Experimental Botany 71, 1659-1667.

Baccelli, I., and Mauch-Mani, B. (2017). When the story proceeds backward: The discovery of endogenous β-aminobutyric acid as the missing link for a potential new plant hormone. Communicative & Integrative Biology 10, e1290019.

Baider, A., and Cohen, Y. (2003). Synergistic interaction between BABA and mancozeb in controllingPhytophthora infestans in potato and tomato and *Pseudoperonospora cubensis* in cucumber. Phytoparasitica 31, 399-409.

Balmer, A., Glauser, G., Mauch-Mani, B., and Baccelli, I. (2019). Accumulation patterns of endogenous β-aminobutyric acid during plant development and defence in *Arabidopsis thaliana*. Plant Biology 21, 318-325.

Balmer, A., Pastor, V., Gamir, J., Flors, V., and Mauch-Mani, B. (2015). The 'prime-ome': towards a holistic approach to priming. Trends in Plant Science 20, 443-452.

Buswell, W., Schwarzenbacher, R.E., Luna, E., Sellwood, M., Chen, B., Flors, V., Pétriacq, P., and Ton, J. (2018). Chemical priming of immunity without costs to plant growth. New Phytologist 218, 1205-1216.

Cohen, Y., and Gisi, U. (1994). Systemic translocation of 14C-dl-3-aminobutyric acid in tomato plants in relation to induced resistance against *Phytophthora infestans*. Physiological and Molecular Plant Pathology 45, 441-456.

Desmedt, W., Kudjordjie, E.N., Chavan, S.N., Desmet, S., Nicolaisen, M., Vanholme, B., Vestergård, M., and Kyndt, T. (2022). Distinct chemical resistance-inducing stimuli result in common transcriptional, metabolic, and nematode community signatures in rice root and rhizosphere. Journal of Experimental Botany 73, 7564-7581.

Huby, E., Napier, J.A., Baillieul, F., Michaelson, L.V., and Dhondt-Cordelier, S. (2020). Sphingolipids: towards an integrated view of metabolism during the plant stress response 225, 659-670.

Kajiwara, K., Muneoka, T., Watanabe, Y., Karashima, T., Kitagaki, H., and Funato, K. (2012). Perturbation of sphingolipid metabolism induces endoplasmic reticulum stress-mediated mitochondrial apoptosis in budding yeast. Molecular Microbiology 86, 1246-1261.

Liljeroth, E., Bengtsson, T., Wiik, L., and Andreasson, E. (2010). Induced resistance in potato to *Phytphthora infestans*—effects of BABA in greenhouse and field tests with different potato varieties. European Journal of Plant Pathology 127, 171-183.

Luna, E., van Hulten, M., Zhang, Y., Berkowitz, O., López, A., Pétriacq, P., Sellwood, M.A., Chen, B., Burrell, M., van de Meene, A., Pieterse, C.M.J., Flors, V., and Ton, J. (2014). Plant perception of β-aminobutyric acid is mediated by an aspartyl-tRNA synthetase. Nature Chemical Biology 10, 450-456.

Magnin-Robert, M., Le Bourse, D., Markham, J., Dorey, S., Clément, C., Baillieul, F., and Dhondt-Cordelier, S. (2015). Modifications of Sphingolipid content affect tolerance to hemibiotrophic and necrotrophic pathogens by modulating plant defense responses in Arabidopsis Plant Physiology 169, 2255-2274.

Nagano, M., Takahara, K., Fujimoto, M., Tsutsumi, N., Uchimiya, H., and Kawai-Yamada, M. (2012). Arabidopsis Sphingolipid Fatty Acid 2-Hydroxylases (AtFAH1 and AtFAH2) are functionally differentiated in fatty acid 2-hydroxylation and stress responses. Plant Physiology 159, 1138-1148.

Park, W.J., and Park, J.W. (2020). The role of sphingolipids in endoplasmic reticulum stress. FEBS letters 594, 3632-3651.

Pieterse, C.M.J., Zamioudis, C., Berendsen, R.L., Weller, D.M., Wees, S.C.M.V., and Bakker, P.A.H.M. (2014). Induced systemic resistance by beneficial microbes Annual Review of Phytopathology 52, 347-375.

Qin, L., Liu, L., Tu, J., Yang, G., Wang, S., Quilichini, T.D., Gao, P., Wang, H., Peng, G., Blancaflor, E.B., Datla, R., Xiang, D., Wilson, K.E., and Wei, Y. (2021). The ARP2/3 complex, acting cooperatively with Class I formins, modulates penetration resistance in Arabidopsis against powdery mildew invasion. The Plant Cell 33, 3151-3175.

Reuveni, M., Zahavi, T., and Cohen, Y. (2001). Controlling downy mildew (*Plasmopara viticola*) in field-grown grapevine with β-aminobutyric acid (BABA). Phytoparasitica 29, 125-133.

Rogers, E.E., and Guerinot, M.L. (2002). FRD3, a member of the multidrug and toxin efflux family, controls iron deficiency responses in Arabidopsis. The Plant Cell 14, 1787-1799.

Roschzttardtz, H., Séguéla-Arnaud, M., Briat, J.-F., Vert, G., and Curie, C. (2011). The FRD3 citrate effluxer promotes iron nutrition between symplastically disconnected tissues throughout Arabidopsis development. The Plant Cell 23, 2725-2737.

Schwarzenbacher, R.E., Wardell, G., Stassen, J., Guest, E., Zhang, P., Luna, E., and Ton, J. (2020). The IBI1 receptor of β-aminobutyric acid interacts with VOZ transcription factors to regulate abscisic acid signaling and callose-associated defense. Molecular Plant 13, 1455-1469.

Shi, L., Bielawski, J., Mu, J., Dong, H., Teng, C., Zhang, J., Yang, X., Tomishige, N., Hanada, K., Hannun, Y.A., and Zuo, J. (2007). Involvement of sphingoid bases in mediating reactive oxygen intermediate production and programmed cell death in Arabidopsis. Cell Research 17, 1030-1040.

Singh, R.R., Ameye, M., Haesaert, G., Deveux, M., Spanoghe, P., Audenaert, K., Rabasse, J.M., and Kyndt, T. (2023). Beta-Aminobutyric acid induced phytotoxicity and effectiveness against nematode is stereomer-specific and dose-dependent in tomato. Physiologia Plantarum 175, e13862.

Thevenet, D., Pastor, V., Baccelli, I., Balmer, A., Vallat, A., Neier, R., Glauser, G., and Mauch-Mani, B. (2017). The priming molecule β-aminobutyric acid is naturally present in plants and is induced by stress. New Phytologist 213, 552-559.

Ton, J., Jakab, G., Toquin, V.r., Flors, V., Iavicoli, A., Maeder, M.N., Métraux, J.-P., and Mauch-Mani, B. (2005). Dissecting the β-aminobutyric acid–induced priming phenomenon in Arabidopsis. The Plant Cell 17, 987-999.

Wu, C.C., Singh, P., Chen, M.C., and Zimmerli, L. (2010). L-Glutamine inhibits beta-aminobutyric acid-induced stress resistance and priming in Arabidopsis. Journal of Experimental Botany 61, 995-1002.

Yassin, M., Ton, J., Rolfe, S.A., Valentine, T.A., Cromey, M., Holden, N., and Newton, A.C. (2021). The rise, fall and resurrection of chemical-induced resistance agents. Pest Management Science 77, 3900-3909.

Zeng, H.-Y., Liu, Y., Chen, D.-K., Bao, H.-N., Huang, L.-Q., Yin, J., Chen, Y.-L., Xiao, S., and Yao, N. (2021). The immune components ENHANCED DISEASE SUSCEPTIBILITY 1 and PHYTOALEXIN DEFICIENT 4 are required for cell death caused by overaccumulation of ceramides in Arabidopsis. Plant Journal 107, 1447-1465.

Zhu, L., Huang, J., Lu, X., and Zhou, C. (2022). Development of plant systemic resistance by beneficial rhizobacteria: Recognition, initiation, elicitation and regulation Frontiers in Plant Science 13, 111807.

Zienkiewicz, A., Gömann, J., König, S., Herrfurth, C., Liu, Y.-T., Meldau, D., and Feussner, I. (2020). Disruption of Arabidopsis neutral ceramidases 1 and 2 results in specific sphingolipid imbalances triggering different phytohormone-dependent plant cell death programmes New Phytologist 226, 170-188.